An Aeroacoustic Study of Airfoil Self-Noise for Wind Turbine Applications

by

Nicholas Tam

A thesis
presented to the University of Waterloo
in fulfillment of the
thesis requirement for the degree of
Master of Applied Science
in
Mechanical and Mechatronics Engineering

Waterloo, Ontario, Canada, 2017

I hereby declare that I am the sole author of this thesis. This is a true copy of the thesis, including any required final revisions, as accepted by my examiners.

I understand that my thesis may be made electronically available to the public.

Abstract

The current study addresses the issue of noise relating to both large and small scale wind turbines. In utility scale applications, larger size rotors in new generations of wind turbines bring an increasing challenge to manage noise emissions. A better understanding of wind turbine noise characteristics, behaviour and generation mechanics can facilitate the development of noise reduction strategies. This can greatly aid in their adoption.

The issue of noise, however, is not exclusive to large scale wind turbines. Small scale wind turbines, operating in laminar or transitional regimes, has the potential to emit tonal noise which can be more audible and of a greater nuisance. Small scale wind turbines can be installed in higher traffic areas closer to human receptors. As such, the understanding of their noise characteristics, behaviour and generation mechanics is important as well.

In Reynolds number regime where small scale wind turbine operates, tonal noise is primarily caused by laminar boundary layer-vortex shedding (LBL-VS) noise generation mechanism. In the controlled environment of a closed circuit wind tunnel, the SD-7037 airfoil profile is examined at $Re_c = 4.0 \times 10^4$. Acoustic measurements are collected when the airfoil is under dynamic oscillation and under various static angles of attack.

Results found evidence to suggest LBL-VS noise originated from the suction side of the airfoil in this study; suggesting noise reduction efforts should be focused on suction side phenomenon in similar low Reynold number flow ($Re_c < 10^5$). Under dynamic oscillation, airfoil self-noise is studied in condition more representative of outdoor conditions. The tonal noise was found to be reduced compared with static low angles of attack results. The tones were also seen as intermittent; appearing at certain phases of the oscillation cycle. Side peaks were also found at the narrowband acoustic spectra; with the cause linked to the dynamic oscillating frequency.

Trailing edge saw-tooth serrations, which have been used on large scale wind turbines, are examined for their noise reduction properties with the SD-7037 airfoil profile. The results were found to be mixed.

For larger scale wind turbines, turbulent boundary layer flow more commonly found on the surface of the airfoil, leading to the generation of broadband noise at the trailing edge. The current study examines a 10 m diameter passive controlled wind turbine at the Wind Energy Group outdoor wind turbine test site. The behaviour of the wind turbine noise with respect to on site parameters such as upstream wind speed, upstream wind direction, wind turbine yaw direction, wind turbine blade pitch angle and wind turbine rotor rpm are examined. The feasibility for performing further acoustic experiments at the Wind Energy Group outdoor wind turbine test site is also assessed.

Acknowledgements

I am indebted to many incredible people over the course of my studies at the University of Waterloo. I must take the opportunity now to express my deepest appreciations for their help and contributions into my research.

First and foremost, I would like to thank my supervisor, Professor David Johnson, for his guidance and patience with me through the years. I am grateful that he has given me the opportunity to pursue this topic of study and I thank him for allowing me to be part of the Wind Energy Group and its continuing research efforts.

I would also like to thank my parents, King Ho Tam & Ever Tam, for their support which allowed me to pursuing my dreams and to pursue this current study. Without their nurture and their encouragements, I would not be the person I am today.

To all my friends and colleagues at the Wind Energy Group: Nigel Swytink-Binnema, Faegheh Ghorbanishohrat, Rifki Adi Nugroho, Farid Samara, Kobra Gharali, Tyler Gallant, Curtis Knischewsky, Ahmed Abdelrahman, Andrea Moscardi, Alison Zilstra, Michael Mckinnon and all the co-op students (in particular Daniel Dworakowski for his assistance in the fabrication of the ground board wind screen), I would like to extend my warmest thanks to them for their daily support, inputs and assistance in many aspects of this study. On top of this, I value the friendship and bonds we have developed outside of our research, and I wish them all the best in current and future endeavours.

To the technical staff of the Engineering faculty, including Andy Barber, Jason Benninger, James Merli, Jorge Cruz and Terry Ridgeway, I thank them for all the assistance in the experimental setup and all the valuable advice in the design process. I would also like to thank James Torriff of University of Waterloo and a member of the Kwartzlab Makerspace community workshop for his generosity and help in the fabrication of the trailing edge extension strips.

To Sharath Sundar and my sister, Jovita Tam, who both are my dearest friends and closest confidants, I thank them for their counsel and for the shrewd prospectives they provided to me over the years. I would also like to thank Obaidullah Younas, Majid Shegow, Winnie Tong, Sophie Yin, Mica Lau, Francine Gilbert and Alexandra Sevestianova for bringing balance to my life outside of my research. I treasure our times together and hope that we can share more moments in the years to come.

Dedication

This work is not dedicated to us but to our children. It is the hope that clean and sustainable energy such as wind can help us to leave a better world for them.

Table of Contents

List of Tables

List of Figures

Chapter 1

Introduction

Wind energy has enjoyed a remarkable growth in the past decades. In Canada, total installed generation capacity of utility scale wind turbines has increased from 137 MW in 2000 to 11,205 MW in December of 2015 [1]; producing 1.5 % of the national electrical output between December 2014 to December 2015 [2]. The same trend is seen around the world; with global installed capacity increased from 17.4 GW in 2000 to 486.7 GW at the end of 2016 [3].

On the road to their adoption, the issue of noise is a cause for much detraction. For utility scale wind turbines, broadband noise emanating from the trailing edge of the wind turbine blade is a large contributor to the overall noise emission. Minimizing their impact, regulatory bodies often sets limits to the noise level observed nearby. For example, in Ontario, wind turbine noise guidelines are determined by the Ministry of Environment. Noise assessed near neighbouring dwellings are restricted to as low as 40 dB in rural environments (known as Class 3 areas) [4]. Further details can be seen in figure 1.1.

As successive generations of utility scale wind turbines develop larger size rotors, there is a growing challenge to manage the greater noise generated from their larger designs. This is an issue of much interest in research.

The issue of noise, however, is not limited to utility scale applications. Small scale wind turbines, operating in laminar or transitional flow regimes, has the potential to create sharp and distinct tonal noise which can be more notable and of more annoyance to receptors than the broadband noise of larger scale wind turbines. At the same time, small scale wind turbines are seeing greater adoption in many stand alone projects and niche applications. They can also be found in urban environments, roof tops and areas that are more densely

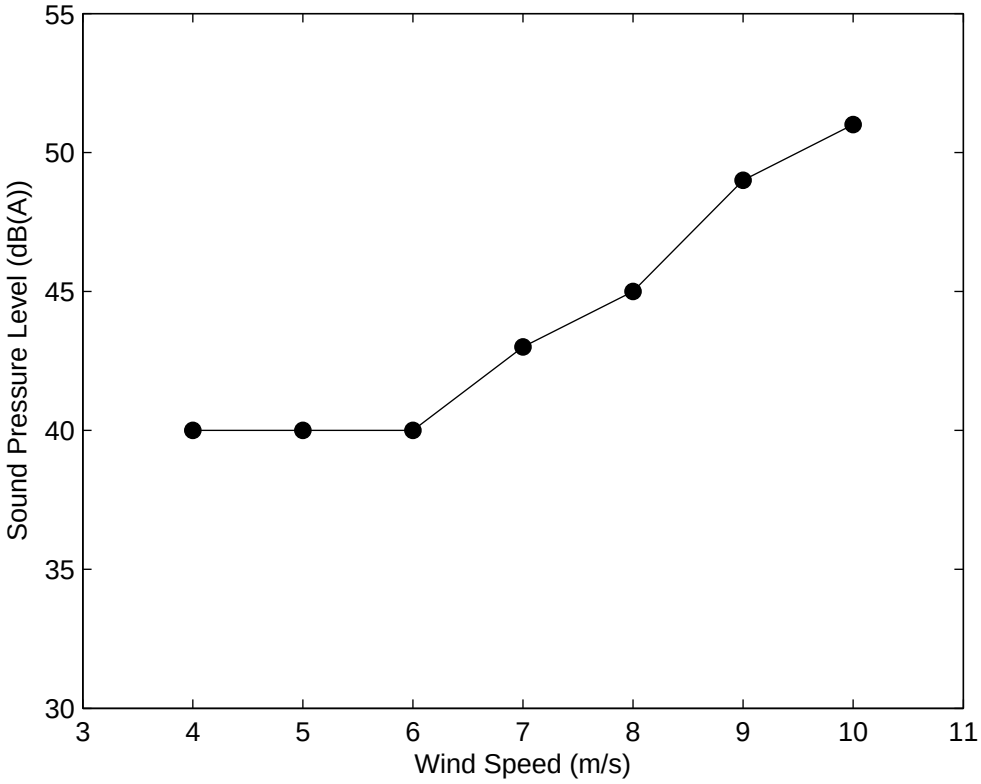

Figure 1.1: Ontario Ministry of Environment guidelines for noise emission with respect to wind speed (10 m height) for wind farm sites, as measured near dwellings in rural areas (Class 3). Adapted from [4]

populated; closer to human receptors than utility scale wind turbines. The issue of noise needs to be addressed for small scale wind turbines as well.

The broadband and tonal noise source found on wind turbines belong to a group of noise source types known as airfoil self-noise. Further information can be found in section 2.1. Understanding their characteristics, behaviour and generation mechanics is crucial to creating better wind turbine designs and developing better noise reduction strategies. Noise reduction devices, such to those reviewed by Barone [5], are promising methods to curtail noise emissions. Further insight into airfoil self-noise and the behaviour of wind turbine noise can greatly improve the effectiveness of these noise reduction devices; further aiding in their adoption.

1.1 Project Motivation and Objective

The following is a study that examines airfoil self-noise mechanisms as they are found on wind turbines during their operation. The goal of this study is to learn more about their characteristics and behaviour as an aid to developing noise reduction strategies for wind turbines. Examining the subject of noise reduction further, the effects of a type of noise reduction device known as trailing edge saw-tooth serrations are examined as a secondary goal. Further details on the saw-tooth serrations can be found in section 2.4 of this thesis.

The current study is divided into two parts:

In the first part, the behaviour of airfoil self-noise is studied under a controlled environment. This is accomplished with the closed circuit wind tunnel of the Wind Energy Group. To examine airfoil self-noise under conditions more reflective to those experienced by wind turbines during their operation, acoustic measurements are also collected under dynamic stall conditions created by pitching oscillation. The dynamic stall condition used in this study was previously studied by Gharali [6]. For comparison, acoustic measurements are also collected for an airfoil specimen under classical conditions at different static angles of attack.

To examine the effects of trailing edge saw-tooth serrations, acoustic measurements are collected for the airfoil specimen with different extension strips attached to it at the trailing edge. As part of a larger study, Particle Image Velocimetry (PIV) measurements are collected for the same experimental conditions [7]. The findings in this portion of the experiments are relevant to the tonal noise generation mechanism found in small scale wind turbines.

In the second part, airfoil self-noise are examined under outdoor field conditions at the Wind Energy Group outdoor wind turbine test site. Acoustic measurements are collected using equipment conforming to the International Electrotechnical Commission (IEC) standard for wind turbine noise measurements [8]. As well, the feasibility of the test site for future acoustic experiments is assessed. The results of this portion are relevant to larger scale wind turbines experiencing broadband noise emission.

1.2 Thesis Organization

Following this chapter, in Chapter 2, a review of the technical background relevant to this study is presented. For a reader unfamiliar with aero-acoustics and aerodynamics concepts, this chapter offers a brief explanation of airfoil noise generation mechanisms and

wind turbine noise sources. A literature review of past studies on trailing edge saw-tooth serrations can also be found in this chapter.

Chapter 3 documents the experimental design portion of this study. Details on equipment specifications,the test specimen used in the experiment, experimental procedures, analysis techniques as well as any experimental considerations are discussed.

Chapter 4 shows the results of acoustic experiments conducted under controlled conditions in the closed circuit wind tunnel under static and dynamic conditions.

Chapter 5 presents the results, analysis and discussion of experiments conducted at the UW outdoor wind turbine test site for the 10m diameter passive yaw turbine.

Finally, a summary of all findings and suggestions for future studies can be found in Chapter 6.

Chapter 2

Background

This following chapter provides a background on key concepts pertaining to this current study. It is organized into four sections.

- The first section is a discussion on airfoil self-noise. It provides a background on the different types of airfoil self-noise generation mechanisms associated with wind turbine blades.
- The second section, on wind turbine noise, provides details on noise associated with wind turbines, their characterization and assessment.
- The third section is a discussion with regards to noise associated with dynamic conditions such as those experienced by wind turbines.
- The final section of this chapter provides a review of past studies regarding trailing edge saw-tooth serrations.

2.1 Airfoil Self-Noise

Airfoil self-noise refers to the noise caused by an airfoil shape from being immersed in a steady and uniform subsonic flow. Brooks et al. [9] described five self-noise generation mechanisms: laminar boundary layer "vortex shedding"(LBL-VS) noise, turbulent boundary layer trailing edge (TBL-TE) noise, blunt trailing edge noise, separation-stall noise, and tip vortex noise. These mechanisms can be seen in figure 2.1.

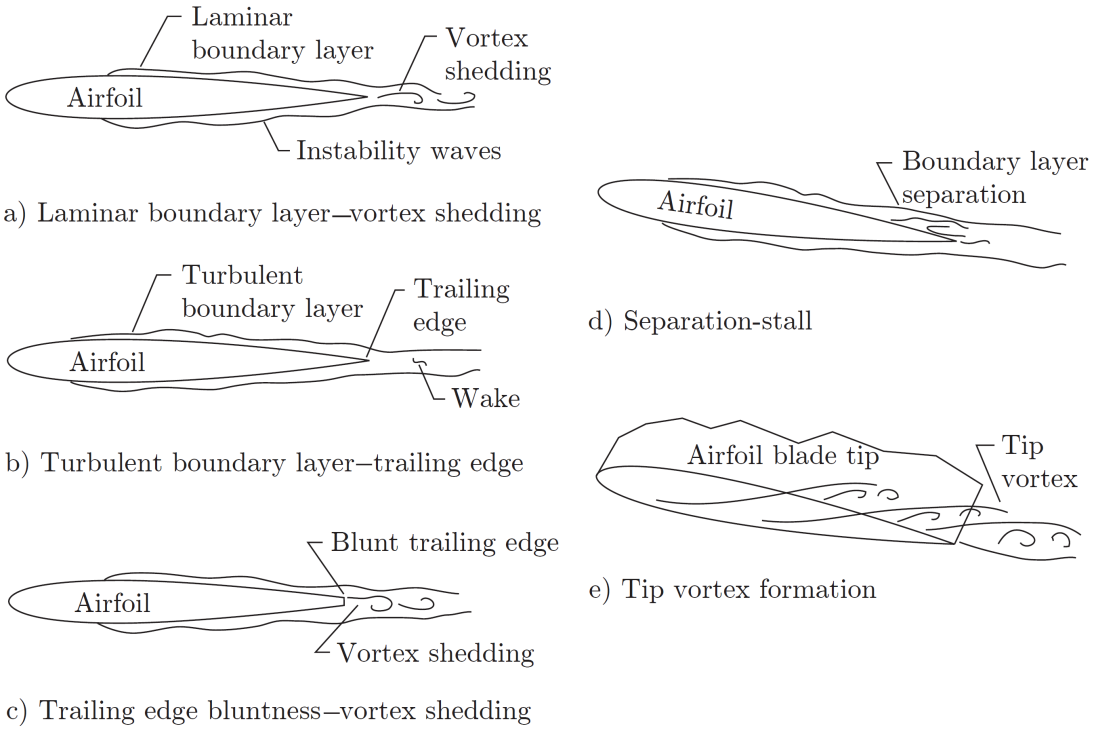

Figure 2.1: Five different airfoil self-noise generation mechanisms as described in Brooks et al. [9], Adapted from Brooks et al. by McPhee [10].

Depending on the wind turbine blade chord length/rotor diameter, blade geometry and the aerodynamic design, all of the mechanisms discussed by Brooks et al. [9] can be found on wind turbines. As the first portion of this study deals extensively with the LBL-VS noise mechanism, it will be discussed in detail. The remaining noise mechanisms, namely TBL-TE noise, blunt trailing edge noise, separation-stall noise and tip vortex noise, are relevent to wind turbines and the current study. However, they are not dealt with in the same depth as the LBL-VS noise and as such, they will only be briefly reviewed.

2.1.1 Laminar Boundary Layer Vortex Shedding Noise

LBL-VS noise refers to the noise created by the airfoil under Reynolds number conditions where laminar flow can be found in the boundary layers of the airfoil. This is depicted in figure 2.1a. As it relates to wind turbines, this type of noise can be found in small scale

wind turbines where the chord Reynolds number Re_c is between 10^4 to 10^6. For example, the Sun Force wind turbine, which has been used previously in some experiments conducted by the Wind Energy Group, has a measured rotor diameter of 1.2 m with typical rotational speed of 400 rpm. With a chord length of 0.05 m, the estimated Re_c is 6.0×10^4 at 75% of the blade.

In terms of characterization, this noise source is noted by its distinct narrowband frequency (tonal) components. Broadband noise components can also be present, although it is not the defining characteristic. An overview of the literature surveyed would find that there are a broad range of aspects that were examined with this type of noise generation mechanism. The study of the "ladder effect"and noise generation mechanism are common. The literature survey would also find some disagreements between the various results in different studies. In comparison with the results of the current study, not all features that have been observed from the different studies are found. Nevertheless, the different findings from previous studies will be summarized as it would be relevant in evaluating the results.

It should be noted that with the disagreements, a number of theories exist regarding the mechanics of the noise generation. While these theories can differ, the models proposed generally involve laminar instability and some or all of the following elements:

- The interaction with the trailing edge
- The formation of certain fluid structures (i.e. coherent vortices, laminar separation bubbles, separated shear layers, etc.)
- The interaction with the above fluid structures
- A feedback mechanism due to acoustic waves or hydrodynamic instability waves. Waves at downstream/trailing edge propagate upstream and reinforce the instability at its source

The various models proposed by different studies are summarized in figure 2.2. They will be discussed in greater detail.

2.1.1.1 Early Research

Aeroacoustic research in LBL-VS noise gained prominence in the 1970s. A noted study from that time conducted by Paterson et al. [11] investigated this phenomenon and attributing the cause of noise to vortex shedding. The Paterson model is depicted in figure 2.2a.

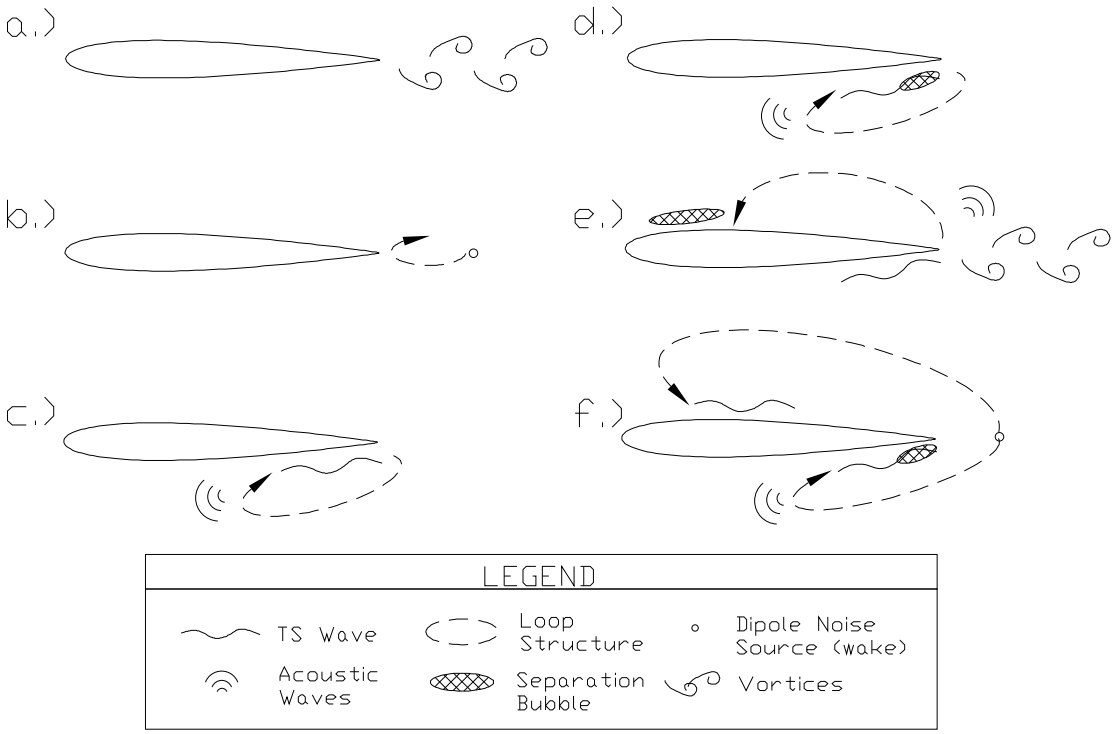

Figure 2.2: LBL-VS noise generation mechanism models proposed from various studies. a.) Paterson et al. [11] b.) Tam [12] c.) Fink [13] d.) University of Bristol studies [14] e.) Akishita [15] f.) Desquesnes et al. [16]

Their experiments showed several behaviours that have been commonly observed in subsequent studies. The acoustic spectra observed consist of multiple tones at various frequencies. For the tone with the greatest sound pressure level (referred to as the main tone), the frequency (f) increased with freestream velocity (U_∞) at a rate of $f \cong U_\infty^{0.8}$ over a small change in U_∞. Given sufficent change in U_∞, the tones "jumped"or followed another 0.8th power relation. This is referred to, in Paterson et al. and subsequent literature, as the "ladder effect". Over a larger range of U_∞, the frequency of the main tone was found to increase at a rate of $f \cong U_\infty^{1.5}$.

Paterson et al. developed an empirical fitted model based on bluff body vortex shedding, relating f and U_∞ by a tuned constant value, as seen in equation 2.1:

$$f = \frac{K_p U_\infty^{1.5}}{\sqrt{c\nu}} \tag{2.1}$$

where K_p is a dimensionless constant tuned by Paterson et al. to empirically fit experimental data for NACA 0012 ($K_p = 0.011$), c is the chord length, and ν is the kinematic viscosity. K_p is derived from assumption that bluff body vortex shedding is at a constant Strouhal number/normalized frequency of 0.2. The Strouhal number (St) is defined in eq. 2.2:

$$St = \frac{fl}{U} \tag{2.2}$$

where l and U represents the length and velocity variable used to normalized the frequency component respectively. Paterson et al. [11] used two times the flatplate laminar boundary layer thickness as l and U_∞ as U.

The Paterson study measured the sound pressure levels of the tonal noise at different velocities and angles of attack. For a given positive angle of attack, the authors noted the sound pressure level of the tonal noise to increase, plateau and then decrease with increasing velocity; corresponding the appearance and disappearance of the tonal noise with the appearance and disappearance of the laminar boundary layer conditions with the changing velocity [11]. Although the study did not discuss the changes with respect to the angle of attack, the sound pressure level of the tonal noise is seen to behave similarly with changing angles of attack.

Later studies by Tam [12] and Fink [13] focused on the nature of the noise generation mechanism. Both of these studies developed their own models involving feedback mechanisms to explain discrepancies or limitations from the Paterson model (i.e. They do not believe vortices are the true source of the tonal noise, the Paterson model did not account for the "ladder effect"). Tam suggested a model which involves acoustic waves in the wake feeding back to excite the instability source at the trailing edge [12]. The Tam model is shown in figure 2.2b. Fink theorized that the feedback loop mechanism is located in the airfoil boundary layer. Acoustic waves created from laminar instabilities/ Tollmien-Schlichting (TS) waves flowing past the trailing edge are proposed to excite the instability source upstream [13]. The Fink model is shown in figure 2.2c.

Arbey and Bataille [17] conducted a study to evaluate the findings up to that point, which included the conclusions of Paterson et al. [11], Tam [12] and Fink [13]. Using a higher resolution frequency analyzer, the frequency spectra of noise from the airfoil were shown to contain a broadband rise in noise with discrete tones at equal spacing (side peaks) imposed on the broadband increase. This is depicted in figure 2.3.

Arbey and Bataille concluded that tonal noise was formed by a feedback mechanism of acoustic waves forcing TS Waves at the source of creation. Different tones are generated

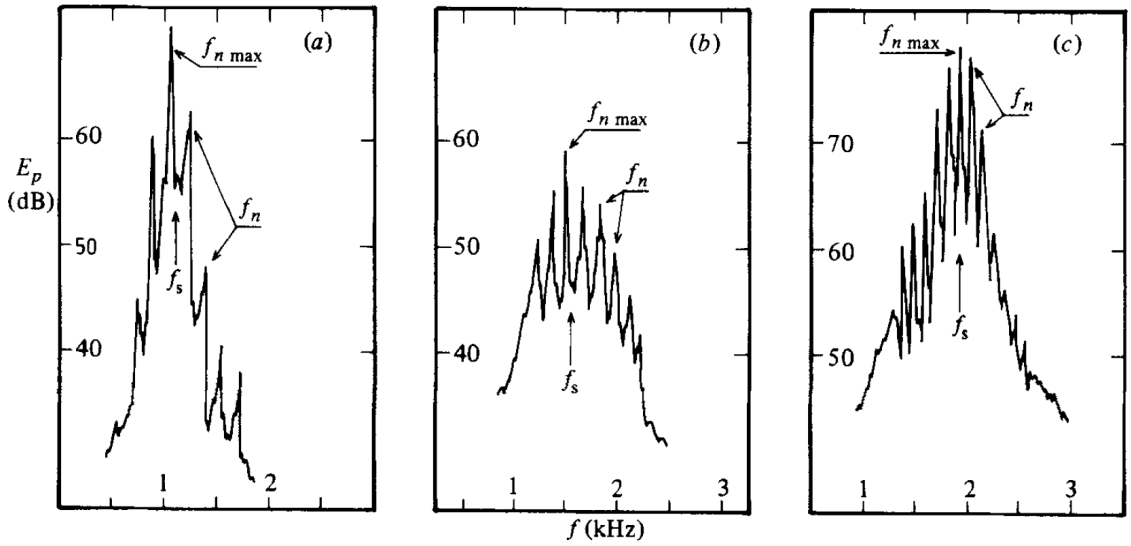

Figure 2.3: Sound pressure level vs. frequency plots from the Arbey and Bataille study. Note the figures feature the main tone ($f_{n\,max}$) and equispaced secondary (side peak) tones (f_n) a.) NACA 0012.8 at $U_\infty = 20.2m/s$ b.) NACA 0012.16 at $U_\infty = 35m/s$ c.) NACA 0012.16 at $U_\infty = 35m/s$ Figure originally presented in Arbey and Bataille [17].

when acoustic waves are in phase with the TS waves. Tone generation is sensitive to the location where the boundary layer velocity is at a maximum and the point of instability begins. Frequency spacing is defined by equation 2.3:

$$f_n = (i + \frac{1}{2})\frac{K_a}{P_m}U_\infty^{0.85} \tag{2.3}$$

where f_n is spacing of the secondary tone, K_a is an empirical constant, i is an integer value representing different discrete tones found, and P_m is location of maximum velocity at the boundary layer. K_a has a value of 0.89 in the units of $m^{1.85}/s^{0.85}$.

As for the broadband noise, Arbey and Bataille concluded the mechanism described by Fink [13], where acoustics waves are formed from TS waves convecting past the trailing edge (diffraction), is responsible for the broadband noise generation. The mechanism functions like the TBL-BL noise generation mechanism (reviewed in section 2.1.2), except instability/transitional boundary layer flow replacing the turbulent boundary layer flow in the model. However, the two different boundary layer flows are interchangeable in the model as they both produce comparable wall pressure fluctuations required for the noise

generation mechanism. Arbey and Bataille also found the broadband noise measured in the farfield of the airfoil matches the wall pressure fluctuations observed near the surface of an airfoil at the trailing edge [17].

2.1.1.2 Semi-Empirical Prediction Model

In 1989, Brooks et al. [9] conducted an experimental study that characterized the different types of airfoil self-noise. LBL-VS noise was included as one of the noise types studied. Their prediction models (known as the BPM models) are semi-empirically scaled and give a prediction of the sound pressure level in a 1/3 octave spectum. As the BPM model for LBL-VS noise is used in the current study, it is reviewed in equation 2.4, with 1/3 octave sound pressure levels denoted as L_{LBL-VS}:

$$L_{LBL-VS} = 10log\left(\frac{\delta_p M^5 S \bar{D}}{d^2}\right) + G_1\left(\frac{St'}{St'_{peak}}\right) + G_2\left(\frac{Re_c}{(Re_c)_0}\right) + G_3\left(\alpha_*\right) \tag{2.4}$$

The first term, $10log\left(\frac{\delta_p M^5 S \bar{D}}{d^2}\right)$, is scaling based on known theoretical and analytical relationships. It should be noted that noise is scaled with δ_p, the boundary layer thickness on the pressure side. M is the Mach number of the freestream flow. S is the span of the airfoil specimen. $\bar{D}$ is a value that accounts for the directivity of the noise. d is the direct distance between source and receiver.

The second term, $G_1\left(\frac{St'}{St'_{peak}}\right)$, determines the shape of the spectral curve, based on the empirical relationship derived from Brooks et al.'s experiments. The relationship is a function of the ratio between the Strouhal number (normalized frequency with boundary layer thickness of pressure side δ_p and U_∞) and its peak value.

The third term, $G_2\left(\frac{Re_c}{(Re_c)_0}\right)$ determines the peak scale level, and is a function of Reynolds number and angle of attack.

The fourth term, $G_3\left(\alpha_*\right)$ augments the shape of the spectral curved based on the angle of attack of the airfoil in question.

Further details of the semi-empirical model and function terms can be found in Brooks et al. [9].

2.1.1.3 Involvement of Boundary Layer Separation and Vortex Structures

Following the Arbey and Bataille study, more extensive investigations on the noise generation mechanism were conducted in the 1990s at the University of Bristol [14] [18] [19] [20]. Lowson et al. [14] examined the NACA 0012 and NACA 23015 airfoils. They proposed the involvement of a separated flow in the noise model which is depicted in figure 2.2d. This model is similar to that of Fink and Arbey and Bataille as it involves TS waves and a feedback mechanism. In this model, it was proposed that the TS waves were strongly amplified by the shear layer in the laminar separation. The strength of the tone depends on when laminar-turbulent transition occurs as the amplification process is interrupted by this process.

Lowson et al. [14] also outlined a region of conditions (with respect to Re_c and angle of attack) where tonal noise is expected to occur for the NACA 0012 airfoil. Later in Probsting et al. [21], a figure was compiled showing this region and summarizing results of several studies examining different points in and outside of the region. This is shown in figure 2.4.

Further studies of Nash and Lowson [18] and Nash et al. [19] explores this model with Laser Doppler Anemometry (LDA) measurements. In Nash and Lowson [18], the authors found that flow near the trailing edge of the pressure side has separated and that coherent vortex structures had formed in the region. The frequency of the velocity fluctuation matched the acoustic tone measured, and correlation of LDA velocity data with microphone data showed direct relations with the flow at the trailing edge (as opposed to the flow before the separation); further supporting their proposed model.

In Nash et al. [19], the authors looked at two cases with a 0.3m chord NACA 0012 airfoil in greater detail; a case with tonal noise at $-4°$ angle of attack ($U_\infty = 29.7$ m/s) and a case without tonal noise at $-3°$ angle of attack ($U_\infty = 8.1$ m/s). Like Nash and Lowson [18], the tonal noise case was again found to have a separated region with a vortex rollup upstream of the trailing edge from the shear layer. The no tone case also contain a separated region. However, unlike the tonal noise case, there were lower r.m.s velocity fluctuation values in the region and a lack of frequency components that were associated with tones or vortex shedding. From the comparison of the two cases, they conclude three main conditions must be present for tonal noise to happen:

1. Amplification of the TS instability mechanism was facilitated by a separated region or inflected flow region near the trailing edge.

2. Periodic structures must be found at the trailing edge and so the separated or inflected flow region must be found nearby

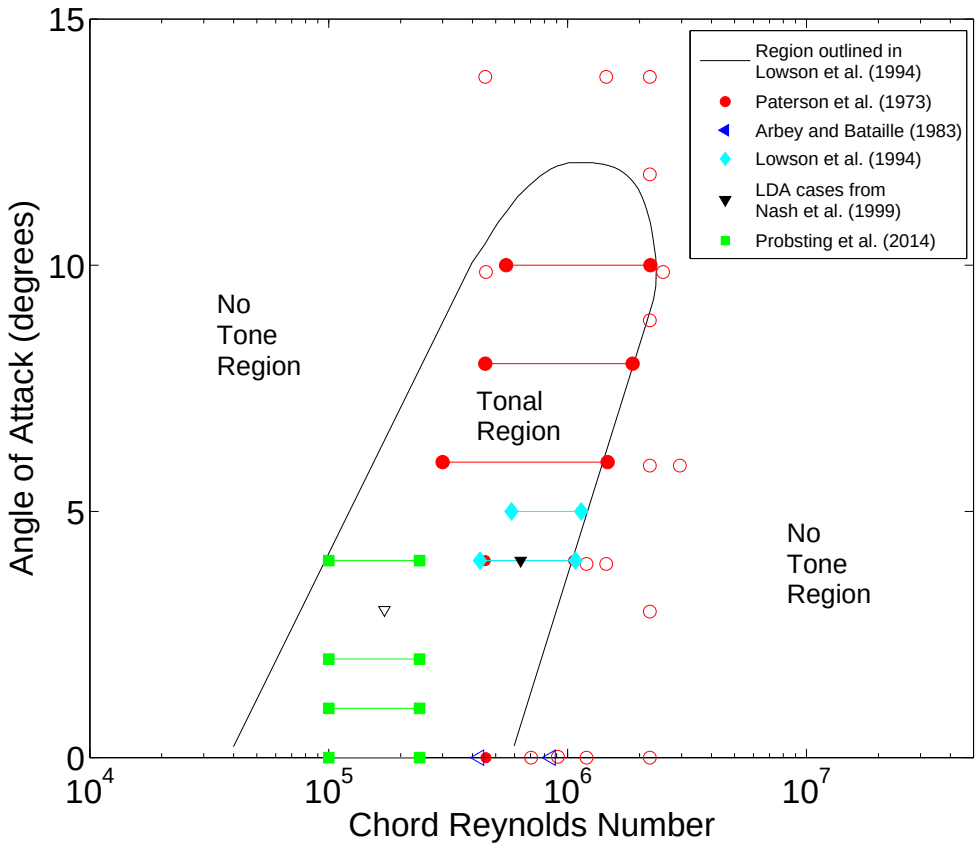

Figure 2.4: Region of Reynolds number and angle of attack where tonal noise can be found for a NACA 0012 Airfoil. Region outlined by Lowson et al. [14], compared with results from: Paterson et al. [11], Arbey and Bataille [17], Lowson et al. [14], Nash et al. [19], Probsting et al. [21]. Filled markers indicate tonal noise was observed while hollow markers indicate no tones were observed. Adapted from Probsting et al. [21]

3. Random or non-coherent turbulence from a strong adverse pressure gradient would affect the noise generation mechanism.

Flow visualization of the airfoil while generating tones showed vortex shedding at the same frequency as the tonal noise. Their studies also examined the laminar instability relationship using the Orr-Sommerfeld equation and Falkner-Skan boundary layer velocity

profiles [19] [20]. The amplification of the TS instability was concluded to be found in the separated region close to the trailing edge, with a frequency matching that of tonal noise. It was noted that the frequency of amplified instability is not just found at the trailing edge location, but throughout the separated region, which begins further upstream than the trailing edge.

Other studies have looked at the contribution of vortices to the LBL-VS noise in more detail. Nakano et al. [22] examined a NACA 0018 airfoil and found tonal noise generated at a small angle of attack; with a vortex shedding frequency matching the tonal frequency (similar to findings of other studies [11] [19]). A separated shear layer was found on the pressure side like the results of Lowson et al. [14]. The authors concluded the vortical structure formed on the pressure side of the airfoil was generating the tonal noise as the vortices convect past the trailing edge; believing that some of the kinetic energy from the vortices would be converted into acoustic energy.

Takagi et al. [23] examined the same setup but under the influence of a cylinder wake. Increased turbulence of the cylinder wake was found to suppress the tonal noise generation mechanism by promoting transition and an attached boundary layer on the surface of the airfoil.

2.1.1.4 Tone Frequency and Angle of Attack

Nakano et al. [22] [24] also examined the acoustic spectra at various angles of attack. The results from [22] are shown in figure 2.5. Tonal noise was seen at 3° and 6°. For these angles, there was only minor variations in frequency of tonal noise as the angle of attack increases. In [24], the authors calculated the Strouhal number of the tone at 2 kHz. The results are comparable to Paterson et al. [11]. The authors believed it is more appropriate to scaled the Strouhal number with the mean boundary layer thickness of the airfoil at the trailing edge. The mean boundary layer thickness of the airfoil at the trailing edge was found to not vary significantly from 0° to 6° degrees. Hence, this may explain why the tone frequency did not vary significantly.

Chong and Joseph [25] examined a NACA-0012 airfoil profile at Re_c of 1.5×10^5. The tonal noise was observed to be at 570 Hz at 0°, 575 Hz at 2°, and not present at 5°. Tonal noise frequency lined up well with the predicted peak in amplification factor estimated from the Orr-Sommerfeld equation. Under turbulent boundary layer flow conditions, either by tripping or by the boundary layer naturally transitioning, the tonal noises were not found. While tonal noise was observed in their study, broadband noises were not resolved. The

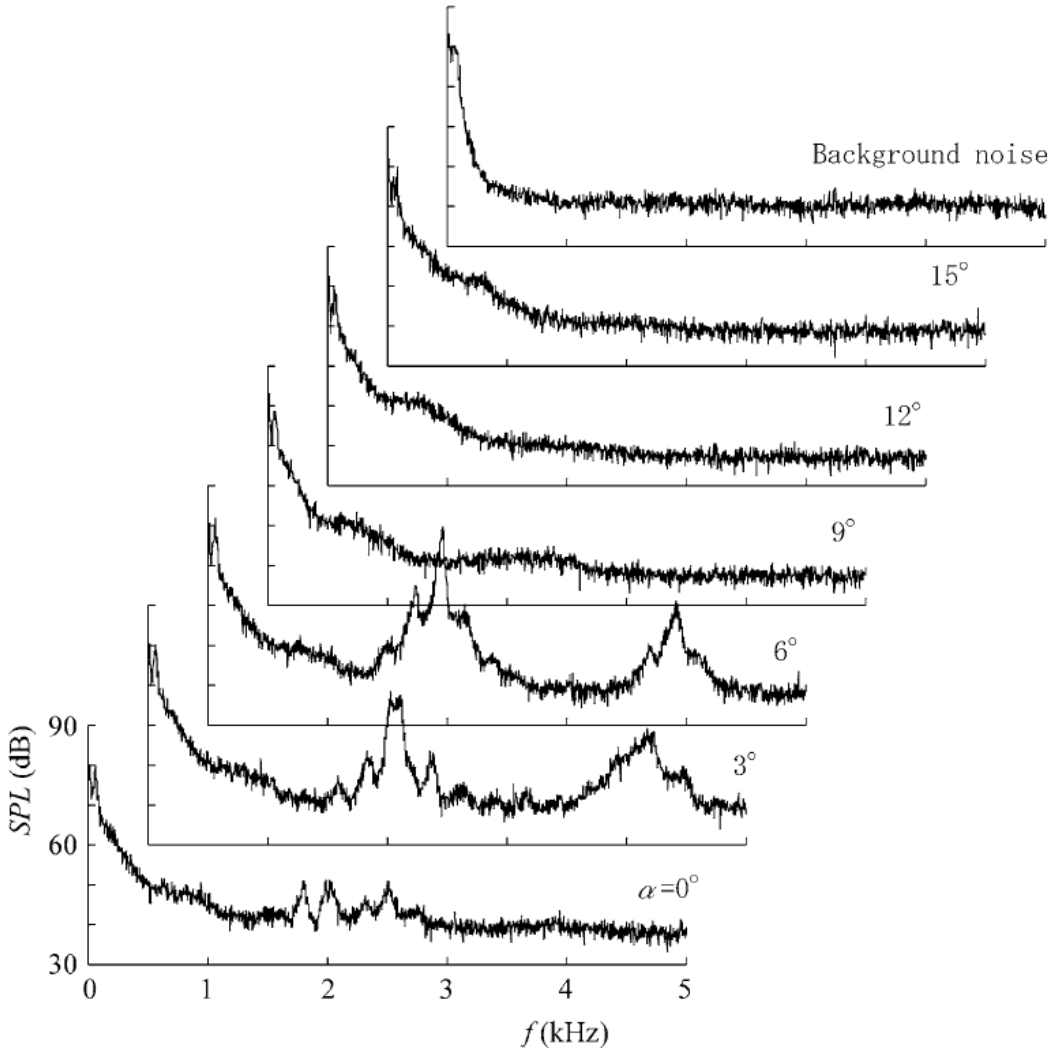

Figure 2.5: Narrowband acoustic spectra of a NACA 0018 airfoil at $Re_c = 1.6 \times 10^5$ for various angles of attack from the Nakano studies. The main tones found at 3° and 6° are consistently located at the sound frequency of 2.1-2.2 kHz. Figure originally presented in Nakano et al. [22]

authors believed the high background noise of the wind tunnel had masked the broadband noise.

Arcondoulis et al. [26] also conducted airfoil noise measurements at various angles of

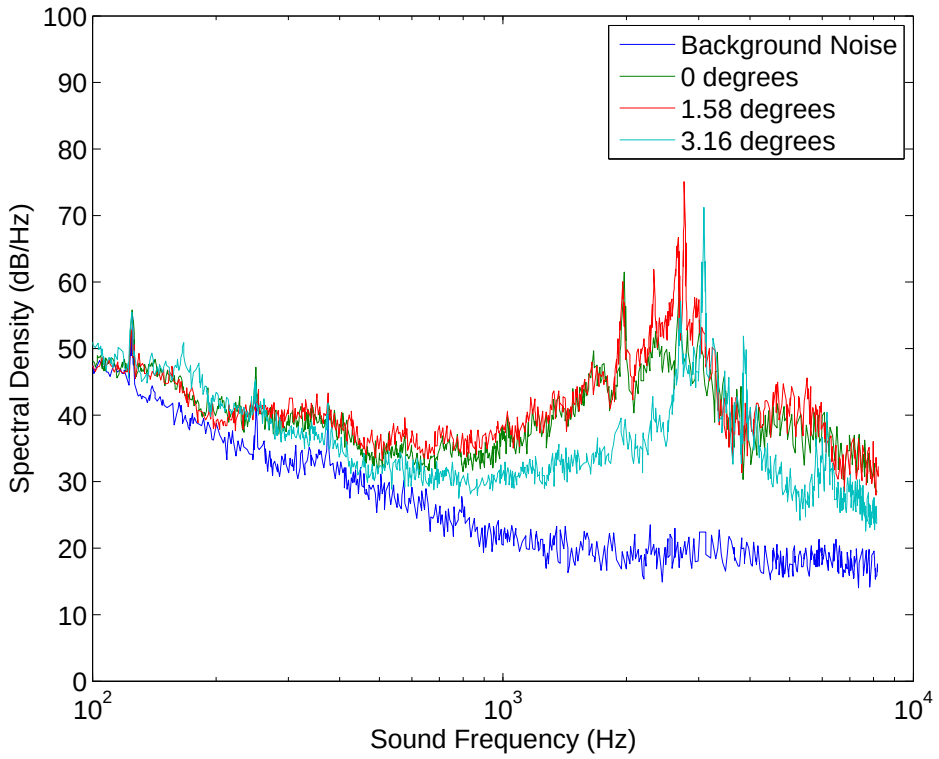

Figure 2.6: Narrowband acoustic spectra of a NACA 0012 airfoil at $Re_c = 1.5 \times 10^5$ for effective angles of attack of 0°, 1.58° and 3.16° from the Arcondoulis study. Figure digitized from Arcondoulis et al. [26]

attack and Reynolds number. With regards to the effects of angle of attack on tonal noise at equal flow conditions, the authors presented acoustic spectra at $Re_c = 1.5 \times 10^5$ for effective angle of attack of 0°, 1.58°, and 3.16°. These are shown in figure 2.6. The authors did not discuss the effects of angle of attack with frequency of tonal noise under constant Reynolds number. However, examining figure 2.6 between 0° with 1.58°, it appears the tones did not have a shift in frequency. Between 1.58° and 3.16°, the tones are only seen to have shifted to a slightly higher frequency.

With numerical studies, Ikeda et al. [27] examined NACA airfoils of 2% to 8% thickness at 20% to 80% chord position with Direct Numerical Simulations (DNS) at Re_c of 1.0×10^4 at Mach number of 0.2. The vortex shedding frequencies at different angle of attack, normalized by airfoil chord and U_∞, were noted for all cases and shown in figure 2.7.

As evident from the figures, the variation of the camber thickness and location of maximum camber had an impact on the vortex shedding behaviour. The vortex shedding frequencies is seen to decrease abruptly after some angle of attack for many case. The authors examined this behaviour by looking at the NACA 4206 airfoil case more closely. At an angle of attack of less than or equal to 4°, the vortex shedding is seen to be primarily induced by wake instability (close to the model shown in figure 2.2b). At the angle of attack of 5° or greater, the vortex formation was clearly found on the suction side surface, and an acoustic feedback loop was part of the mechanism (close to the model shown in figure 2.2d). The shedding frequency is also seen to be relatively consistent before and after the abrupt change.

2.1.1.5 Involvement of the Suction Side

From the studies reviewed so far, the majority of the results have found that the source of the LBL-VS noise to originate from the pressure side of the airfoil. However, some studies have noted or investigated the involvement of mechanisms causing tonal noise originating from the suction side.

Akishita [15] studied a NACA 0015 airfoil at Re_c of 8.0×10^4 to 3.2×10^5. In his model, shown in figure 2.2e, Akishita suggested the TS waves from the pressure side to be the source of the initial acoustic wave generated in the wake. The feedback loop on the suction side then amplifying the acoustic wave at certain frequencies to into the prominent discrete tones.

In tripping the boundary layer into transition on the surface of the airfoil, Akishita found the tonal noise to disappear when separately tripping the suction side and pressure side. Trips on the pressure side had varying affects on the tonal noise. However, on the suction side, tonal noise was unaffected unless the trip was placed near the trailing edge. The author noted that this conflicts with his proposed model as such a trip would eliminate the key structure (the laminar separation bubble) needed for the feedback loop.

Desquesnes et al. [16] conducted a DNS simulation to investigated the involvement of the suction side in the noise generation mechanism. Their findings suggested a model where the suction side was involved in a secondary feedback loop that contributes to the generation of the equi-spaced discrete tones/side peaks. The Desquenes model is depicted in figure 2.2f. The pressure side is responsible for the main tone produced in the acoustic spectra. The mechanics of the mechanism on the pressure side is the same as the Lowson model in figure 2.2d. The acoustic waves generated in the wake then forms the secondary

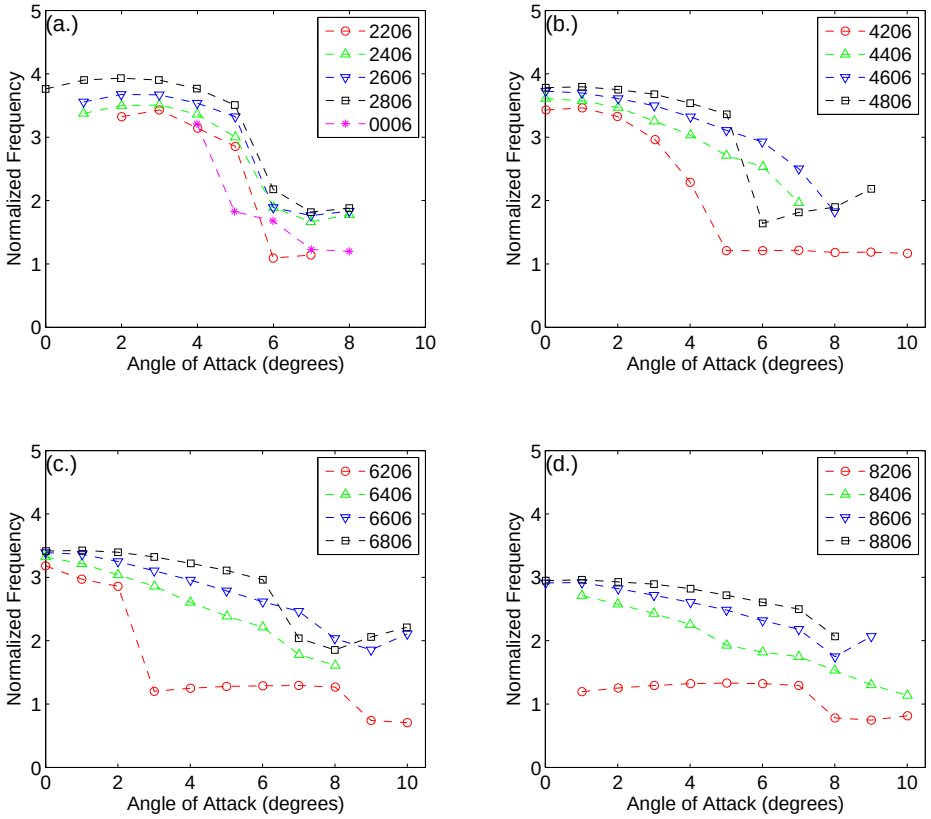

Figure 2.7: Normalized frequency of vortex shedding from the Ikeda study for various NACA cambered airfoil families at $Re_c = 1.0 \times 10^4$. Frequency normalized by airfoil chord and U_∞ a.) NACA 2X06 family with NACA 0006 airfoil b.) NACA 4x06 family c.) NACA 6x06 family d.) NACA 8x06 family. Figures digitized from Ikeda et al. [27]

feedback loop on the suction side which is responsible for the equi-spaced discrete tones/side peaks.

However, experiments by Probsting et al. [21] and Plogmann et al. [28] found discrete tones/side peaks to exist in absent of suction side contributions. Further discussion regarding to the equi-spaced discrete tone/side peak phenomenon is found in section 2.1.1.6.

The studies of Akishita [15] and Desneques et al. [16] have suggested a suction side mechanism to be a part or secondary contributor to the noise source. Other studies have

found the suction side structures to be the primary cause for LBL-VS noise.

Probsting and Scarano [29], who examined a NACA-0012 airfoil at Reynolds number similar to this study, had found that the noise came from the suction side of the airfoil. The authors provided a reasonable explanation for why the noise was observed on the suction side instead of the pressure side. At the low Reynolds number regime which covers the current study and the study of Probsting and Scarano, it is typical to find the phenomenon of shear layer separation and vortex roll up occuring on the suction side of the airfoil. A pressure side boundary layer would experience very late transition (if at all) and therefore not likely to see the same phenomenon. It should be noted that with high Reynolds number, the conditions are more favourable for the pressure side boundary layer to separate and roll up in to a vortex while the suction side begins to transition into turbulence. Hence, at higher Reynolds number, the mechanism on the suction side disappears and is found on the pressure side; leading to the observations of the various studies reviewed.

Reviewed previously, the study of Ikeda et al. [27] was conducted at a Reynolds number range similar to this study. Vortex shedding/roll up phenomenon that were normally seen on the pressure side with other acoustic studies were found on suction side for their studies as well.

2.1.1.6 Equi-spaced Discrete Tone/Side Peaks

As mentioned previously, Desquesnes et al. [16] investigated into the occurance of equi-spaced discrete tones/ side peaks, in the acoustic spectra from their DNS simulations. The authors suggested the cause to be related to the amplitude modulation of the main tone. The phase difference of the TS wave/vortices shedding between the suction and pressure side interacts constructively and distructively; leading to periodic amplitude modulation of the acoustic wave at the main tone frequency. The secondary feedback loop on the suction side is responsible for the phase difference on the suction side.

Probsting et al. [21] conducted wavelet analysis on their acoustic measurements to examine both frequency and time domain of the signal (Desquenes et al. [16] examined their signal with respect to frequency and time domain as well). The results were found to be similar results to that of Desquesnes et al. [16] as both studies found amplitude modulated acoustic signal. However, when Probsting et al. examined a case with a boundary layer trip attached to the suction side, the equi-spaced discrete tones/side peaks still remains.

As such, the equi-spaced discrete tones/side peaks is found to be caused by amplitude modulated acoustic signal. The cause of the modulation is unknown and requires further

study and is not necessarily caused by suction/pressure side interaction as Desquenes et al. [16] suggests.

2.1.1.7 Summary

In summary, LBL-VS noise was first thought to be caused by vortices shed from the airfoil [11]. Later studies [12] [13] [17] suggest the involvement of a feedback mechanism; where acoustic waves created downstream of the airfoil reinforces the instability mechanisms created upstream. The behaviour, physical mechanism and the role of vortices is further explored [14] [18] [19] [20] [22] [23].

In review of the studies, the effect of angle of attack with respect to the behaviour of the tone is not seen to be discussed extensively. Presented results from various studies [24] [25] [26] [27] show minimal changes to the frequency with respect to the angle of attack. The involvement of suction side is also discussed in some literature [15] [16] [29] [30]; noting that suction side can be involved for low Reynolds number flow. The appearance of side peaks are also examined in literature [16] [21]. It was found to be related to amplitude modulation of the main tone. However, the exact cause of the modulation is still in question [21].

2.1.2 Turbulent Boundary Layer Trailing Edge Noise

Turbulent boundary layer trailing edge noise, as the name implies, is noise generated by the airfoil when a turbulent boundary layer flows past the trailing edge. It is depicted in figure 2.1b. The cause of TBL-TE noise can be described as a diffraction process of turbulent eddy waves in the boundary layer as they convect past the trailing edge [31]. The pressure fluctuations of the eddies, which can be considered as acoustic waves, encounter an abrupt change in acoustic impedance [32] (due to the discontinuity of the trailing edge) and scatter as a result.

In the context of wind turbines, this type of noise is associated with large scale wind turbines, where the blade Re_c typically exceeds 10^6. Although it should be noted that TBL-TE noise can be found at Re_c lower than 10^6, as long as the boundary layer at the trailing edge is turbulent. As such, it is seen in small scale turbines as well depending on flow conditions. The noise is characterised by a broadband increase in noise over mid range acoustic frequencies [33]. Unlike LBL-VS noise, tonal components are not associated with this type of noise.

In terms of prediction models, a semi-empirical model similar to the one presented previously in section 2.1.1.2 was also developed by Brooks et al. [9] for TBL-TE noise. It is not reviewed in this section. Further details can be found in Brooks et al. [9].

The analytical theories of this type of noise also exist. They are well reviewed and studied by Howe [31], with noted contributions to the area from the works by Powell [34], Ffowcs-Williams and Hall [35], and Amiet [36]. The mathematical treatment is beyond the scope of the current study and as such it is not be extensively reviewed.

In brief, it can be said that the noise source has been considered by looking at the near field pressure fluctuations in order to determine the far field acoustic spectrum [36]. In Ffowcs-Williams and Hall [35], the rms pressure fluctuation in the farfield (sound pressure) is found for flows over a semi-infinite flat plate at low Mach number. The relationship is scaled with geometric and fluid flow parameters as shown in equation 2.5:

$$\langle p^2 \rangle = \rho_0^2 v'^2 \frac{U_c^3}{c_0} \left(\frac{S\mathcal{L}}{d^2} \right) \bar{D} \tag{2.5}$$

where $\langle p^2 \rangle$ is the rms pressure fluctuation (sound pressure) as seen in the observer's position, v' is the velocity fluctuation of flow past the trailing edge, U_c is the convection velocity of the turbulence past the trailing edge, ρ_0 is the density of the fluid (air in this case), S is the spanwise width of the airfoil under examination, d is the distance between the airfoil and the receiver, $\mathcal{L}$ is the turbulence length scale of convected turbulence, $\bar{D}$ is the directivity factor, same as that described for the LBL-VS noise model and c_0 is the speed of sound.

As the relationship from equation 2.5 shows, noise levels can be affected by a number of parameters. Reduction can therefore be achieved by targeting and reducing some of these parameters. To begin, it should noted that the density of the fluid medium p_0 and speed of sound c_0 are fixed for a given condition and therefore are of little interest in consideration of noise reduction. The increase in distance between the noise source and receiver, d is an effective means of reducing the impact of TBL-TE noise on the receiver. In practice, this imposes a restriction in turbine placement (an example of this would be setback limits mandating minimum distance between residential locations and wind turbines) at a wind farm site and limits the site's potential. It is therefore worthwhile to look at other variables as well.

From equation 2.5, it can be shown that the sound pressure level is known to be related to the freestream velocity U_∞^5 as the convection velocity U_c and velocity fluctuations v' are on the same order as U_∞ [9]. It would appear that targeting the U_∞ to be the

most worthwhile reduction due to the higher order relationship. Some wind turbine noise reduction efforts have targeted this parameter by reducing the tip speed of the rotor. However, such reduction inevitably comes at some expense with loss in power production.

Other research efforts have been focused on reducing the turbulence length scale, $\mathcal{L}$. In this case, the turbulence convected past the trailing edge is scaled with the boundary layer thickness δ because the boundary layer is responsible for noise generation. Hence, reducing boundary layer thickness is another means to reduce noise emissions [5]. This is typically done by selecting an airfoil profile that minimizes this parameter or designing a suitable airfoil profile during the development stage of the turbine.

The spanwise length of the airfoil under examination, S, can also be targeted to reduce the sound pressure level emitted from the trailing edge. This is accomplished by reducing the effective spanwise length of the airfoil trailing edge at the section in question. Serrations, to be discussed in greater detail in section 2.4, is one such method of altering this parameter in trailing edge noise radiation.

2.1.3 Remaining Noise Generation Mechanisms

2.1.3.1 Blunt Trailing Edge Noise

Blunt trailing edge noise is the type of noise that is associated with vortex shedding in the wake from a notable separation/thickness between the two surfaces at the trailing edge. It is depicted in figure 2.1c. Ideally, the two sides of the airfoil surfaces converge to a point at the trailing edge and this type of noise would not occur. However, with practical considerations given during manfacturing of wind turbine blades, a certain degree of thickness does exist at the wind turbine blade trailing edge. It has been suggested that this is typically not of concern for wind turbine blades [33]. This type of noise is characterized as a tonal noise [37].

Blake [38] noted that blunt trailing edge vortex shedding can be evaluated by a bluntness criterion defined by two parameters: average boundary layer displacement thickness between the pressure and suction side δ^*_{avg} and trailing edge thickness t. An airfoil experiencing laminar flow (with Re_c potentially up to 2.0×10^6) can expect to experience blunt trailing edge noise if the ratio δ^*_{avg}/t is within $0.1 - 3$. For turbulent boundary layer conditions, the existence of blunt trailing edge noise was said to occur if ratio t/δ^*_{avg} is greater than $0.3 - 0.5$ [38].

Blunt trailing edge noise is modeled by Brooks et al. [9] in a manner similar to those previously discussed.

2.1.3.2 Stall-Separation Noise

Stall-separation noise refers to the noise generated by regions of detached flow on the airfoil. It is depicted in figure 2.1d. Although it is not desirable to find a separated/ stalled region on a wind turbine blade, it is nevertheless a condition experienced during its operation. This type of noise is described to be low frequency and broadband in nature (like noise from a bluff body) [9]. Brooks et al. [9] has modeled this mechanism.

2.1.3.3 Tip Vortex Noise

Tip vortex noise refers to noise generated from the three dimensional flow at a blade tip due to flow leakage from the pressure to the suction side and the resulting tip vortex flow structure. It is depicted in figure 2.1e. This type of noise is broadband in nature [37]. The tip vortex noise was modelled by Brooks et al. [9].

Migliore and Moriarty [39] employed the BPM model for tip noise in NRELs FAST code. The authors noted that this noise type was highly dependent on tip geometry. In practice, the estimates would need to be tuned for each design and therefore, accurate results are difficult to obtain.

While tip vortex noise is not expected to be the most significant noise source for a wind turbine, it can be notable under certain conditions [33]. However, this noise is not expected to be significant in the current study.

2.2 Wind Turbine Noise

In the previous section, the concept of airfoil self noise was introduced. Although airfoil self noise has noted contributions to noise generation with wind turbines, there is another noise generation mechanism to consider with wind turbines situated in outdoor environment. In this section, this other noise generation mechanism is introduced. As well, this section discusses how wind turbine noise is estimated and assessed. This section provides background to readers unfamiliar to this subject in aid of understanding the design of outdoor experiments and the discussion of experimental results, as discussed in Chapter 3 and Chapter 5 respectively.

2.2.1 Turbulent Inflow Noise

Airfoils in outdoor environments experience very different conditions from those placed in controlled wind tunnel environments. For one, the fluctuating flows or turbulence seen by an airfoil profile induce a type of noise that is different than the airfoil self-noise mechanisms already reviewed in section 2.1. This noise source that is due to the fluctuating upstream flow is called turbulent inflow noise.

Wagner et al [37] provided a description and overview of turbulent inflow noise as it relates to wind turbine applications. Upstream turbulence is characterised by the length scales of the eddies. They can be found in a variety in sizes in atmospheric flow but typically, length scale are in the order of 100 m. Noise is generated when the eddies interact with the airfoil profile. For eddies that are relatively large compared with the chord of the airfoil, interaction causes global load fluctuations and correspondingly, the wavelength of sound emitted is expected to be large (creating low frequency noise). This situation is referred to as an being "acoustically non-compact" [37].

An acoustically compact case occurs when eddies are of length scales which are relatively small compared with the airfoil. Noise is generated by fluctuations localized at the leading edge instead. The associated wavelength of sound would be small (creating high frequency noise).

Given the typical wind turbine blade chord length and the length scale of the turbulence encountered, the likely turbulent inflow noise for wind turbines belongs to the former case. Observed noise is broadband in nature and typically dominates the lower frequencies of the acoustic spectrum.

Amiet [40] conducted the study of turbulent inflow noise with a flat plate and modelled the sound pressure level relationship with several flow and physical variables. For use with application to wind turbines, Lowson used Amiet's finding to prediction of wind turbine noise. The relationship is reviewed by several authors [39] [41] [42] .

Guidati [43] developed a prediction code for turbulent inflow noise which corrects the Amiet model for airfoil profiles. A computationally less intensive version was also developed with the details of its development is reviewed by Moriarty and Guidati [44].

2.2.2 Wind Turbine Noise Prediction

In the discussion of the current study, it is useful to compare the experimental results with estimates from known prediction models. There are generally two main considerations

for estimating wind turbine noise: predicting the noise at the source and estimating the propagation effects from the noise source to the receiver. In this study, only the former will be discussed. The latter is excluded as it is not expected to have significant effect in the current setup. The propagation of noise in an outdoor environment consider effects due to atmospheric attenuations, directivity, amplitude modulation, convective amplification, Doppler effect, etc. Readers who wish to know more are referred to Bowdler et al. [33], Zhu et al. [45] and Scheper et al. [46].

For estimating the noise at the source, there is a method that is well studied in literature [39] [41] [42] [45] [46] [47] [48] [49]. In this literature review and current study, it is referred to as the Acoustics of Blade Elements (ABE) method. The noise is estimated by dividing the wind turbine blade into different sections, and calculating the contribution of each section individually. The summation of the contributions from each section would give the estimate for the total noise. This method is similar to the blade element momentum (BEM) analysis method used for rotor performance assessment. In fact, it is convenient to couple this analysis technique with BEM analysis to estimate the velocity inputs need in the airfoil acoustic models. For more information on the BEM method, please see Manwell et al. [50].

To calculate the noise from a particular blade section, a two dimensional airfoil profile representative of that blade section is used. The noise is then estimated using known prediction models for airfoils. By using prediction models that estimates the noise from different types of generation mechanisms separately, the degree of their contributions relative to each other can also be assessed.

The total noise from the blade section, $(L_p)_s$, is found by summing the contributions from the different types of noise generation mechanisms. Equation 2.6 shows this summation process (for sound pressure levels) as used in the reviewed studies [39] [41] [42] [45] [46] [47] [48] [49]:

$$(L_p)_s = 10log\left(10^{\frac{(L_p)_{TBL}}{10}} + 10^{\frac{(L_p)_{LBL}}{10}} + 10^{\frac{(L_p)_{SEP}}{10}} + 10^{\frac{(L_p)_{BTE}}{10}} + 10^{\frac{(L_p)_{TIP}}{10}} + 10^{\frac{(L_p)_{TI}}{10}}\right) \quad (2.6)$$

where $(L_p)_x$ is the sound pressure level of the different types of noise in decibels. x represents the various types of airfoil noise (previously reviewed in section 2.1 and section 2.2.1): turbulent boundary layer trailing edge noise (TBL), laminar boundary layer/vortex shedding noise (LBL),blunt trailing edge (BTE), separation/stall noise (SEP), tip noise (TIP) and turbulent inflow noise (TI).

The noise for the entire rotor is then estimated by summing the noise for all individual sections. The reviewed studies [39] [41] [42] [45] [46] [47] [48] [49] typically estimates the sound pressure level of the rotor, in the manner as shown in equation 2.7:

$$(L_p)_{TOTAL} = 10log \sum_{s=1}^{n} 10^{\frac{(L_p)_s}{10}} \tag{2.7}$$

Where $(L_p)_Y$ is the sound pressure level in decibels. The subscript Y represents either the total noise or the noise contributions from the blade section s. The blade is divided into n number of sections.

Readers wishing to learn more about the extent of research and findings for the ABE method are referred to the references mentioned previously. Some of the findings are found to be relevant for the current study (and perhap relevant for a future continuing study as well):

- Nearly all reviewed studies for ABE method employed the BPM models [9] as the method of predicting airfoil self-noise (only exception is Kamruzzaman et al [48]) while the relationship of Amiet/Lowson [40] [51] is used for estimating turbulent inflow noise model. Although not used in any of the reviewed studies, the Guidati models [43] [44] would also be appropriate for use in this application.

- Moriarty and Migliore [39] examined the accuracy of the BPM model by comparing model predictions with the airfoil self-noise of two different 2D airfoils profiles (NACA 0012 and S822) in the wind tunnel. Their results can predict the general trend and spectral shape of each noise generation mechanism. In other studies [41] [43], using the program Xfoil [52] to estimate boundary layer parameters has found to further improve the accuracy of the BPM model estimates.

- The contribution of turbulent inflow noise and airfoil self-noise to the ABE method noise estimate is found to vary between the reviewed studies. While some found one type of noise to be dominant over the other type of noise [42] [49], turbulent inflow noise is generally found to be dominant at low frequencies while airfoil self-noise is found to be greater than turbulent inflow noise in mid/high frequency range (>1 kHz) [39] [41] [47]. Migliore and Moriarty [39] noted results can differ with different rotor size (with smaller rotors experience turbulent inflow noise at higher frequencies). The parameters for estimating turbulence (i.e. turbulent length scale) also have an impact in obtaining an accurate estimate; with the authors noting the limitation in their estimates.

- For the ABE method noise estimates from the various studies, different types of airfoil self-noise have been seen as the dominant noise source in the mid to high range of frequencies. In some studies, LBL-VS and blunt trailing edge noise were excluded from consideration [41] [42], citing their presence to be unlikely due to the high levels of turbulence experienced by the rotor. TBL-BL and separation/stall related noise is found to be prominent in these studies. Moriarty and Migliore [39] predicted LBL-VS noise and/or blunt trailing edge vortex noise in their ABE noise modeling and observed corresponding results in their wind turbine noise measurements between the frequency of 1 to 2 kHz. Indeed, the rotor diameter of the wind turbine studied by Moriarty and Migliore [39] is smaller than the other studies (15 m vs. 30 m as those studied in [41] [42]). The consideration of LBL-VS noise may be appropriate given the smaller scale of the wind turbine studied.

2.2.3 Wind Turbine Noise Measurement in Outdoor Settings

The noise emitted from wind turbines situated in an outdoor environment has been studied by both research and industrial endeavours. In research, a summary of early measurement techniques can be found in Wagner et al. [37]. More recently, the use of an acoustic microphone array has been popular with the purpose of identify noise source locations. Oerlemans and Schepers [53] conducted studies with an outdoor megawatt scale wind turbine using a microphone array. The dominant noise source was found to be in the outer regions, but not at the tip of the blade.

Industrially, wind turbine noise is assessed as part of the regulatory process and is governed differently depending on jurisdication. However, the International Electrotechnical Commission (IEC) standard 61400, which contains a section for wind turbine noise assessment (Part 11), is widely used as a reference for local regulations. The standard has also been used in some wind turbine noise research studies. The details from IEC-61400-11 version 2.1 [8] are summarized below:

- The microphone equipment used must be a type 1 sound level meter as per IEC standard 60804. Instruments that are capable of recording overall sound pressure level data for a set period (standards require one minute averages). Functions such as frequency spectrum analysis, 1/1 or 1/3 octave level monitoring and digital recording are required for additional analysis.

- The microphone must be placed on an acoustic hard surface of specified construction, at a location depending on the tower height and radius of the turbine. The location

of the microphone must be downstream of the rotor and within an alignment of 15° of the wind direction. As well, wind speed and wind direction upstream of the turbine must be collected within a specified region. Please see figure 2.8 for illustration.

- A-weighting is applied to the noise measurements. A-weighting is decibel level correction that varies with acoustic frequency bands. It is designed to represent human ear response by attenuating levels at very low and high frequencies where human ears are not sensitive. Application of A-weighting is common in industrial or environment noise assessment [33]. The level reduction of A weighting can be seen in figure 2.9.
- The sound power level of the wind turbine can be calculated if the overall sound pressure level of the turbine is 6 dB above the associated background noise. This is to ensure the signal to noise ratio (SNR) is adequate (6 dB is two times the pressure level). From the IEC standard [8], It is defined by equation 2.8.

Sound power level (SWL) is calculated by:

$$P = L_{bk-A} - 6 + 10log_{10}(\frac{4\pi R_1^2}{s_0}) \tag{2.8}$$

where P is the sound power level of noise emitted by the wind turbine, L_{bk-A} is the background corrected A-weighted overall sound pressure level, R_1 is the direct and diagonal distance from hub to the microphone position as depicted in 2.8 and s_0 is the reference area ($s_0 = 1m^2$).

The IEC standard covers further details with the experimental setup, collecting and analysis of sound data. The current study uses IEC 61400-11 version 2.1 as a basis in experimental design.

In practice, the process of using this standard to measure noise from a utility scale commercial wind turbine can be extensive and labour intensive. Favourable conditions must be met in order for the data points to be collected. Turbine controls are typically available so the turbine can be yawed, and turbine on-off to facilitate noise measurements.

With small scale wind turbines, the assessment of noise by this standard can pose some challenges. For one, small scale wind turbines can have passively controlled systems, which can be difficult to hold constant during measurement. Migliore et al. [54] conducted noise measurements of several small scale wind turbines using the procedures based on the IEC standard (Further details and results of the NREL studies can be found in [55] [56] [57] [58] [59].). The authors modified the sampling procedures by reducing the average time of each data point from 1 min. to 10 s to better reflect the changing dynamic conditions.

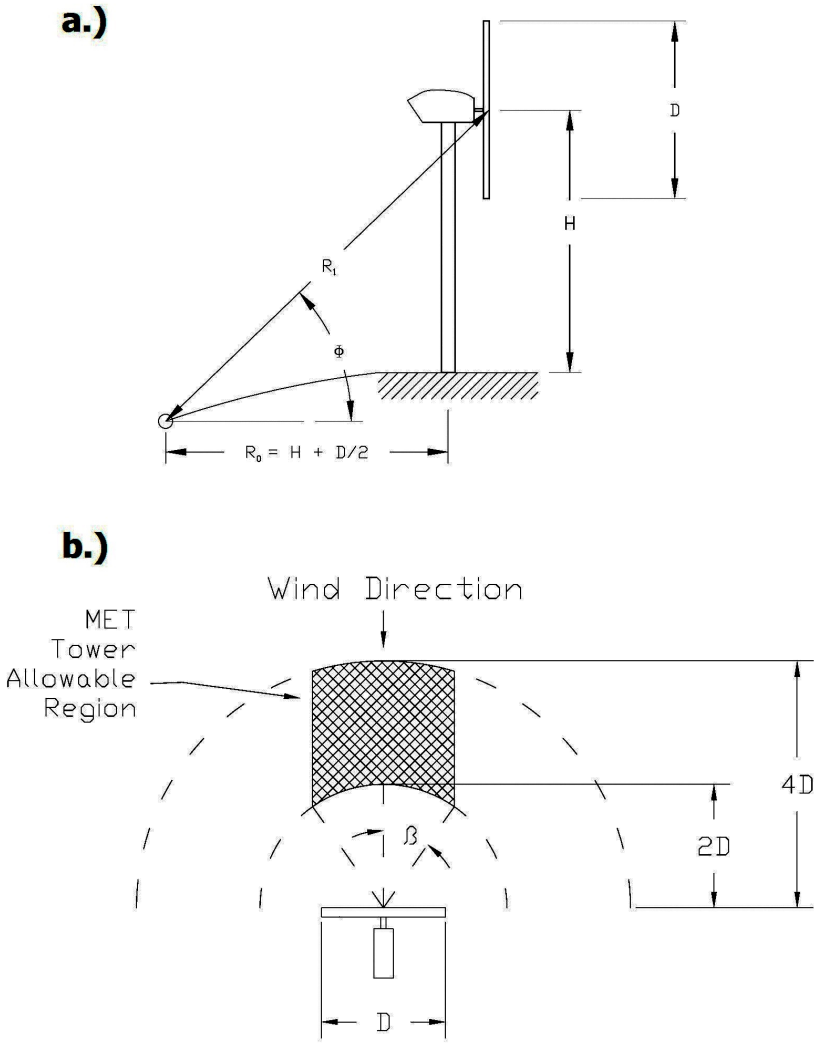

Figure 2.8: Location Guidelines defined in the IEC standard 61400-11 [33]. a.) Microphone and soundboard measurement location b.) 10m MET tower for measuring upstream wind speed and wind direction. Diagrams adapted from [33]

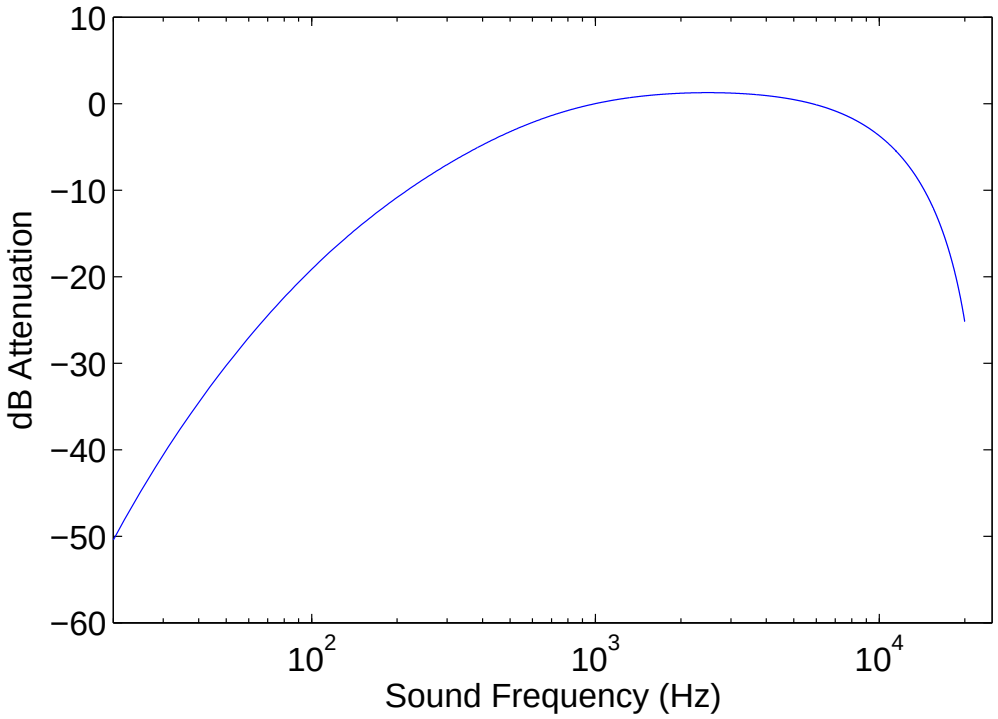

Figure 2.9: Sound pressure level attenuation vs. sound frequency for A-weighted filter. Source:[60]

2.3 Dynamic Conditions

In section 2.1, airfoil noise generation mechanisms under steady air flow conditions were described. When wind turbines are operating under field conditions, the flow seen by the turbine rotor can be far from a steady flow situation. Aside from high levels of inflow turbulence, occurrences of wind shear, cross-flow, yaw-misalignment and wind gusts can cause the blade to dynamically stall; drastically affecting the behaviour of the flow field in comparison to classical aerodynamics. As such, it is important to understand that the airfoil self-noise generation mechanism would be affected by such phenomena.

The complexities of dynamic stall phenomenon will not be reviewed here. Readers unfamiliar with the behaviour of dynamic stall can see McCroskey [61] for more details. Gharali [6] can provide some background on dynamic stall as it related to current experiments.

In terms of noise associated with dynamic stall phenomenon, to the best of this authors

knowledge, there has been very little published on the subject. Larato et al [62] hypothesized noise due to dynamic stall to be related to large scale vortices and counter-rotating vortices interaction. In the former, low frequency spectral peak, as observed by Moreau et al. [63], is speculated to occur while the latter is suggested to contribute to a thumping periodic component.

Nagarajan and Lele [64] and Nagarajan et al. [65] examined noise of airfoil under oscillating conditions. However, the study focused on the prediction results of URANS and Ffwocs-Williams acoustic analogy and no discussion relevant to this study was found.

2.4 Trailing Edge Saw-Tooth Serrations

The following section is a review of past studies investigating trailing edge saw-tooth serrations. Trailing edge saw-tooth serrations were found to be promising due to the relative ease of implementation, robustness, and effectiveness [66]. The use of trailing edge saw-tooth serrations have been explored by turbine manufacturers such as General Electric and Siemens. They are now beginning to see adoption in utility scale commercial turbines.

The review is divided with respect to the high Reynolds number regime and low Reynolds number regime. They are found in their respective subsections. Serrations have been found to reduce noise emissions for both turbulent boundary layer noise and LBL-VS self-noise generation mechanisms. These noise mechanisms were previously discussed in sections 2.1.1 and 2.1.2.

As reviewed in section 2.3, no studies have been found regarding noise associated with the dynamic stall phenomenon. This includes cases where serrated airfoils are exposed to dynamic conditions. Related to this thesis, Gharali et al. [7] examined the aerodynamic effects of a serrated airfoil under dynamic stall with reduced frequency k of 0.08.

2.4.1 Effect of Serrations in High Reynolds Number Regime

The use of trailing edge serrations for airfoil noise reduction was first investigated analytically by Howe in the sinusoidal configuration [67] and later, in saw tooth configuration [68]. Trailing edge noise is created when turbulent eddies of the boundary layer flow at a normal direction to the trailing edge. The intent of serrations is to create a trailing edge which is misaligned with the main components of turbulent eddies. The serrated configuration can be thought of as reducing the effective length of the trailing edge where the noise is generated [68].

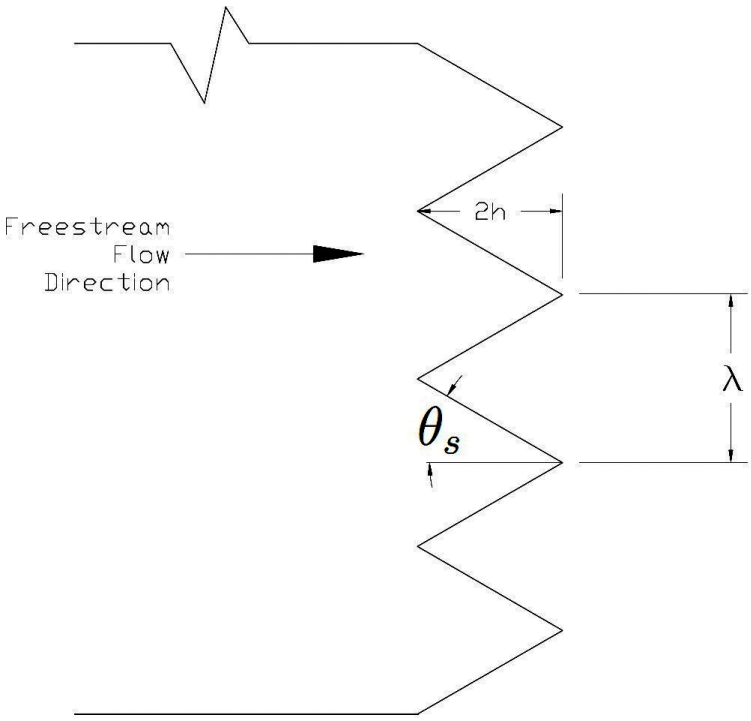

Figure 2.10: Physical parameters used to describe trailing edge saw-tooth serrations. Adapted from Howe [68]

Howe modeled the situation as a semi-infinite flat plate with low Mach number attached flow. Shown in figure 2.10, his definitions of the physical parameters for serrations are commonly adopted in subsequent studies. The sound pressure level reduction in dB, as a function of the physical parameters of the serrations, was estimated in equation 2.9:

$$L_{reduction} = 10log\left(1 + (\frac{4h}{\lambda})^2\right) \tag{2.9}$$

where $L_{reduction}$ is the sound pressure level in dB that is reduced, h and λ have been defined previously.

Howe noted that noise reduction was found to occur when the acoustic wavelength is small enough to be affected by the serrations. The condition that satisfies this is when the non-dimensional sound frequency/ Strouhal number $St_H = \omega h/U_c$ is $>> 1$, where ω represents the angular frequency of sound, h is the amplitude of the serrations defined by

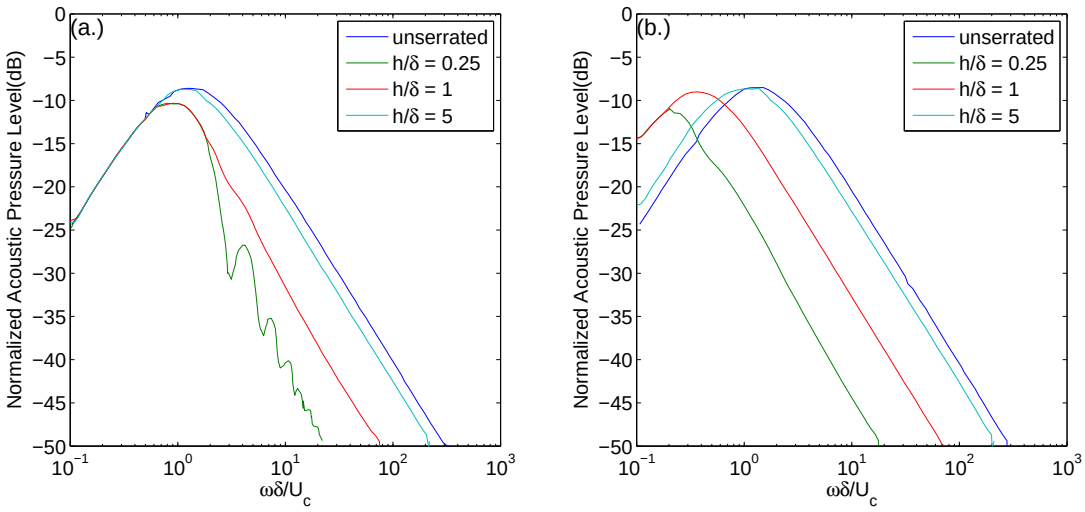

Figure 2.11: Normalized Acoustic Pressure level (dB) vs. non-dimensionalized sound frequency for serrated and unserrated trailing edge as predicted in the Howe study. a.) $h/\delta = 1$ b.) $h/\delta = 10$. Figure digitized from Howe [68]

figure 2.10 and U_c is the convection velocity of turbulence experienced by the surface of the airfoil.

At the minimum, the physical dimensions of the serration, both amplitude h and wavelength λ, should be at least on the order of the boundary layer thickness. The tooth angle of the serration, θ_s, should be less than 45° for them to be sufficiently misaligned with the main components of turbulent eddies to be effective.

From the h/λ term in Equation 2.9, it can be shown that narrower serrations were more effective in reducing noise. This is also seen in figure 2.11, where the predicted noise reduction of serrations was plotted with respect to the acoustic spectrum for different serration dimensions. Narrower serrations, represented by curves with smaller λ/h values, achieved higher levels of noise reduction. The same figure also shows the level of reduction to be increasing with increasing acoustic frequency/Strouhal number.

Subsequent studies have further insights into the performance and behaviour of serrations; with results different than Howes analytical conclusions in some instances. The European Union project STENO (Serrated Trailing Edge Noise) [69], one of the first experimental studies of airfoils with trailing edge serrations, showed narrow serrations to be more effective in reducing trailing edge noise. When examining 4 different airfoil profiles

and five different serrated flat plates between Re_c 7×10^5 to 1.4×10^6 at zero angle of attack (flat plates) and lift coefficient C_l of 0.0, 0.5 and 1.0 (airfoils), they reported reductions from various serrated specimens when examining them in an open jet anechoic wind tunnel [70] . However, the overall noise reductions were found to be below those predicted by the Howe model.

Project STENO also investigated the impact of serration orientation with respect to the flow. However, this will not be reviewed for the current study.

As part of the European Union project SIROCCO (Silent Rotors by Acoustic Optimization), Oerlemans et al. [71] measured noise of a turbine blade on a utility scale wind turbine with serrations mounted on the last 12.5 m of one blade (for a blade 47 m in length). Acoustic measurements were collected using a microphone array with beam-forming techniques at wind speeds of 6-10 m/s (reference wind speed measured at 10 m).

An overall sound pressure level reduction of 3.2 dB was observed. Again, this reduction level was found to be less than Howe's prediction. Noise was found to be dominant near the outer radius of the rotor, with blade noise directed downward with the movement of the blade. Reduction was found in lower frequencies but there was an increase in noise at higher frequencies, similar to the observations from Braun et al. [69]

Gruber [72] conducted an extensive experimental campaign examining serrations parametrically in an open jet wind tunnel. Thirty seven interchangeable configurations were tested on a NACA 65(12)-10 airfoil platform of varying wavelength λ and serration amplitude h. As with the studies mentioned earlier, Grubers results also showed similar discrepancies with Howes prediction. As seen in figure 2.12, Grubers result showed noise reduction being far less than those predicted by Howe under the same condition, with the trend of increasing noise after a certain threshold (as already seen by Project STENO and Oerlemans [71]).

With respect to sound frequency, the range of noise reduction was found to occur roughly for Strouhal number (St_δ) of $0.3 < f\delta/U_\infty < 1$. The Strouhal number used by Gruber (St_δ) was based on frequency f (in Hz), boundary layer thickness δ and U_∞. It should be noted that Howe's Strouhal number St_H was based on angular frequency ($2\pi f$), serrations amplitude h and convection velocity ($U_c = 0.7\ U_\infty$).

For the range of frequencies greater than $St_\delta = 1$, noise levels were found to be increased. The velocity spectrum obtained from a hot wire probe suggests that the cross flow from the pressure side to the suction side to be the cause (as Braun et al. [69] had speculated earlier). Similar thresholds of noise reduction and increase were also seen in the study conducted by Finez et al. [73] as well.

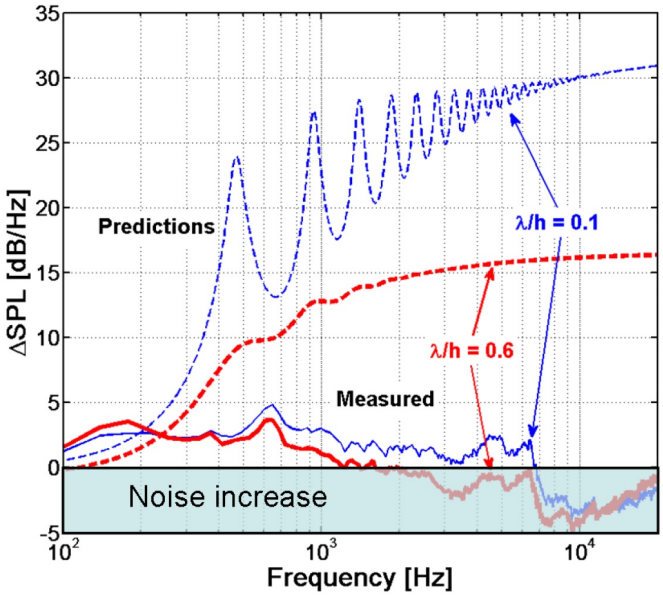

Figure 2.12: Comparison of Howes prediction model with Grubers experimental results. Aspect Ratio $\lambda/h = 0.1$ and 0.6. Figure originally published in Gruber [71]

Noise reduction, from observations of sound power level, was found to increase with decreasing wavelength λ (also with ratio of λ/δ) at low to mid frequencies. At high frequencies (range where $St_\delta > 1$), noise was found to be above the baseline configuration, with increasing noise with decreasing wavelength λ (with ratio of λ/δ as well).

With regards to amplitude h, Gruber found serrations were effective when the ratio $h/\delta > 0.25$. Serrations smaller than this criteria were found to have no effect in noise reduction as they were too small compared with the turbulent eddies. This trend seemed to hold when the amplitude is normalized by ratio λ or δ. A greater amplitude was found to cause greater reduction in low/med frequencies while increasing noise levels at higher frequencies.

Angle of attack was not found to cause significant changes in the reduction behaviour in the two aspect ratios of serrations tested. However, for noise increase at $St_\delta > 1$, increasing the angle of attack increased the noise levels, with narrow serrations showing greater reduction from the baseline. The cause was reported to be due to the increase in pressure difference, leading to stronger cross flow in the mechanism described previously.

Gruber examined the near field pressure spectra of flat-plates with serrated and un-

serrated trailing edges using remote microphone probes. It was proposed that the noise reduction mechanism is related to the reduction of phase velocity of pressure fluctuation at low frequencies (from interference of backscattering pressure).

Finez et al.[73] studied two sets of serrations and compared with a baseline case: $\lambda = 2$ mm, $h = 6.5$ mm and 10 mm. They examined a serrated NACA 6512-10 airfoil in a cascade configuration at $Re_c = 5.5 \times 10^5$ ($M = 0.23$, 0.1 m chord length, 17° angle of attack) using time resolved PIV and microphone measurements. The Strouhal number ranges of noise reduction and increase for Finez et al. [73] were found in agreement with Gruber's [72] results.

Finez et al. [33] found that the attached turbulent boundary layer is "blown off"due to cross-flow through the serrations from the pressure side (enhanced mixing). Similar observations were found in Grubers experiments, whose boundary layer thickness increased by 12% from the root to the tip of the serrations, relative to the straight edge. They speculated this phenomenon facilitated noise reduction by reducing the efficiency of the edge in scattering noise. Serrations also caused reduced coherence with the vortex shedding at the trailing edge, which also pointed to a less effective noise scattering process.

Flow structures around a serrated trailing edge have been explored by Probsting [74], who examined a serrated NACA-0012 airfoil using tomographic PIV. The serrations used were cut into the airfoil profile instead of being a thin trailing edge as seen in other investigations. The added bluntness caused significant blunt trailing edge noise and no reduction was seen.The Tomographic PIV study found the formation of coherent structures in the shape of Hairpin/cane vortices (small scale) and Horseshoe vortices (large scale) on the surface of the airfoil. However, the disccusion of these flow structure are beyond the scope of the current study and will not be reviewed.

2.4.2 Effect of Serrations in Low Reynolds Number Regime

The effects of serrations under low Reynolds number flow regime have been mainly investigated by Chong et al. [75] [76] [77], Moreau et al. [78] [79] [80] [81] and numerically by Jones and Sandberg [82] [83] [84].

Chong et al. examined serrations and their effects on the laminar instability noise mechanism featuring Tolmien-Schlichting wave feedback. This mechanism was discussed in section 2.1.1. The NACA 0012 airfoil profile was studied with serrations cut into the airfoil similar to the model from Probstings investigation; referred to as broken type serrations by the authors in [76]. Unlike Probsting [74], however, the blunt trailing edge of the serrations was not found to be the cause of any major noise source [76].

The airfoil profile was tested between Re_c 1.0×10^5 to 6.0×10^5 in an open jet anechoic wind tunnel throughout the three studies. The studies showed there were some notable differences between the behavior of serrations in the laminar and turbulent regimes. Large narrowband reductions of up to 20 dB when $Re_c = 2.4 \times 10^5$ were observed [77]. In [75], the impact of serrations was found not to be on the broadband aspect of the airfoil self-noise but on suppressing the tonal qualities. Wider serrations were found to be more effective at suppressing the noise caused by LBL-VS mechanisms, as opposed to narrower serrations for turbulent boundary layer noise. Later studies [77] found that greater serration angle (θ) and amplitude ($2h$) improved noise reduction abilities.

The cause of the noise reduction was suggested to be due to the interference on the laminar separation bubble at the pressure side and near the trailing edge. The separation bubble, in particular the length of the region, was key to the feedback mechanism and noise generation. From [77], greater serration angles were found to inhibit the formation of laminar separation. With the increase in serration amplitude, the serrations cut into more of the chord, reducing the length of the region where the separation bubble is located. In terms of the behaviour of serrations with respect to angle of attack, it was found that reductions were more noticeable with higher angles of attack. This is proposed to be due to the shift in the separation bubbles toward the trailing edge [75].

Moreau et al. [78] [79] [80] [81] examined serrations in a flat plate configuration in an open jet wind tunnel. Two sets of serrations were examined: $\lambda/h = 0.2$ and $\lambda/h = 0.6$. Like the Chong studies, wider serrations were found to be more effective than narrower serrations. In [78], they found that attenuation fell into two regimes for the range of Reynolds number studied; with the low speed regime ($Re_c < 1.7 \times 10^5$) achieving attenuation when $St_\delta < 0.7$, and higher speed regime ($1.7 \times 10^5 < Re_c < 4.5 \times 10^5$) achieving reducing from $0.7 < St_\delta < 1.4$. It should be noted that the Strouhal number range is similar to those of Gruber [72]. Although for Moreau et al. [78], the serrations behave differently then Gruber. According to the authors, the difference was attributed to the difference in airfoil specimen geometry and Reynolds number.

From [79], the effects of serrations for $1.7 \times 10^5 < Re_c < 4.5 \times 10^5$ were discussed. Both narrow and wide serrations achieve attenuation of blunt trailing edge vortex noise between $0.7 < St_\delta < 1.4$ and a general noise attenuation at a low Strouhal number ($St_\delta < 0.13$ for narrow serrations, $St_\delta < 0.2$ for wide serrations). The range of Strouhal number in between saw an increase in noise for narrow serrations while no effect was observed for wider serrations. For $Re < 1.7 \times 10^5$, experimental results from [81] are summarized in table 2.1. Wide serrations achieved broadband reduction at low frequencies. Locally, the rate of reduction can be up to 16 dB/Hz. The narrow serrations also achieved reductions but created an increase with two notable tones, as seen in figure 2.13, which can negated

Table 2.1: Overall sound pressure level (250 Hz to 4 kHz) reduction for wide and narrow serrations at various U_∞ from Moreau et al. [81]. Negative values indicates increase in sound pressure level.

U_∞ (Re_c)	Wide Serrations, OASPL reduction (dB)	Narrow Serrations, OASPL reduction (dB)
12 m/s (1.3×10^5)	1.4	-4.1
11 m/s (1.2×10^5)	4.4	-4.1
10 m/s (1.1×10^5)	8.0	-1.0
9 m/s (1.0×10^5)	10.9	1.8

the noise reduction benefits.

Further discussion on the mechanics can be found in [80] and [81] for high and low speed regime respecitively but will not be reviewed for the current study.

Jones and Sandberg examined a NACA 0012 airfoil with saw-tooth trailing edge serration extensions at angle of attack of 5°, Mach number M of 0.4, Re_c of 5.0×10^4 using direct numerical simulation (DNS). Two sets of serrations were examined: both having wavelengths of $\lambda = 5$ mm, with one having amplitude h of 3 mm and the other having amplitude h of 6 mm. Longer serrations were found to provide greater reduction and over a greater range of frequencies [82].

Under this condition, the pressure side consists entirely of laminar boundary layer flow while the laminar/turbulent exists on the suction side at mid chord [82]. The latter mechanism is noted by the authors as a noise source that dominates trailing edge noise at higher frequencies [82].

Detailed results are discussed in [83]. The serrations did not have an effect on the laminar/turbulent boundary layer transition on the suction side of the airfoil. The serrations did have an effect of the mechanism at the trailing edge, affecting pressure side boundary layer flow and seem to have an affect in reduction noise originating from pressure side source at the trailing edge.

Further findings on flow structure can be found in [82] and [84] but will not be reviewed for the current study as it is beyond of scope of discussion.

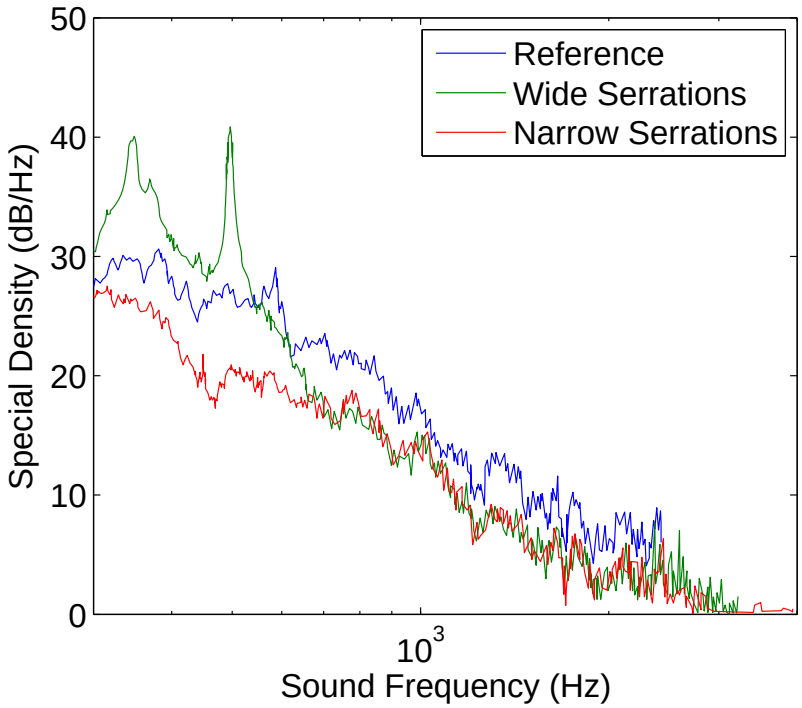

Figure 2.13: Acoustic Spectra of serrated and reference flatplate at 11 m/s ($Re_c = 1.2\times10^5$) from the Moreau study, Figure digitized from Moreau et al. [81]

Chapter 3

Experimental Setup

In this section, the experimental setup and considerations for the two sets of experiments, namely the indoor controlled environment experiments conducted on campus at the University of Waterloo and the outdoor field experiments conducted at the Wind Energy Group outdoor wind turbine test site, are discussed.

The discussion for each set of experiments is divided into four subtopics:

- Description of the experiment platform (wind tunnels or test site) and instrumentation
- Details regarding the test specimen in the experiments (airfoils and serrations)
- Experiment plan and data collection procedures
- Techniques to analyze the data collected from the experiments

3.1 Experiments in a Controlled Environment

The first portion of this study examines the aerodynamic and aeroacoustic effects of serrations as they relate to small scale wind turbines. With small scale wind turbines operating in low Reynolds number regime (as low as 10^4) and in a highly dynamic environment, experimental conditions should reflect these qualities. Examining the experiment platform available to conduct experiments, it was found that the closed circuit wind tunnel of the

wind energy group to be the most suitable choice. Previously studies conducted by Orlando [85] and by Gharali [6] also used this experiment platform to conduct aeroacoustic and dynamic stall studies respectively.

The following experiment use the SD-7037 airfoil profile, which was previously studied by Gharali [6].

3.1.1 Equipment

3.1.1.1 Closed Circuit Wind Tunnel

The closed circuit wind tunnel was originally constructed by Sperandei [86]. Later, the tunnel was modified for aeroacoustic experiments by McPhee [10], Orlando [85] and for dynamic stall studies by Gharali [6]. The details of the tunnel specification and the extent of modification can be found from these sources. In this section, only details pertinent to the experiment are discussed. General descriptions of the wind tunnel are summarized in table 3.1. The wind tunnel schematics is shown in figure 3.1. A diagram depicting the test section features, dimensions and current experimental setup is seen in figure 3.2.

Gharali [6] made modifications to the wind tunnel for the purpose of studying dynamic stall effects on airfoils under pitching oscillation. A servo motorized mount was installed. The servo motor has a rotational movement resolution of 22 counts per degree, or movement increments of 0.05° for every count. Under dynamic pitching oscillation, the positioning error of the servo motor is within 8 counts (0.36°). The accuracy of the servo motor static positioning is within 2 counts (0.1°).

In preparation for this study, it is also important to determine the current state and calibration of the wind tunnel. In particular, there are three factors of interest: test section wind speed calibration, turbulence intensity, and background noise levels.

Figure 3.3 shows the test section wind speed calibration at the time of the study. It was found that the calibration has changed since the time of Orlando [85], with maximum wind speed (when fan frequency is at 60Hz) to be lowered by roughly 4 m/s.

A change was also observed with the turbulence intensity of the wind tunnel. The difference between observations of Gharali [6] and that of the current study can be seen in figure 3.4. The turbulence intensity was found to have increased from the time of Gharali [6] as well; with turbulence intensity level $\sim 0.8\%$ before to around $\sim 1\%$ currently.

The change was attributed to the maintenance of wind tunnel. It is suspected that leakage between wind tunnel wall sections and some build up of residue inside the wind

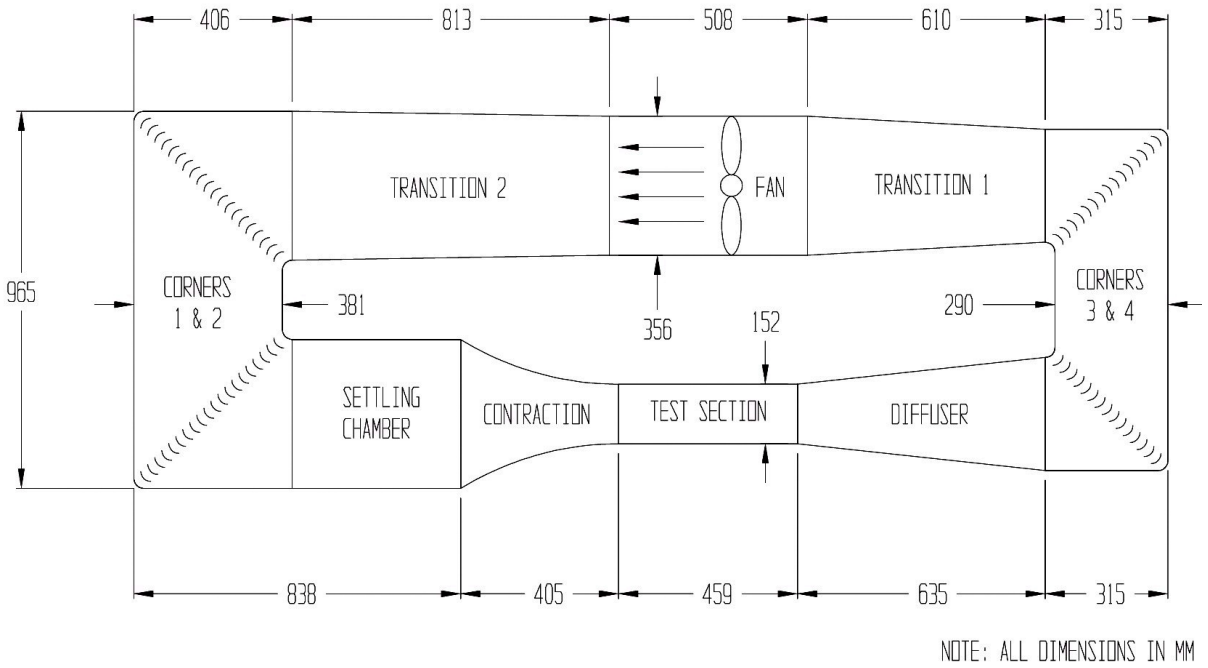

Figure 3.1: Schematic of the closed circuit wind tunnel. Figure originally presented in Sperandei [86].

tunnel (from smoke fluid flow seeding in other experiments) to have contributed to the cause.

To improve the conditions of the wind tunnel, an extensive overhaul of tunnel is needed, which due to the scheduling and demand of tunnel at the time of the study, was not possible. Despite the changes in condition of the wind tunnel, however, it can still achieve the conditions needed for the study.

For the acoustic measurements, the change in the wind tunnel background noise can have an impact in the current study. The shift in variable frequency drive (vfd) fan frequency vs. wind speed (U_∞) calibration is expected to increase the wind tunnel background noise. This is illustrated in figure 3.5, where the wind tunnel background noise measured during the study of Orlando [85] is compared with the background noise measured during the current study. The background noise measurements were taken using the same equipment and techniques as Orlando [85] (to be described in following sections). The results show an increase in noise levels at the same wind speed condition.

The current background noise sound pressure level at 25 m/s (near the experimental

Table 3.1: Summary of wind tunnel parameters

Specification	Details
Test Section Dimensions	152.4 mm × 152.4 mm (6" × 6") cross-section by 460 mm length [86]
Specimen Mount Location	180 mm downstream of test section inlet [86], as seen in figure 3.2
Wind Speed	Up to 31 m/s @ 60 Hz fan Speed, see figure 3.3 for wind speed calibration
Turbulence Intensity	near 1 %, varies with wind speed, see figure 3.4
Modifications	Recess microphone port in McPhee [10], Acoustic Foam lining to reduce background noise in Orlando [85], Servo motor controlled pitching oscillation mount for dynamic stall study in Gharali [6]
Specimen Mount Location	180 mm downstream of test section inlet [86], see figure 3.2
Microphone Port Location	180 mm downstream of inlet [10], see figure 3.2
Background Noise	around 40 dB beyond acoustic frequency of 2 kHz (sound pressure level measured at recess microphone port at bandwidth of 0.75 Hz). See figure 3.5

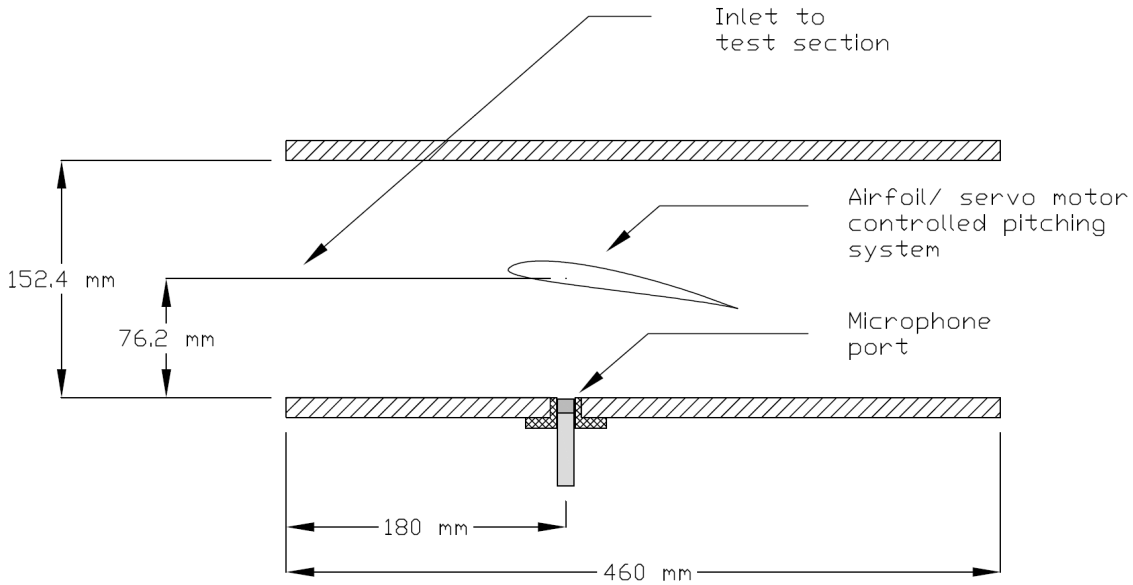

Figure 3.2: Not to scale diagram depicting the test section features and dimensions. The current experimental setup is also depicted.

point) is shown in figure 3.6. It is expected the background noise to be at a sound pressure level of 40 dB or above at the frequency range of interest to this study (2 kHz to 7 kHz).

3.1.1.2 Open Jet Blow Down Wind Tunnel

Subsequent experiments on the airfoil specimen was conducted with the open jet blow down wind tunnel at the University of Waterloo main campus. This portion of the experiment subjects the airfoil specimen to the same flow condition but in an open jet environment without the potential for resonance from the wind tunnel's hard walls.

Figure 3.7 shows the configuration of the wind tunnel at the time of experiments while figure 3.8 depicts the schematic of the wind tunnel with as well as the airfoil/microphone setup. The wind tunnel consists of a Buffalo Forge Model 7e centrifugal blower, expanding to a 1.83 m $\times$ 1.83 m (6' x 6') section with equipped with honeycomb straighteners and screens. This is followed by 2 contractions (a 9:1 contraction, and a 2.12:1 contraction), which reduces the outlet area to 0.5 m $\times$ 0.35 m. Wind speed is checked at the outlet of the contraction using a pitot static tube with a digital manometer (Omega Engineering Model HHP-90). A maximum wind speed of 48 m/s can be achieved.

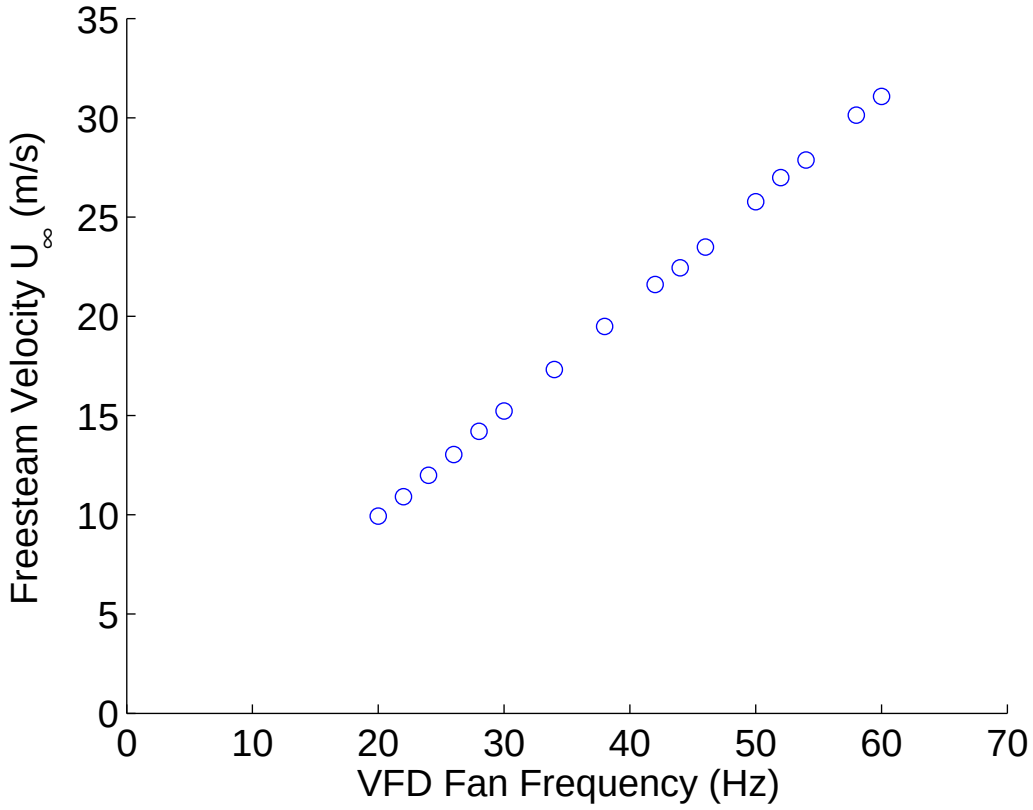

Figure 3.3: Calibration of the closed circuit wind tunnel at the time of the study.

The airfoil specimen was mounted on a lab stand with a condenser microphone placed at a distance of 76.2 mm (3") beneath the airfoil to replicate the closed circuit wind tunnel setup. The background noise of the wind tunnel was measured during experiments. Although the background noise of the wind tunnel is substantial, the airfoil tonal noise found was well above that of the background noise.

The turbulence intensity of the wind tunnel was not characterized but is expected to be much higher than that of the closed circuit wind tunnel. Although the increased turbulence is not considered as an issue in the current experimental plan.

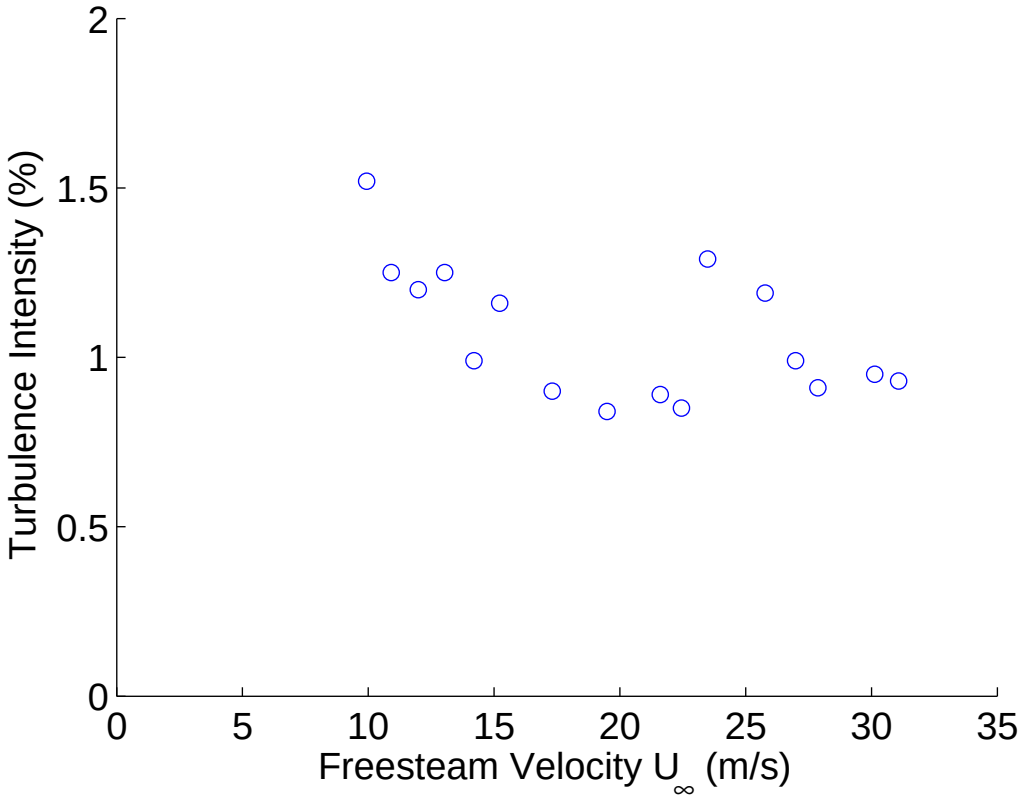

Figure 3.4: Turbulence intensity of the closed circuit wind tunnel at the time of the study.

3.1.1.3 Microphone Equipment

The experimental equipment first used by McPhee [10] was used to investigate the aeroacoustic effects in this portion of experiments. They are shown in figure 3.9. The acoustic equipment consists of a Bruel and Kjaer (B&K) Type 4189 condenser 12.7 mm (0.5") microphone and a B&K Nexus conditioning amplifier. The amplifier was then connected to a National Instrument PCI-6251 PCI based data acquisition board, where its analog input is taken by a custom program originally written by McPhee [10]. The system is set to create samples of 100 s in duration at a sampling frequency of 4.2×10^4 Hz.

The B&K Nexus amplifier was set to an output sensitivity of 31.6 mV/Pa. The microphone was mounted in a recess of the tunnel wall to reduce induced noise from the boundary layer flow. No overload was observed during the experiments with the airfoil.

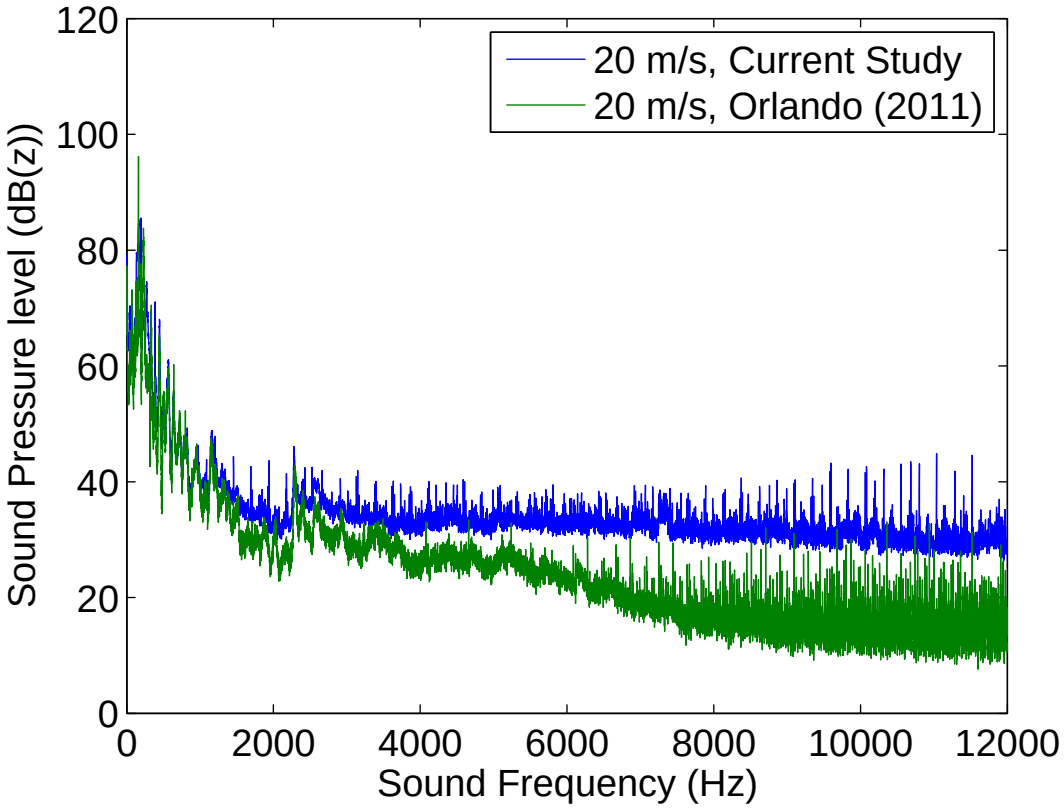

Figure 3.5: Comparison of the closed circuit wind tunnel background noise from Orlando [85] and the current study at $U_\infty = 20$ m/s.

The mount was flush with the wind tunnel with a Dacron fabric membrane between the microphone and flow of the wind tunnel. This is shown in figure 3.10. It was found that the microphone response is affected by the placement of the microphone within the port, with greater attenuation to response at higher frequencies when the microphone was set at a greater recess from the wall surface. Increased depth is detrimental according to McPhee [10] due to the creation of a Helmholtz resonance cavity. The microphone was fitted tightly with a 2 mm recess from the edge of the port mount as specified by McPhee [10]. This was checked prior to each experiment to ensure there were no changes in the system prior to experiments each day. Day to day repeatability was observed.

Further details of the microphone equipment and setup have been discussed by McPhee [10] and Orlando [85].

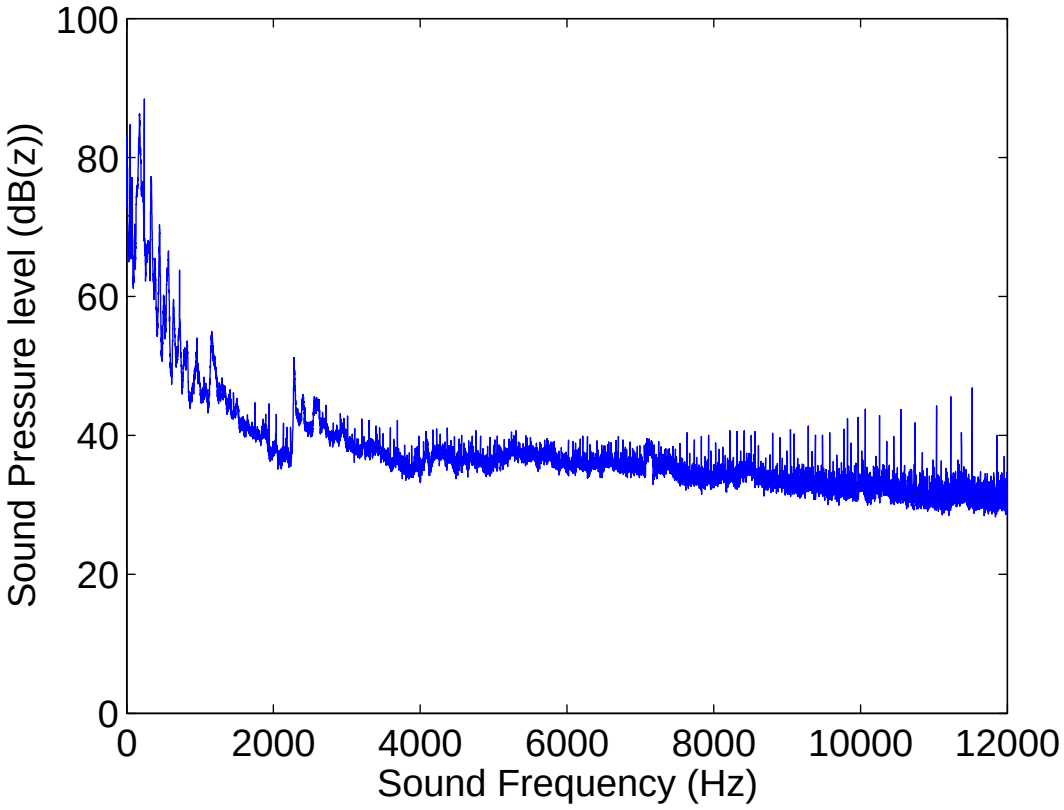

Figure 3.6: Sound pressure level of the closed circuit wind tunnel background noise at 25 m/s.

While another set of microphone equipment, the B&K Type 2250 sound level meter with a Type 4192 12.7 mm (0.5") condenser microphone, is available, the equipment used by McPhee [10] was selected for the following reasons. First, the setup of McPhee [10] was capable of a higher frequency resolution for narrowband/fast fourier transform (FFT) analysis in comparison with the sound level meter unit. Secondly, the equipment was the same as that used by Orlando [85]. This would not introduce instrumentation bias error with initially assessing the wind tunnel condition.

However, for simplicity of setup, the B&K Type 2250 sound level meter was used later in the verification experiments at the open jet wind tunnel. The B&K Type 2250 sound level meter was also used as the microphone instrument in the outdoor portion of this experiment as it is an rugged and integrated instrument that is more suitable for use in the

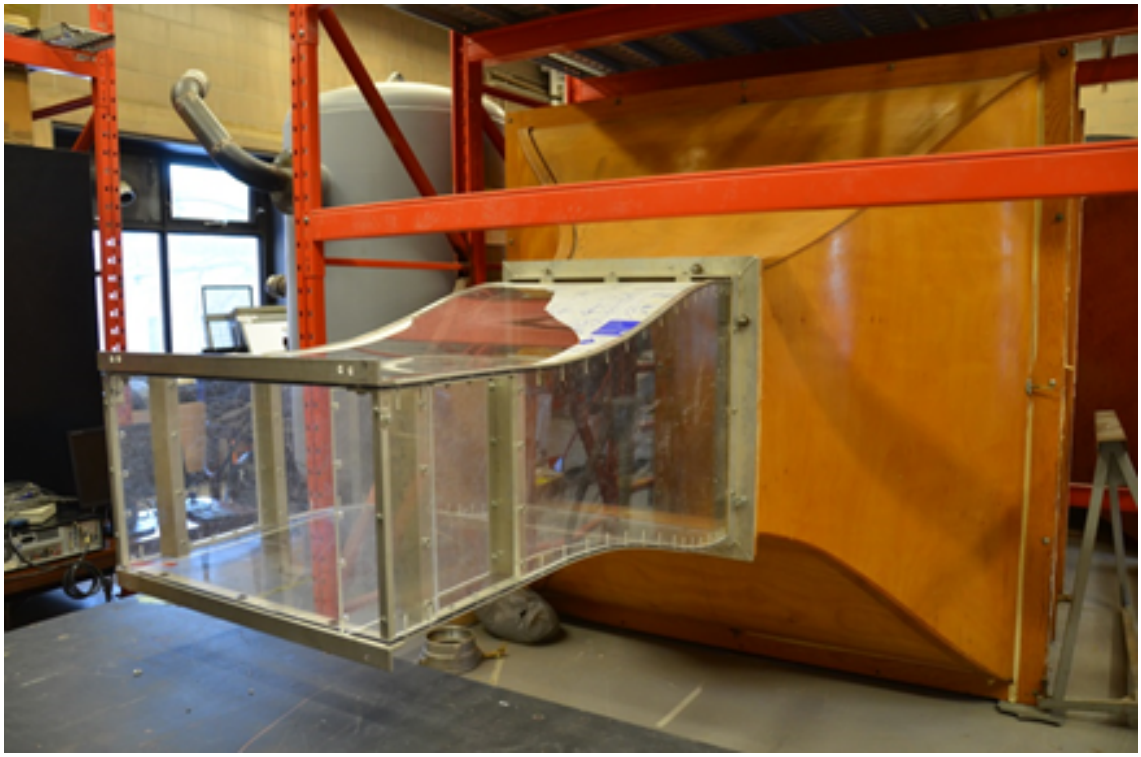

Figure 3.7: The open jet blow down wind tunnel, shown here with the two contractions attached.

field environment. Details of the sound level meter system are discussed in section 3.2.1.3.

3.1.2 Test Specimen

3.1.2.1 SD-7037 Airfoil

The airfoil used in this experiment was manufactured in the same manner as the airfoil used by Gharali [6]. A five axis CNC machine milled the SD-7037 airfoil profile of the test specimen from aluminum stock. The specimen was later lightly sanded to remove surface machine grooves and anodized to give a smooth and non-reflective finish. The chord length of this new airfoil specimen was found to be 25 mm.

During his study of a S822 airfoil with a chord length of 50 mm, Orlando [85] discovered the closed circuit wind tunnel to be affected by Parker β mode resonance. Given the chord

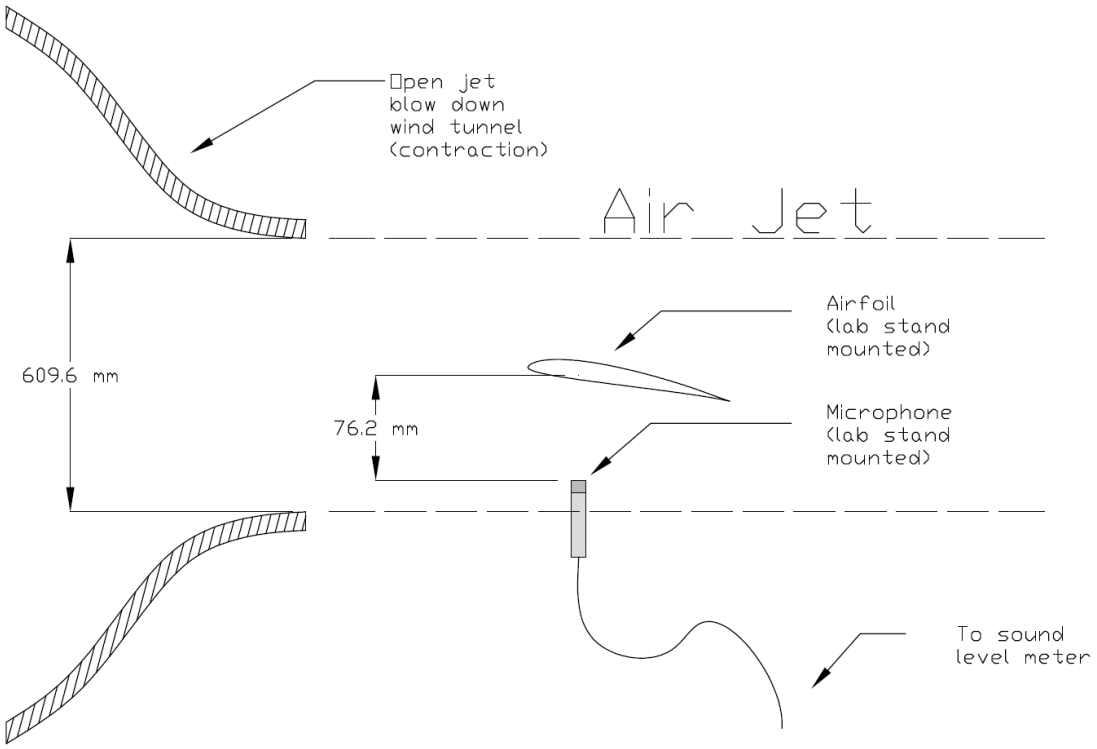

Figure 3.8: Schematic of the experimental setup at the open jet blow down wind tunnel (not to scale)

length of the SD-7037 airfoil is smaller than the threshold where resonance is expected to occur [87], this was not considered as an issue at the time of the experiment design.

However, from the results of experiments in the current study, the effects of resonance is speculated to have influenced the results. In search of other studies with discussions on the subject during the analysis of the experimental data, the study of Ikeda et al. [88] was found to be relevant. Ikeda et al. [88] investigated the effects of resonance with an airfoil in a hard wall test section configuration with a $Re_c = 1.0 \times 10^4$. The authors suggested the resonance is not purely acoustic in nature and that the resonance mechanism can alter the behaviour of the feedback noise generation mechanism. Two types of resonance are examined: anti-symmetric and symemtric resonance. Higher modes of resonance were found to be dominant.

Further discussion regarding the possible resonance effects involves discussing the experimental results from the current study. This discussion is continued in section 4.1.2.

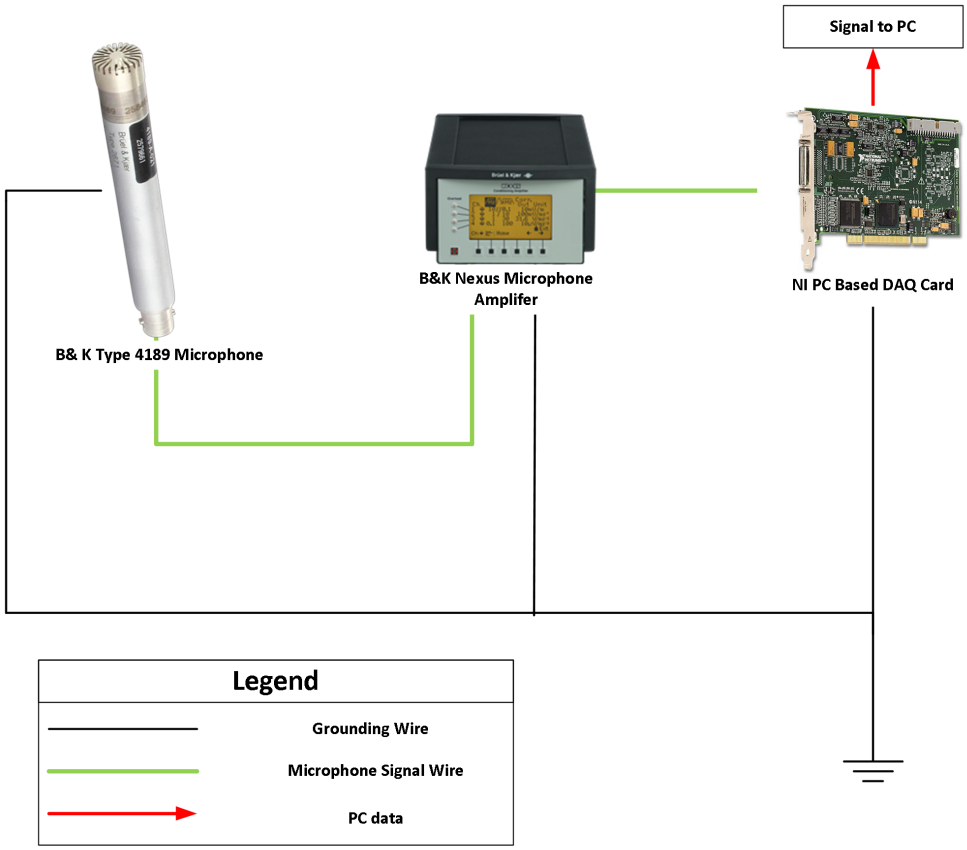

Figure 3.9: Diagram of the microphone and data acquisation equipment setup for closed circuit wind tunnel experiments

3.1.2.2 Serration Design and Construction

The design of serrations for the SD-7037 airfoil has been bound by several constraints and considerations:

Tunnel Blockage Barlow et al. [89] recommends that the cross-sectional area of the airfoil specimen should be less than 7.5% of the test section cross-sectional area. Given the dimension of the closed circuit wind tunnel, the chord length of the SD-7037 airfoil specimen and the maximum angle of attack tested, this limits the serration length to be less than 5.5 mm.

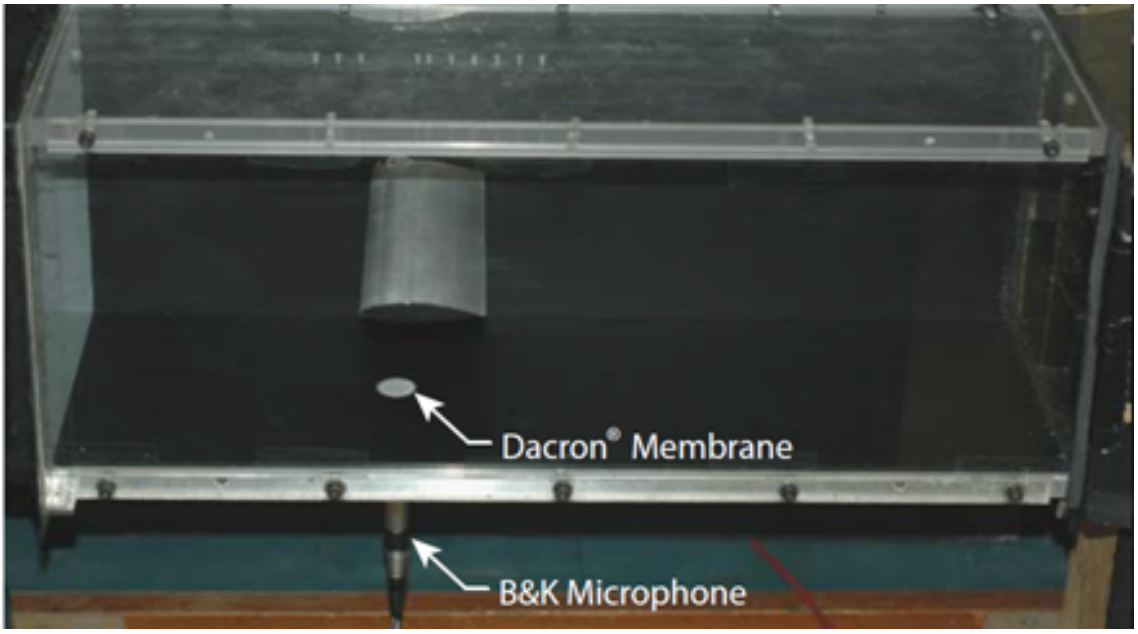

Figure 3.10: Microphone system installed in the wind tunnel during the Orlando study [85]

Parker β Mode Resonance Even with the maximum allowable length for serrations as limited by wind tunnel blockage restrictions (5.5 mm), the airfoil specimen chord length would still be below the threshold where resonance is expected to occur [87]. As such, this was not considered as an issue at the time of designing the serrations.

Bluntness Parameter The trailing edge extension added to the airfoil must introduce a thickness such that airfoil will not produce trailing edge bluntness noise. The convex nature of the trailing edge with the unmodified airfoil specimen means it could be machined to a sharp point without any difficulty. Given the low Reynolds number condition, using Blakes bluntness criterion [38], as discussed in section 2.1.3.1, the thickness of the trailing edge is near 0.3 mm or less.

Manufacturing Constraint Due to the dimensions of the airfoil specimen, the serrations associated with it would likely have wavelength and amplitude dimensions on the order of 1 mm. The concave nature of the sawtooth pattern between teeth is an issue given that traditional manufacturing methods are limited by the diameters of the cutting tool.

Given these considerations, the length of the extension of serrations was selected to be 4 mm (h = 2 mm). This length was determined based on a balance of serration teeth dimension from limitations in the manufacturing process and matching the extension to original chord ratio values found in other studies. Here, the extension to original chord ratio is 16%, which is similar to studies reviewed previously.

In terms of the aspect ratio λ/h (previously defined in section 2.4), two were selected: 0.67 and 1.33. An aspect ratio of 0.67 was selected because it is similar to the aspect ratio that was found effective in the study of Moreau et al. [79]. As it was found that wider serrations were more effective for laminar boundary layer cases, another set of serrations doubling the wavelength was examined. This has an the aspect ratio of 1.33. Manufacturing constraints (the finest serration) were also taken into consideration, with wide serrations being able to be manufactured with greater fidelity. They are referred to as the narrow serration case (NSR) and the wide serration case (WSR) respectively.

For comparison with serrations, other test cases were made. The flat plate case (FPL) consists of an un-serrated flat plate extension length of h. This is illustrated in figure 3.11. This case represents an airfoil with a rectangular trailing edge extension that has the same wetted area as the serrated cases. This case is mainly included because it is used to compare the drag effects of the airfoil in the companion investigation to the study which examines the aerodynamic effects with PIV measurements. The acoustic effects is expected to be less significant but is examined in this study nevertheless.

To examine the effects of the attachment method, a zero length attachment (ZLA) case consist of a 2 mm rectangular strip was also included. This strip, attached to the pressure side of the trailing edge of the airfoil specimen and does not protrude beyond the trailing edge. This would differentiate the reduction, if any, caused by the interference by serrations and by the attachment method.

For comparison with all the other test cases, the original trailing edge case (OTE), which is the unmodified SD-7037 airfoil, is also examined. All five test cases of trailing edge configurations are shown in figure 3.12.

In terms of construction, several materials were considered. Previous studies have employed different materials: from cardboard [72] [79], thin sheet metal [71] [72] to aluminum foil or masking tape [90]. It was desirable to seek a thin, rigid and non-reflective material.

Serrations were manufactured out of polyester shim stock 0.127 mm (5 mil) in thickness in order to satisfy the bluntness criterion. The serration pattern was cut from a laser cutter (G. Weike Model LG900N) from Kwartzlab MakerSpace, a community organized machine shop in Kitchener, Ontario. The laser cutter is capable of cutting non-metallic and non-

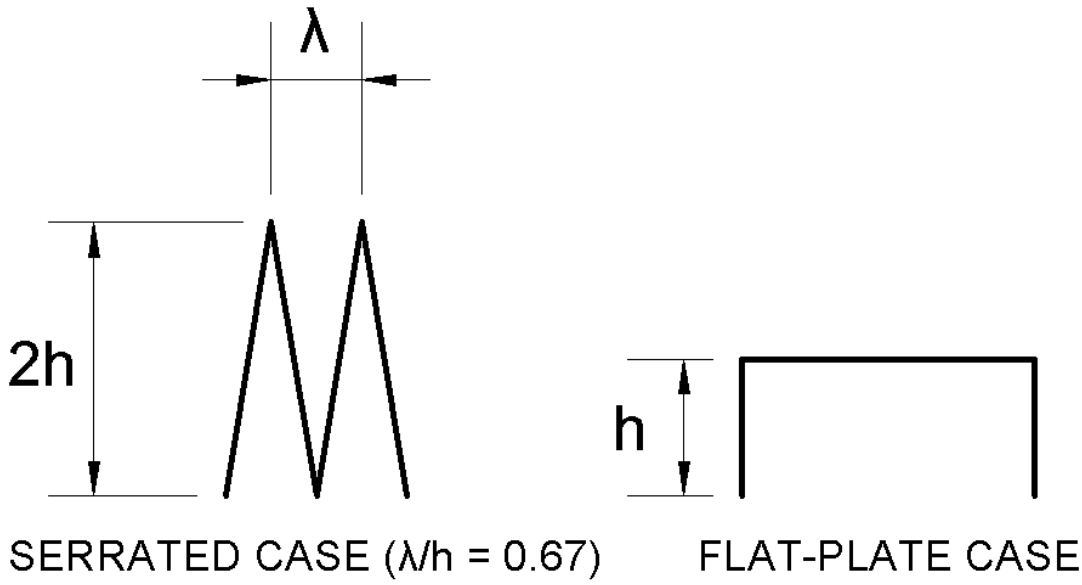

Figure 3.11: Diagram comparing serrated case and flatplate case.

chlorinated sheet materials. A beam width of 0.1 mm provided sufficient fidelity of the serration valley and introducing a minimal fillet, as shown in figure 3.13.

The extensions are placed on the pressure side of the trailing edge of the airfoil specimen with a 2 mm attachment overlap. Cyanoacrylate adhesives was manually applied using a fine brush to the airfoil trailing edge before the strip was pressed on to the airfoil surface. Excess adhesive running off from the contact surfaces was cleaned by cotton swab dipped with solvents. Cotton swabs with solvents were also used to clean the adhesive residue on the airfoil after the extensions were removed.

With the aluminum surfaces well covered, the extensions are then spray painted matte black to further reduce reflection from the laser.

3.1.3 Experimental Plan

This experiment examines five different trailing edge configurations: original trailing edge (OTE), narrow serrations (NSR), wide serrations (WSR), flat plate extension (FPL) and zero length attachment (ZLA). The airfoil specimen was subjected to a flow of Re_c =

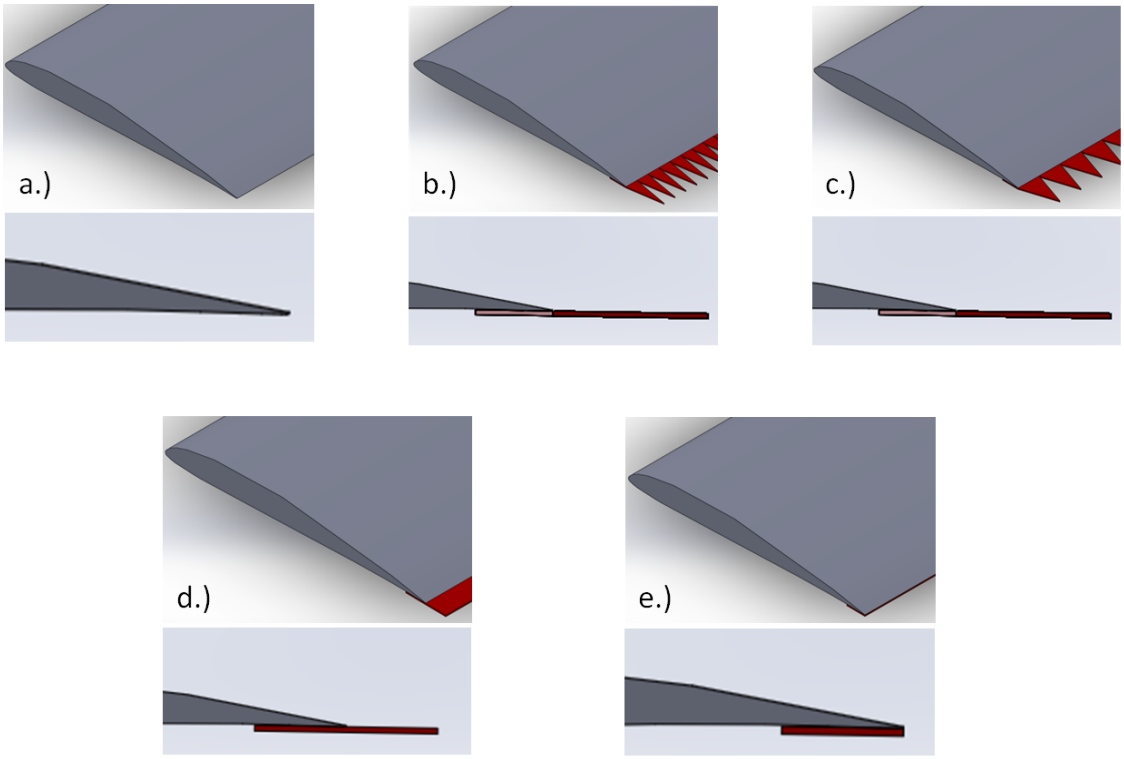

Figure 3.12: The five trailing edge cases examined in the current study. a.) Original trailing edge (OTE) b.) Narrow serration (NSR) c.) Wide serration (WSR) d.) Flat plate (FPL) e.) Zero length attachment (ZLA)

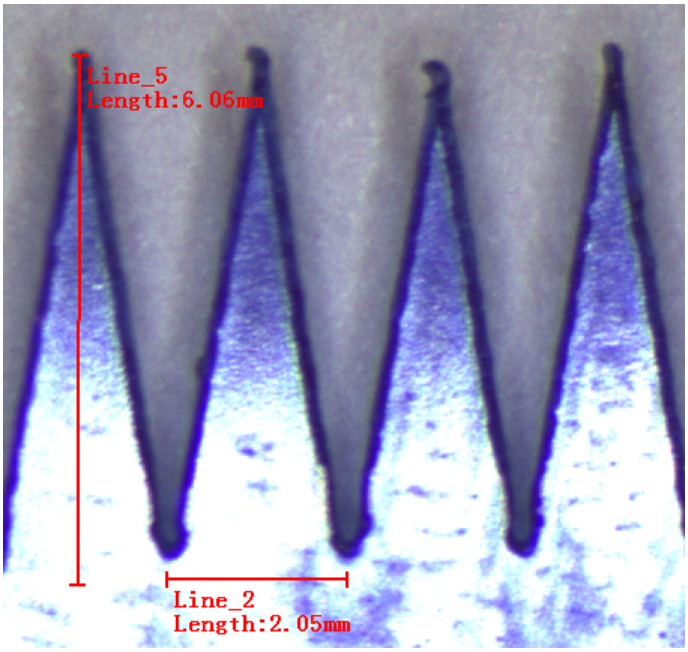

Figure 3.13: Magnified view of the NSR case serrations cut on polyester shim stock

4.0×10^4 in the closed circuit wind tunnel. The placement of the airfoil specimen in the closed circuit wind tunnel was previously shown in figure 3.2.

For the dynamic case, the reduced frequency, k, of the oscillation is defined in equation 3.1:

$$k = \frac{\pi f c}{U_\infty} \tag{3.1}$$

where the reduced frequency k for all experiments in this study is 0.08, f is the frequency of oscillation of 25 Hz, c is the chord length of the airfoil of 25 mm and U_∞ is 24.8 m/s. The airfoil is pitched sinusoidally according to equation 3.2:

$$\alpha = \alpha_{mean} + \alpha_{amp} sin(2\pi f t) \tag{3.2}$$

where α_{mean} is the mean angle of attack (11°), α_{amp} the maximum amplitude of angle of attack during oscillation (11°), t is time in seconds and f is the frequency of oscillation in Hz. The SD-7037 airfoil was previously studied under the same condition with regards its aerodynamic and dynamic stall behaviour by Gharali [6].

Using the microphone equipment described in section 3.1.1.3, each trailing edge configuration were examined under dynamic oscillation and at static angles of attack (0°, 1°, 2°, 3°, 5°, 10°, 15°, 20°). The microphone equipment measured noise from the airfoil at the respective states continuously for 100 s. For the static cases, the acoustic measurement would represent the results from the airfoil while the angle of attack is at steady state. For the dynamic cases, the acoustic measurement would represent the different angles of attack at all phases of the oscillation cycle (instead of a phase-wise condition at a particular part of a cycle). The data acquisation was not configured to match the phase of the oscillation with the acoustic measurements.

Two acoustic measurements of the wind tunnel background noise were measured for each set of experiments with a particular trailing edge configurations: before the airfoil specimen was inserted into the test section and after the airfoil specimen was removed from the test section when the experiments at the various cases are completed. The background noise did not vary significantly during the experiment (before or after) or between the experiments with different trailing edge configurations.

In order to understand the tones observed from experiments in the closed circuit wind tunnel, the same airfoil specimen is placed in the open jet blow down wind tunnel. The experimental condition of the close-circuit wind tunnel is replicated with the expection of the hard wall in order to access the resonance effect. As such, the airfoil is subjected a flow at $Re_c = 4.0 \times 10^4$. The setup of this portion of the experiment was previously discussed in section 3.2.1.3.

3.1.4 Analysis Techniques

The following analysis techniques were used to examine the acoustic measurements obtained from the experiments:

1/3 Octave Spectra The acoustics measurments were examined in 1/3 octave spectra for general comparison. The microphone voltage signal were converted to dynamic pressure values and post processed in MATLAB to derive the 1/3 Octave Spectra. The MATLAB code used a 1/3 octave filter banks conforming to ANSI S1.11 specifications.

Fast Fourier Transform FFT analysis was conducted to obtain the narrowband acoustic spectra of the experimental results; resolving tonal qualities in the frequency spectrum. The acoustic measurements were processed by the code developed by McPhee

[10] (Please see McPhee for the full details of the analysis setup). The FFT results are an ensemble averaged of the acoustic measurements when divided into 100 segments (each segment is 1 s in duration, Hamming window applied). The FFT analysis has a frequency resolution of 0.75 Hz. For the verification experiments conducted at the open jet blow down wind tunnel, the FFT analysis was conducted internally by the B&K Type 2250 sound level meter; examining sound at a frequency between 2-7 kHz at 0.8 Hz frequency resolution. Further details regarding the sound level meter can be found in section 3.2.1.3 and 3.2.4.

Wavelet Analysis Wavelet analysis is later performed to examine the microphone signal with respect to the frequency and time domain. A full description of the method can be found in Torrence and Compo [91]. This technique was used by Probsting et al. [92] in their study of LBL-VS noise to investigate side peaks. For the current experiment, Morlet wavelets were used to compare with the microphone voltage signal using the continuous wavelet transform function from MATLAB wavelet toolbox [93].

Airfoil Self-Noise Estimate The observations from the current experiments for the OTE static cases are compared with airfoil self-noise prediction models. The airfoil self-noise estimates are primarily calculated using the program NAFNoise [94] created by the National Renewable Energy Laboratory (NREL). The program estimates airfoil self-noise in 1/3 octave sound pressure levels using the BPM models [9] along with the turbulent inflow noise models of Amiet [40].

Further regarding to the airfoil self-noise estimates, the BPM model was originally created to predict airfoil self-noise for the NACA 0012 airfoil only. To improve results and applicability of the BPM model for other airfoil profiles, the boundary layers parameters, which are required as inputs to the BPM model, is estimated for the airfoil profile of interest (instead of using the empirically derived boundary layer parameters for NACA 0012 from the study of Brooks et al. [9], which is the default for the BPM model.) This technique is a common practice and was employed by several studies reviewed previously in Chapter 2, yielding responsible results.

The boundary layer parameters are calculated by the program Xfoil [52] in the current study. Xfoil is a 2D airfoil analysis tool using panel method to calculate various aerodynamic parameters for a given set of airfoil profile coordinates. The Xfoil boundary layer calculation function is internally integrated into the NAFNoise software.

In the analysis of the current study, there is a further need to examine the LBL-VS noise estimates from the BPM model when they are calculated from boundary layer inputs

other those allowed by the NAFNoise software programming. As it was not possible to override or modify the internal calculations in the NAFNoise software, the LBL-VS noise model, as shown in eq. 2.4, was programmed into MATLAB. The boundary layer inputs for the specific cases were calculated in XFoil and entered as input in the MATLAB program to calculate the 1/3 octave sound pressure level estimate of the BPM model. Further discussion is found in section 4.2.1.

3.2 Outdoor Experiments

The second portion of this experiment examines airfoil self-noise as it relates to larger scale wind turbines. The experiments were conducted at the Wind Energy Group outdoor wind turbine test site as it is the only suitable experiment platform for this type of experiment. The experimental design uses IEC standards 61400-11 version 2.1 [8] for wind turbine noise measurement as a basis.

3.2.1 Experimental Equipment

3.2.1.1 Turbine Test Site

The Wind Energy Groups outdoor turbine test site is the location where the outdoor field experiments were conducted. Established on the grounds of the Waterloo Regional Emergency Service Training Complex (WRESTC), the site is situated within the city of Waterloo, on the western borders of its city limits.

This site has been the setting of two previous studies [95] [96]. The geography and meteorological conditions of the site are well documented by these sources and a summary can be found in table 3.2.

As it is further explained in section 3.2.1.2, it is of interest to this study to know the dominant wind direction at the site. Lam [95] observed that the winds mainly come from the NW direction. This can be seen from the wind rose from the 10 minute average data of the 50 m MET tower at 30 m and 50 m elevation in figure 3.14. This observation is consistent with the yaw direction of the Wenvor Turbine, which has been found to be predominantly from 260° to 320°. For the purpose of data collection, prior to a site visit, the forecast of wind direction and condition was checked on the website Windfinder [97]. The forecast generally predicted the wind condition on site well.

Table 3.2: Turbine test site details

Dominant Wind Direction	NW [95]
Coldest Temperature	$-30°$ [96]
Average Wind Speed/Maximum Wind Speed	4.61 m/s /30.6 m/s [95]
Weibull scale and shape factor (λ and k) at 30 m	4.97/1.97 [95]
Terrain Description	Site situated on a hill, with forest area to the north and east. Open rural lands with some buildings and obstacles to the south and west.
Terrain Roughness Length	1.74 m [95]
Turbulence Intensity at 30 m	0.205 [95]

For this study, it is also important to understand the sound sources from the surrounding area. In terms of areas surround the WRESTC facility, at the time of the study in 2014 to 2015, the site was neighboured by open rural area and sparsely developed land. During evenings and weekend hours, there was minimal traffic passing by the area. This makes it ideal for acoustic measurements.

However, immediately adjacent to the turbine test site, on the grounds of WRESTC, is a landfill biogas plant (at roughly 100 m from turbine base). The plant operates continuously and it is characterized as a low frequency broadband interference to the site. The wind turbine noise, however, can still be discernable, and hence a study can still be conducted. The plant is accounted for in the background noise.

Next to WRESTC is the landfill site for the Region of Waterloo. During the landfill business hours, there was notable noise from vehicles and machineries which can interfere with noise measurements. As such, all sound recordings were measured during the off-hours of the landfill. This is not an issue during evenings and weekends.

Another common issue and noise source for outdoor sound measurements comes from wildlife. Sources such as birds, insects and vegetations may introduce unwanted and intermittent noise in the sound measurements. The experiment attempted to minimize this by taking measurements during the winter and spring months. Insects are not an issue during this time. This is also advantageous as blade fouling due to insect collisions, as shown in figure 3.15, will not occur. Blade fouling may act as a tripping mechanism affecting the

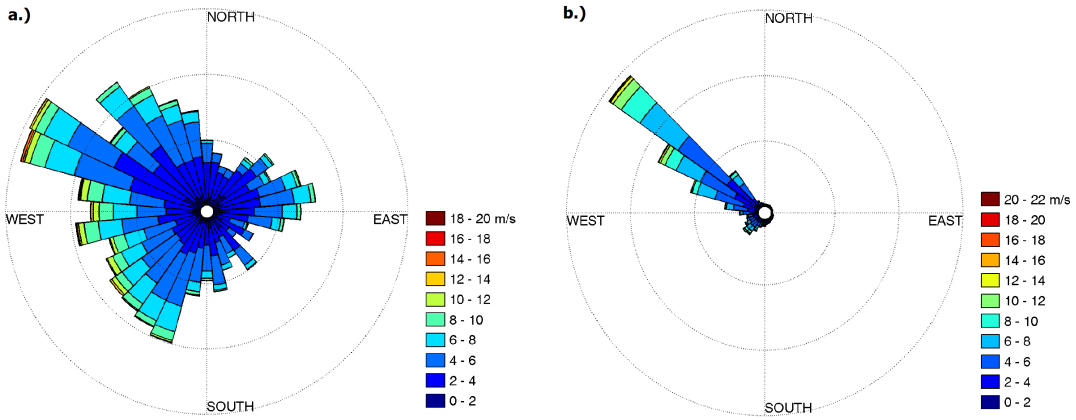

Figure 3.14: Wind rose from the 50 m MET tower. a.) at 30 m b.) at 50 m. Figures originally published in Lam [95]

results of experiments. Some of the experiments were conducted when noise from birds on site can be an issue. The sound measurements were extensively screened for intermittent bird calls.

3.2.1.2 Wenvor Turbine and Instrumentation Network

In this section, the details of the wind turbine and instrumentation found at the Wind Energy Group outdoor turbine test site will be discussed.

The wind turbine examined in this study is a 30 kW passive yaw wind turbine manufactured by Wenvor Technologies Inc [98]. The turbine is shown in figure 3.16 and the turbine specifications are summarized in table 3.3.

The turbine and its surrounding environment are monitored by a network of instruments connected to a PC-based data acquisition (DAQ) system. The instruments are located onboard the turbine, at the 50 m Metrological (MET) Tower that is 100 m south of the turbine and in the General Electric G30 programmable logic controller of the turbine situated at the control center. An existing list of parameters monitored on the turbine and by instrumentation in the surrounding area is shown in figure 3.17.

Many of the instruments described in figure 3.17 were also used by Swytink-Binnema in his study. For details on the specifications and their development, please see Swytink-Binnema [96], Tam et al. [99] and Swytink-Binnema et al. [100].

Figure 3.15: Insect fouling on the leading edge of the wind turbine blade

For this experiment, the existing monitoring system and sensor network is modified to adapt to the current experimental plan. A 10 m meteorological (MET) Tower was installed upstream of the turbine and aligned with the dominant wind direction of the site. The location of the MET tower was selected at a location 25.5 m away from the base of the tower, bearing 283°. The locations are found on site using a Sokkia GRX1 GPS unit with accuracy within 0.01 m. Placement closer to the tower would allow for a wider angle of coverage but there was concern with the tower being too close to the turbine tower guy wire points in the event of falling. At this location, the tower would be in the allowable region outlined in figure 2.8b when the wind turbine yaw direction angle is between 260° to 305°. An upstream view of the turbine, the 10 m MET tower and the 50 m MET tower is shown in figure 3.18. The 10 m MET Tower is the small tower located at the right of the image.

On the 10 m MET tower, a NRG #200P vane and NRG #40C cup anemometer were installed to monitor on the upstream wind. The instruments and specifications can be seen

Table 3.3: Specifications of the Wenvor WTI-30 turbine

Operating Blade Pitch Angle	2.7°-2.8°
Number of Blades	2
Rotor Diameter/ Tip Speed	10 m/ 62.8 m/s
Yaw	Passive controlled
Re_c	around 1.0×10^6 at the outer diameters of the blade
Rotor rpm	122 rpm during grid connection, up 140 rpm during freewheel at high winds, 0-122 rpm during low wind freewheel
Hub Height	30 m
Pitching Mechanism	Passive controlled

in table 3.4.

Potential microphone measurement positions were found downwind of the turbine, as described in figure 2.8a. The primary measurement location is located at 37.5 m away from the base of the tower, bearing 110.85°. ϕ, the angle subtended by the wind turbine and the tower to the microphone measurement position (as defined in figure 2.8a), is 38°.

This location allows the wind turbine yaw direction and upstream wind direction to vary between $275° - 305°$ and be within $\pm 15°$ alignment of the measurement location. During the experiment, there are further considerations with this setup location. The discussion is continued in section 5.2.1.

The location of the Wenvor wind turbine, 50m MET tower, control center, 10m MET tower and the primary microphone measurement position can be seen in the aerial image shown in figure 3.19.

The National Instruments Labview based data acquisition program used in this experiment was created by Swytink-Binnema [96]. Minor modification has been made to the program to accommodate new additions. Instruments on the MET tower replaced two of the inputs originally meant for the instrumentation on the turbine tower in the Swytink-Binnema setup. Specifically, the wind vane located on the 10 m MET tower has replaced the 20 m RMY wind vane input on the USB DAQ. The cup anemometer on the 10 m MET tower has replaced the 10 m cup anemometer of the turbine tower in the USB DAQ input. Two 50 m signal cables ran from the instruments on the 10 m MET tower to the

Figure 3.16: Wenvor WTI-30 30 kW wind turbine. Image source: [98]

turbine base enclosure and connected to the DAQ during the experiments. The Tower USB acquisition within the data logging program has been reconfigured to sample at 2 Hz. This allows the AC sine reading program to sample more 0 V passage during the sample time, and increase anemometer resolution to 0.5 m/s.

During the experiments, there were several issues that arose with the onsite sensor and DAQ system. They are as follows:

- The wind turbine hub wind speed sensor was blown off and was destroyed. As a result, hub wind speed data could not be examined in this study.
- The wireless system has been noted to disconnect during periods of heavy chattering and strong vibrations of the turbine. This is usually seen in high wind/ cross-wind condition. While there were interruptions to data collection during these moments, they were intermittent and did not cause an issue to the overall data collection process.
- The 10 m cup annemometer on the 10 m MET tower was giving erroneous readings on March 15, 2015. For comparison with experimental results from the other days of experiments, the 20m RMY annemometer data was used in the analysis of data for the current study.

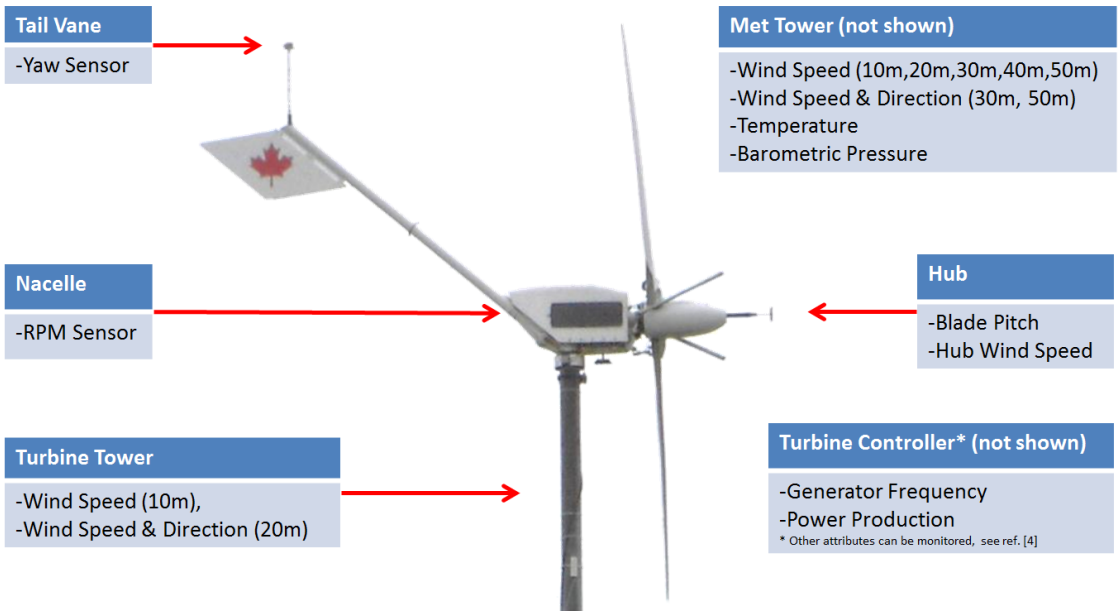

Figure 3.17: List of instruments located at the Wind Energy Group wind turbine test site. Source: Tam et al. [99]

The yaw sensor was previously noted by Swytink-Binemma [96] to be problematic during his experiments. However, it was not found to be an issue during collection of data in this thesis. While the exact cause of the problem has not be identified, it is suspected that improved weather sealing and favorable weather conditions has allowed the sensor to function during this time.

3.2.1.3 Sound Level Meter

Due to the harsh environment at the turbine test site during favorable experimental conditions, the microphone setup used for the controlled environment experiments was not suitable for use in this set of experiments. Instead, this experiment uses the B&K Type 2250 sound level meter [102] equipped with a Type 4189 12.7 mm (0.5") microphone.

The B&K Type 2250 Analyzer and the Type 4189 microphone are Class 1 microphone instruments, capable of real time analysis, from one input source, of overall sound pressure level (OASPL), various fractional-octave spectrum and FFT as well as any statistical and weighting considerations. The system automatically adjusts gain levels, hence there is no concern for overload during recording for playback.

Figure 3.18: View of the Wind Energy Group wind turbine test site from the north. For the towers shown, from left to right: wind turbine tower, 50 m MET tower, 10 m MET tower

For this experiment, the sound level meter was set on logging function, which continuously records and calculates, in a predetermined interval, the A-weight sound pressure level, third octave spectra and other statistics during the operation of the turbine.

The sound level meter is independent of the turbine site DAQ system. As such, in order for the data from both systems to be matched and comparable, both systems must be synchronized. This is done manually and checked hourly during the experiments on site. The systems were synchronized within 1 s during the experiments.

Table 3.4: Specifications of Instruments found on the 10 m MET tower

Make/Model	NRG/#40C Cup Anemometer	NRG/#200P Wind Direction Vane
Variable Measured	Wind Speed (Non-directional)	Wind Direction
Signal Type	AC Sine Wave of variable frequency f_{AC} = 0-125Hz	Linearly variable DC voltage, from potentiometer and supplied 5 VDC
Calibration Curve	Cup Anemometer Reading $U_{cup} = 0.765 f_{AC} + 0.35$	Linear, proportional to supplied voltage
Range	1 to 96 m/s	0-360 degrees, dead band up to 8 degrees
Accuracy	$\pm$ 0.14 m/s at 10m/s	Within 1% linearity

3.2.1.4 IEC Ground Board

In order to conduct noise measurements at the outdoor site with the sound level meter, it is necessary to provide an acoustically hard surface for sound to be uniformly reflected to the microphone. The design for such a ground board is outlined in the IEC standard [8].

The ground board used in this experiment is fabricated from 12.7 mm (0.5") thick plywood 1 m in diameter. The board was then sealed with a vanish coating to protect the wood from moisture and snow. A semi-hemispherical primary windscreen was made, by cutting in half, from a 90 mm diameter B&K UA-0237 windscreen.

For the secondary windscreen, a 0.5 m in diameter semi-hemispherical metal frame was fabricated from 4.8 mm (0.1875") carbon steel rod. This is to ensure the windscreen is of sufficient rigidity and mass as not to move or bend during high wind events. Open cell foam matching specifications [8] was used to cover the windscreen. The foam was cut into wedge shapes and sewn to the frame with narrow gauge cotton thread.

While validation of the secondary windscreen to ensure there is no effect on the frequency response is recommended, a suitable testing procedure was not developed or obtained to examine the constructed windscreen. However, as it was made following the description from the IEC standard, it is not expected to introduce significant deviations.

To remove the microphone from the sound level meter so it can be placed on the ground

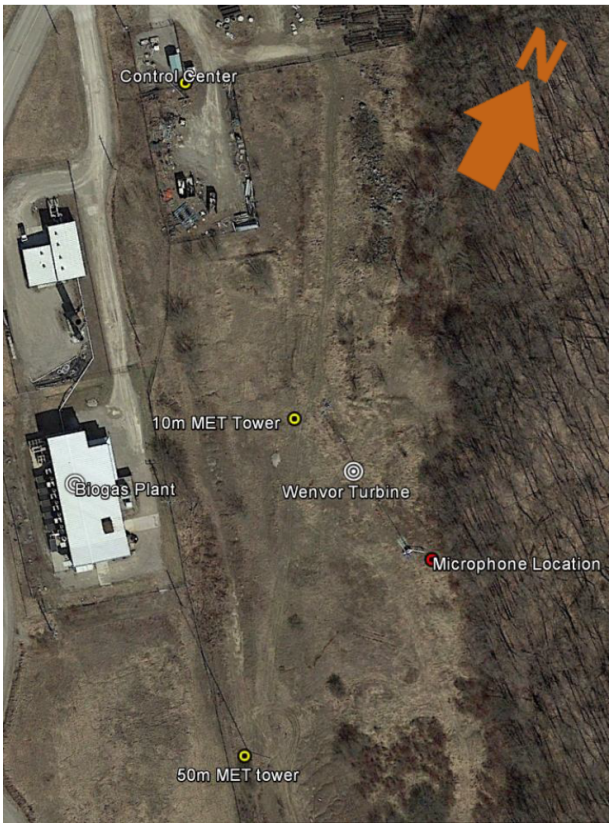

Figure 3.19: Satellite image of the Wind Energy Group wind turbine test site. Source: Google Earth [101]

board, a 3 m microphone extension was used. The typical setup of the ground board with the sound level meter is seen in figure 3.20.

3.2.2 The Wenvor Wind Turbine Blade

In the outdoor portion of this study, the test specimen of interest is the Wenvor wind turbine blade. Although the airfoil profile and aerodynamic design is unknown, the blade profile at various radial distances were digitized by Gu [103], with chord length measured in Swytink-Binnema et al. [100]. The profiles can be seen in figure 3.21. The equation for the chord length at various radius along the Wenvor turbine blade is shown in equation 3.3:

Figure 3.20: Ground board with secondary windscreen

$$c^2 = \left[430^2 - 320000(\frac{r}{R} - 0.27)^2\right]^{0.5} \tag{3.3}$$

where c is the chord length in m, r is the radial distance of interest and R is the length of a single blade ($5m$).

The digitized airfoil profiles and chord length information are useful for estimating the sound pressure level of airfoil self-noise generated by the wind turbine blade. Further details can be found in section 5.3. These sound pressure level estimates can aid in the interpretation of data collected during the experiments and can also aid in the design of trailing edge serrations for the Wenvor wind turbine.

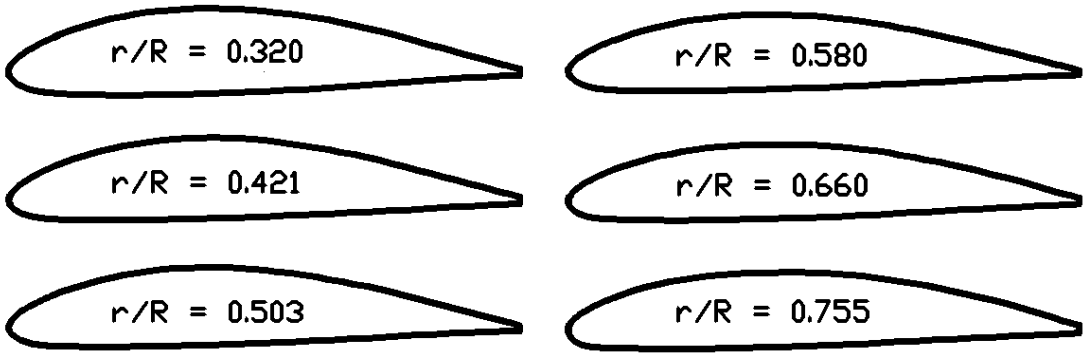

Figure 3.21: Airfoil profiles of Wenvor wind turbine blade at various radial distance (r/R). Profiles coordinates digitized from the Gu study [103]

3.2.3 Experimental Plan and Rationale

Experimental design of aeroacoustic experiments encompasses the operating conditions that the Wenvor turbine is expected to encounter during its operation. A special emphasis is given to the operating point (when the turbine is grid-connected, rotating at 120 rpm with a blade pitch angle of 2.7° to 2.8°), where the turbine was designed to function.

While the IEC standard provides a procedure to collect sound measurements for wind turbines, due to the passive nature of the Wenvor turbine, some modifications were made. By observation, the yawing nature of the Wenvor Turbine is very dynamic. Averages taken within 1 min. can contain large variations which may not be representative of the events occurring during that time. Migliore et al. [54] has noted this phenomenon in their studies and have suggested collecting data within 10 s averages. Examination of the wind turbine yawing behaviour has found that 1 min. averages vary too excessively and a 10 s interval is more suitable, as in the case of Migliore [54]. As such, this is adopted in the current study.

The background noise measurements are collected in between times of turbine operation in order to collect noise data at similar wind speed range. As a matter of practicality, due to the passive nature of the wind turbine, it is difficult for the turbine to achieve operating pitch angle at will. The unpredictable nature of this system has the turbine reaching its operating pitch in matter of seconds to hours. As the operating point is a subject of interest in the study of this turbine, some measurements have been taken back to back without taking background noise inbetween (which would require stopping the turbine/braking)

in order to collect sufficient noise data at particular blade pitch angle and wind speed. Background noise is subsequently collected and all wind speed background noise data are still well represented in this study.

Collection of data occurred during Spring to avoid or minimize noise associated with insects, birds, and vegetation. These concerns were explained previously in section 3.2.1.1. While some noise associated with vegetation and birds was found, the sound recording was analyzed extensively and any intermittent effects have been noted and excluded. Consistent and continuous contributions which did not originate from the turbine are be accounted for with the subtraction of background noise and hence is not a concern.

3.2.4 Analysis Techniques

The outdoor experiments examined the combined (wind turbine and background) and background noise with respect to the OASPL and 1/3 octave band sound pressure levels. The calculations of the 10 s average values were performed internally by the Bruel and Kjaer Type 2250 sound level meter, which was previously introduced in section 3.2.1.3. This portion of the study examines the OASPL and 1/3 octave sound pressure levels with an A-weighting applied (see 2.9).

During the experiment, several unplanned narrowband acoustic spectra (FFT) measurements were performed. The sound level meter also conducted the FFT analysis internally. The FFT analysis examined at the sound frequency between 0-20 kHz with a frequency resolution of 3.25 Hz.

Further details regarding to the operation of the sound level meter can be found in the operations manual [102].

For the 10 s OASPL and 1/3 octave sound pressure level data, the results are further organized in integer wind speed bins for the analysis. The bins span ± 0.5 m/s about the integer wind bins; with a wind speed bin only being valid if there are data points above and below the integer value. The binned integer values are then fitted to a second order regression to determine the sound pressure level at a given integer wind speed (see [8]).

The background corrected wind turbine noise sound pressure level at a particular wind speed (denoted as L_{bk-A} previously in equation 2.8) is then derived from logarithmically subtracting the second order regression values of the combined noise measurements with their background noise counterparts. Given when the wind turbine noise (L_{bk-A}) is well resolved from the background noise, the sound power level of the wind turbine can be calculated by equation 2.8.

For some further analysis with respect to different parameters on site, the integer wind speed bin data is further divided with respect to the different variables (ex. upstream wind direction, yaw direction). As the values in the bins were found not to be Gaussian in nature, bootstrap sampling was used to resample the data amd determine some statistics required for their analysis. This was accomplished using the MATLAB function bootstrp (1000 sets of resample).

The uncertainties related to the regression analysis and instrumentation are further discussed in Appendix A.

Chapter 4

Experiments in a Closed Circuit Wind Tunnel

The following chapter presents the results of experiments conducted at the closed circuit tunnel of the Wind Energy Group in the University of Waterloo. As discussed earlier, this portion of the experiments examines airfoil self-noise in a controlled environment under both static and dynamic conditions. The purpose of these experiments is to understand the effects of dynamic conditions on airfoil self-noise as it relates to small scale wind turbines. Because LBL-VS noise can be found on small scale wind turbines at low Reynolds number regime, it will be the focus in this portion of the study. The details of the experimental setup can be found in section 3.1. A review of the LBL-VS noise generation mechanism and its characteristics can be found in section 2.1.

4.1 Preliminary Assessment

Before the experiments on the SD-7037 airfoil can be analyzed, it is important to identify and characterize any potential effects the wind tunnel and the experimental setup have on the microphone measurements. This way, the noise characteristics that are native to the wind tunnel background and the noises that are artefacts of the experimental setup would not be attributed to the mechanism of interest. As well, if the experiment setup alters the behaviour of the mechanism of interest, the effect should be identified and taken into account during the analysis.

4.1.1 Wind Tunnel Background Noise

To understand the various noise sources present in the wind tunnel, the narrowband acoustic spectra for the wind tunnel background noise are examined. A typical background noise acoustic spectrum was previously shown in figure 3.6. The following observations can be made:

- In general, the sound pressure level magnitudes of the background noise decrease with increasing sound frequency.
- At low frequencies, the wind tunnel background noise has high sound pressure levels due to airflow noise and mechanical noise from wind tunnel components. At frequencies of 1 kHz or less, there are multiple tones found in the spectra. The highest magnitude was observed at nearly 90 dB. A region of elevated levels found near 200 Hz corresponds with the fan blade passing frequency. Comparing the tunnel background noise with the airfoil noise acoustic spectra, there are very few differences below 2 kHz. Indeed, the airfoil is not expected to emit noise at significant levels below 2 kHz. As such, the airfoil acoustic spectra below 2 kHz should resemble the background noise. For this study, LBL-VS noise is found at frequencies well above 2 kHz, the high levels of background noise observed do not impact the current study objectives.
- Between the frequencies of 2.2 kHz to 2.3 kHz, the wind tunnel background noise sound pressure levels abruptly increase by nearly 15 dB. Again, as LBL-VS noise are not found at these frequencies, this has no impact on the current study.
- At frequencies greater than 2.3 kHz, the spectrum does not contain any notable tonal noise features. The noise levels at this range are less than 40 dB.
- As discussed previously in section 3.1.3, the background noise of the wind tunnel is measured after every set of measurements. The results between the different background measurements have excellent repeatibility.

4.1.2 Considerations with Experimental Setup

This section examines the various noise generation mechanisms and other experimental setup artefacts that were previously discussed in earlier chapters. Assessing the noise generation mechanisms (aside from LBL-VS Noise) that could also be present when the

airfoil is in the wind tunnel at experimental conditions, the following conclusions can be made:

TBL-TE and Separation/Stall noise is expected to appear at higher angles of attack given the airfoil boundary layer would eventually transition from laminar to turbulent regime. As reviewed in section 2.1.2, these noise mechanisms are characterized as a broadband increase in the acoustic spectrum. The onset of TBL-TE noise would be accompanied by the decrease and disappearance in tonal noise quality from LBL-VS noise. This effect is naturally occuring and does not interefere with the analysis of the current study.

Turbulence Inflow Noise is unlikely to be an issue as the turbulence intensity of the closed circuit wind tunnel is relatively low comparing to outdoor environments. As well, turbulent inflow noise is broadband in nature, which like TBL-TE noise, is a mismatch to the tonal qualities of LBL-VS noise.

Blunt Trailing Edge Noise is a noise generation mechanism that produces tonal noise components. The airfoil was machined such that the trailing edge sharpness satisfies Blake's bluntness criterion [38]. Blunt trailing edge noise is not expected to occur. Likewise, for the trailing edge extension cases, the serration extensions 0.127 mm (5 mil) in thickness were selected to ensure bluntness noise was not an issue. Comparing the acoustic spectra of the FPL case with the OTE case, as seen later in section 4.3, shows there are no additional tones created by the change in thickness of the trailing edge. This suggests blunt trailing edge noise is also not an issue for the trailing edge extension cases.

Tip Noise is not expected to be present as the closed circuit wind tunnel contains hard walls which block the flow of air from the pressure to suction side of the airfoil.

The presence of acoustic resonance in the hardwall wind tunnel test section is a concern as well. During the experiments, it was not apparent that the airfoil emitted any distinct tonal noise at high angles of attack. This would be consistent with known airfoil boundary layer behaviour. However, from the analysis of the experimental data, it was found that small tones persist at high/stalled angles of attack in small sound pressure level magnitudes. These tones were found to remain at roughly the same frequencies where tonal noise was prominently observed at lower angles of attack. Further details are found in section 4.2.2. This suggests a resonance effect is present in the current setup.

In the previous study conducted by Orlando [85], it was concluded that Parker β resonance was present in the experimental setup. However, it is believed that Parker β

resonance is not the cause of the observed tonal noise in this case. In this experiment, the airfoil was made sufficiently small such that the chord to pitch ratio of the current setup is below the values for Parker β resonance onset threshold. In this experiment, the prominent tones located at 3.4 kHz and 4.1 kHz are well above the highest values of Parker β resonance predicted.

To determine the nature of the tones, the airfoil was placed at low angles of attack in the open jet wind tunnel of the University of Waterloo. In the absence of a hard wall, the narrowband acoustic spectrum of the airfoil shows two tonal noise components are present. The result is shown in figure 4.1. These two prominent tones are located approximately at the same frequencies to those found with the airfoil in the closed-circuit wind tunnel at static low angles of attack and the dynamic case. This suggests the tones are caused by the LBL-VS noise generation mechanism.

Nevertheless, the presence of the tones at higher angles of attack requires further explanation. Even if the current setup is not affected by Parker β resonance, other types of resonance can exist in this experimental setup.

Discussed previously in section 3.1.2.1, Ikeda et al. [88] found two types of resonance discussed in their study: anti-symmetric and symmetric resonance. The first mode frequencies are respectively calculated to be 1.1 kHz and 2.2 kHz for the current study. The 3.4 kHz tone would roughly corresponds to the 2nd mode of anti-symmetric resonance. The 4.1 kHz tone could be the 2nd mode of symmetric resonance, however, the agreement is very poor. Likewise, the weaker tones found at higher frequencies poorly correspond to higher modes of resonance.

Given these observations, it is possible that the observed tones from the current study are affected by resonance. This should be taken into consideration in the analysis of the experimental data.

4.2 Airfoil Self-Noise under Static OTE Case

Since the preliminary assessment has identified the noise characteristics relevant to the current study, the following section discusses the observed behaviour of these noise characteristics with respect to different static angles of attack. The understanding of the noise characteristics under different static angles of attack can aid in the understanding of the results observed during the dynamic case.

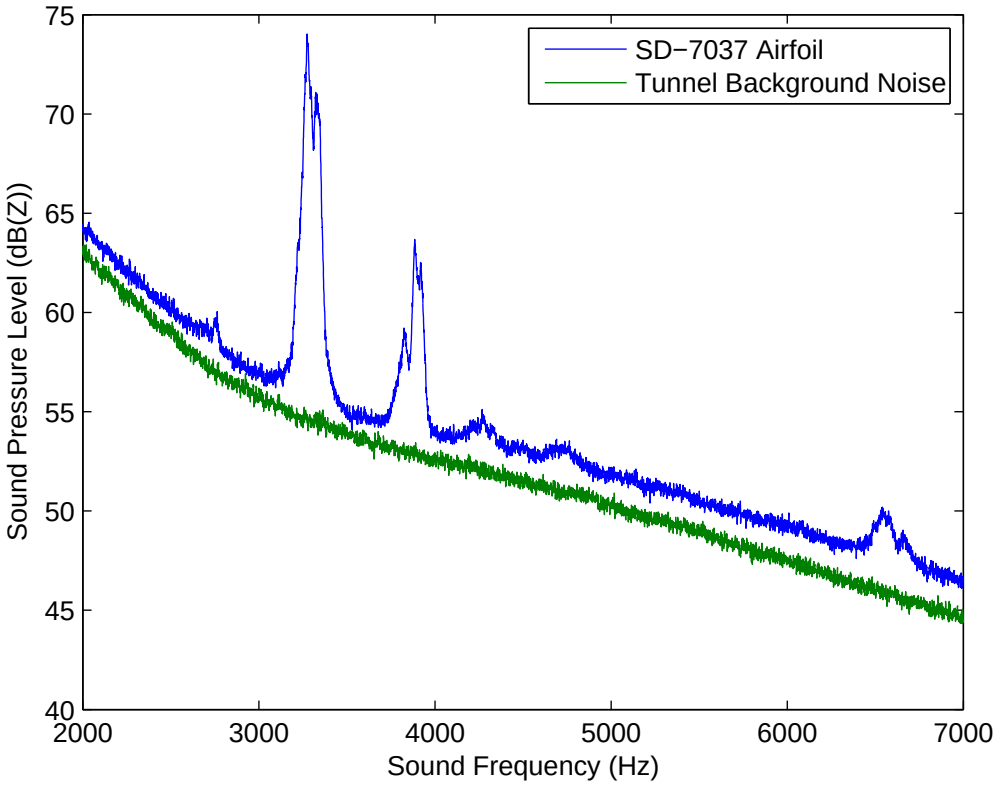

Figure 4.1: The acoustic spectra of the SD-7037 airfoil in the open jet blow down wind tunnel at $Re_c = 4.0 \times 10^4$.

4.2.1 1/3 Octave Spectra

Figure 4.2 shows the 1/3 octave sound pressure levels of the SD-7037 airfoil at low angles of attack (0° to 5°). As the airfoil noise was mainly found between the bands of 2 kHz to 6.3 kHz, those results are displayed in the figure. For comparison, the sound pressure levels for the wind tunnel background noise are also included.

For all the 1/3 octave bands shown, the sound pressure levels tend to increase from 0° until their maximum levels at 1° or 2°. Thereafter, the sound pressure levels tend to decrease with increasing angles of attack. This behaviour is well observed with LBL-VS noise studies that were previously reviewed. For most of the 1/3 octave bands shown, the sound pressure levels at 5° are at higher levels than their counterparts at 3°. This behaviour could be attributed to resonance effect.

A different trend is seen at the 2 kHz band where the sound pressure levels do not change significantly with changing angle of attack. As discussed previously, the airfoil noise at frequencies below 2 kHz is not significant and the airfoil acoustic spectra are obscured by the wind tunnel background noise. The 2 kHz band represents sound between the frequencies between of 1780 Hz and 2240 Hz. As such, a flat response with changing angles of attack is expected.

The highest sound pressure levels of the airfoil noise are seen at 3.15 kHz and 4 kHz bands. In section 4.2.2, the narrowband acoustic spectra will show that the high sound pressure levels at these bands correspond with the observed tonal noise at those frequencies.

The 1/3 octave spectra for the airfoil at higher angles of attack (10°, 15°, 20°) are shown in figure 4.3. Comparing with the acoutic spectra at low angles of attack, the sound pressure levels are generally lower in magnitude. The sound pressure levels at 3.15 kHz and 4 kHz bands for the high angle of attack acoustic spectra are also not significantly above their neighbouring bands as seen with some of the low angle of attack cases. As seen with the narrowband acoustic spectra in the following section, this is due to the reduction or effective disappearance of tonal noise at high angles of attack.

Between the different high angles of attack, it can be seen that the sound pressure levels increase slightly (1-3 dB) as the angle of attack increases. This behaviour is likely attributed to the increase in broadband noise as the airfoil enters further into stall.

Due to the resonance effect noted earlier in section 4.1.2, the observed 1/3 octave spectra should be compared with known prediction models to see if there are changes in the behaviour. The 1/3 octave spectra are compared with estimates calculated from the program NAFNoise [94]. The airfoil self-noise models of Brooks et al. [9] (the BPM

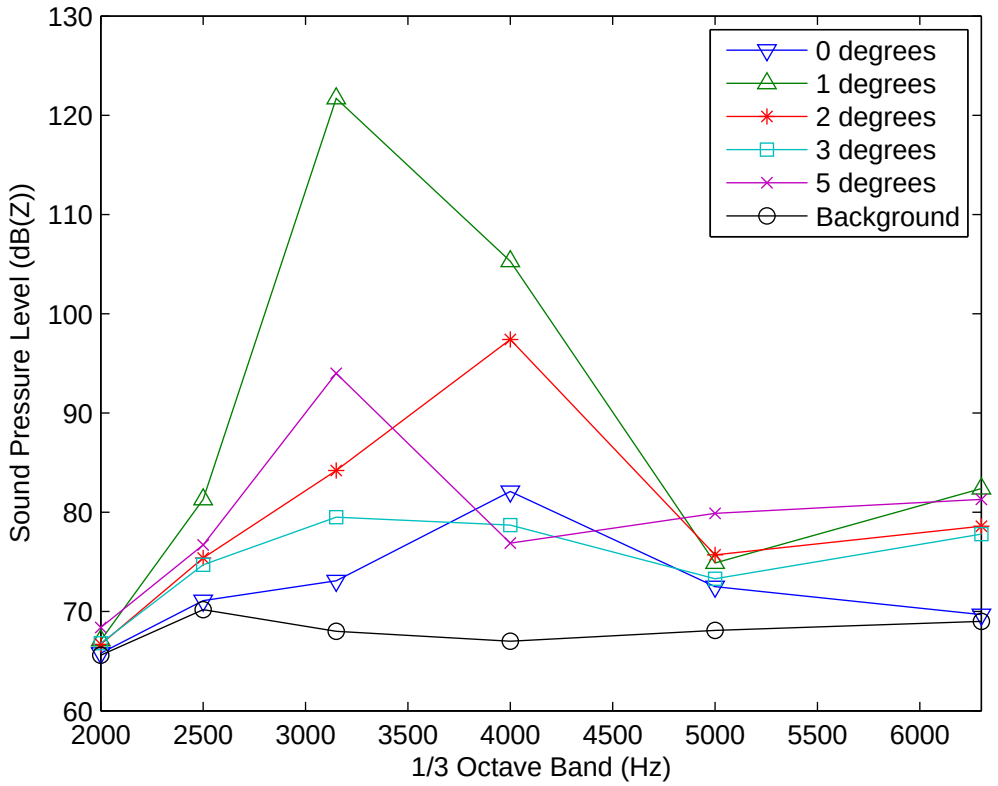

Figure 4.2: 1/3 octave spectra of measured airfoil noise in the closed circuit wind tunnel at low angles of attack.

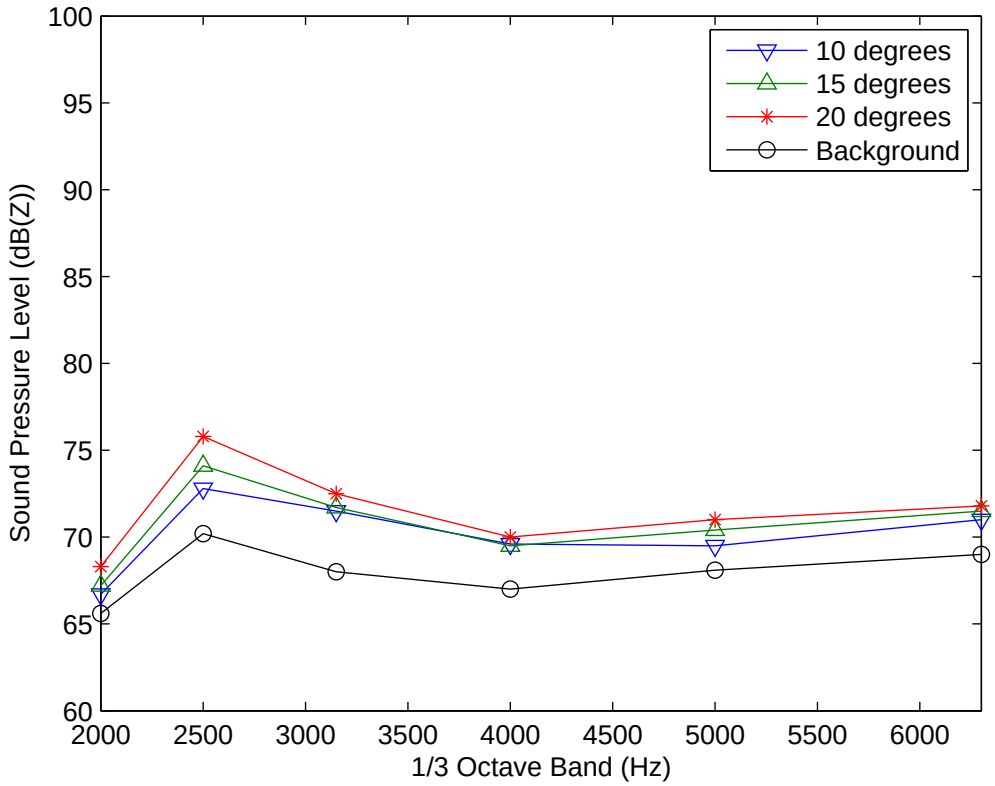

Figure 4.3: 1/3 octave spectra of measured airfoil noise in the closed circuit wind tunnel at high angles of attack

models) and turbulent inflow noise model of Amiet [40] are selected for use for the current analysis. The boundary layer conditions are calculated using XFoil [52].

Figure 4.4 shows the NAFNoise estimates for the airfoil at low angles of attack of 0°, 1°, 2°, 3° and 5° respectively in sub-figures a to e. Each type of noise associated with the airfoil is calculated individually: TBL-TE noise (on the pressure side (TBL-TE,PS) and suction side (TBL-TE,SS) separately), LBL-VS noise, Separation/Stall Noise (SEP) and Turbulent inflow (TI) noise.

Although empirical models exist for tip noise, it is not calculated by NAFNoise. For the current experimental setup, the ends of the airfoil are blocked by the test section walls. As such, the estimation of the tip noise is unnecessary. Likewise, blunt trailing edge noise is also not estimated in this study because the airfoil is manufactured with a sharp trailing edge. An initial estimate for a small blunt trailing edge thickness value has found the values to greatly disagree with experimental observations. Hence, blunt trailing edge noise is discarded from further consideration.

By initial inspection, the estimates appear to differ greatly from the experimental results. To begin, the estimated sound pressure levels for various airfoil noise components do not sum to similar levels as the sound pressure levels observed from the experiment. Comparing the values from figure 4.2 and figure 4.4, the estimated levels are orders of magnitude below the experimental counterparts.

As well, given the Reynolds number of the current study, it is expected that LBL-VS noise would be a dominant component of the estimated sound presure levels. In figure 4.1, the prominent tones attributed to LBL-VS are noted to be the major contribution to the measured sound pressure levels in 3.15 kHz and 4 kHz 1/3 octave bands. The estimated LBL-VS noise should exhibit similar behaviour. However, this is found not to be the case in figure 4.4. The estimated LBL-VS noise is only prominent at 0°. With increasing angles of attack, the LBL-VS sound pressure levels are obscured by other types of airfoil noise. The location of the highest estimated sound pressure level for LBL-VS noise is located at frequencies of 5 kHz or higher. This is inconsistent with the maximum sound pressure levels at 3.15 kHz and 4 kHz observed from the experiments.

Because LBL-VS noise estimates behave differently with sound pressure levels generally lower than other noise sources, the total sound pressure levels of all estimated airfoil noise sources are largely influenced by two other noise sources instead: TBL-TE noise on the pressure side and the TI noise. It should be noted that separation/stall noise and TBL-TE noise on the pressure side also have comparatively low sound pressure level values. Their contributions to the total sound pressure levels are minimal as well.

TBL-TE noise on the suction side and TI noise sound pressure levels remain relatively

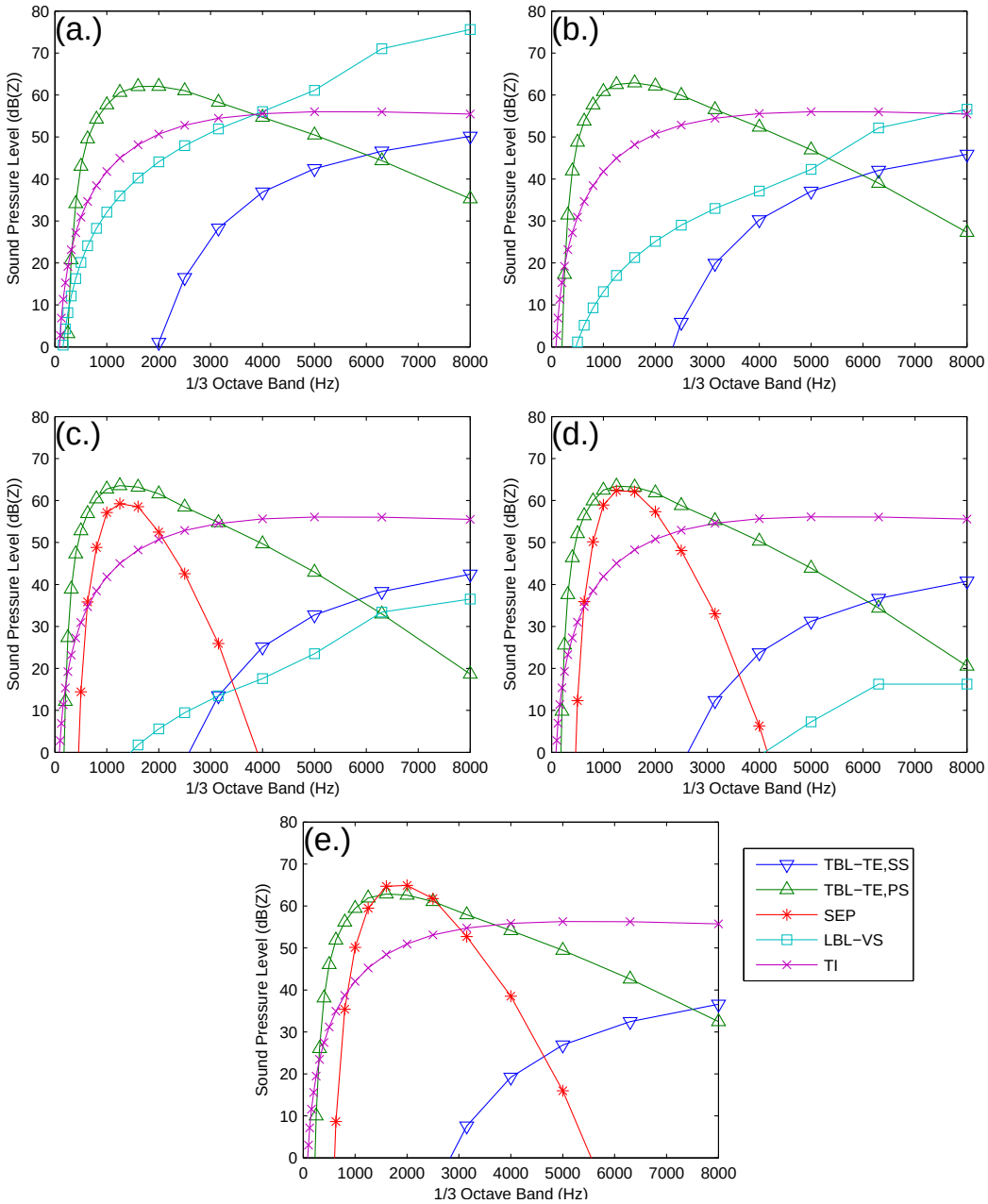

Figure 4.4: NAFNoise estimates at various low angles of attack for SD-7037 airfoil: a.) 0°, b.) 1°, c.) 2°, d.) 3°. e.) 5°

the same at all angles of attack. As such, the change in total sound pressure level is flat with respect to changing angles of attack. This trend is significantly different than the tonal influence results seen in the experiments.

From these differences, it appears NAFNoise does not accurately estimate the results of the experiment. On initial inspection, it may be reasonable to attribute the differences to the resonance effect. However, upon further consideration, it is believed that the BPM models [9] to be the source of the discrepency.

As reviewed previously in section 2.1.1.2, the LBL-VS prediction model uses δ_p, the trailing edge boundary layer thickness on the pressure side, as a scaling parameter in estimating the LBL-VS noise. In a review of past studies of different airfoils, this may seem appropriate as many studies have found LBL-VS noise to originate from the pressure side of the airfoil. However, for the current study, it is believed that tonal noise originates from the suction side of the airfoil.

Suction side noise generation has recently been seen in the studies of Probsting and Scarano [29] and Ikeda et al. [27]. Like the current study, their studies were conducted below Re_c of 10^5. In contrast, most other studies are conducted at a Reynolds number well above 10^5. LBL-VS noise is typically found to be generated on the pressure side of the airfoil in those studies.

From Probsting and Scarano [29], with decreasing Reynolds number, the boundary layer transition point tends to shift towards the pressure side trailing edge and away from the suction side trailing edge. At some point, favourable conditions for boundary layer separation and vortex formation needed for LBL-VS noise generation are no longer found on the pressure side. At the same time, the condition to develop LBL-VS noise appears on the suction side with transition point shifting forward. As such, it is reasonable to find LBL-VS noise on the suction side given the low Reynolds number flow of the current study.

To determine if LBL-VS noise orginated from the suction side in the current study, a boundary layer trip was applied near the leading edge on the suction side of the airfoil. The tonal noise disappeared when boundary layer trip were placed there. When a boundary layer trips was placed on the pressure side, the tonal noise remained. This indicates a laminar boundary layer mechanism located on the suction side of the airfoil is responsible for the tonal noise observed.

Since using the pressure side boundary layer parameter is not suitable for the current setup, the acoustic spectra estimates are recalculated using suction side boundary layer parameters. The results are shown in figure 4.5. In contrast with the original NAFnoise results, TBL-TE noise on the pressure side and TI noise are not major contributors to the total sound pressure level for all low angles of attack. TBL-TE noise is only relevant at

low frequencies and at high angles of attack as LBL-VS noise decreases. TI noise is only relevant at higher angles of attack at higher frequencies.

For LBL-VS noise, because it is scaled with boundary layer thickness, the increased thickness of the suction side boundary layer greatly affects the results. The new estimates are found to have the highest sound pressure levels at lower frequency bands. The sound pressure levels are also much greater in magnitude compared with the original estimates. LBL-VS noise is now found to be the dominant noise for all low angles of attack. The sound pressure levels for LBL-VS noise are at similar levels in comparison to the experimental results in figure 4.2.

For further comparison, the total 1/3 octave sound pressure levels at each low angle of attack are plotted in figure 4.6. The original NAFNoise estimates, the suction side NAFNoise estimates and the experimental results (shown previously in figure 4.2) are included in the figures. For the original NAFNoise estimates, the results are orders of magnitude below the experimental values. The plot also shows the sound pressure levels remain relatively flat at 60 dB with changing angles of attack. As noted earlier, they do not match the experimental results well.

For suction side NAFNoise estimates, the total sound pressure levels for each band are seen to be more closely matched with the experimental results. Although there are some discrepencies present, the general trend of the experimental results is followed by the suction side based estimates.

The magnitudes of the sound pressure levels where the main tones are found are not well predicted. However, the trend where the maximum sound pressure levels can be found are in reasonable agreement. For example, at 1°, the maximum sound pressure level of the estimate is 26 dB below the maximum sound pressure level observed in the experiment. However, the maximum sound pressure levels were predicted to be near 2.5 kHz and 3.15 kHz, where it was found at 3.15 kHz in the experiments. In general, the highest sound pressure levels for the various angles of attack are observed between 2 kHz to 3.15 kHz for the suction side NAFNoise estimates; with the peak level tending to shift to lower frequencies with increasing angles of attack. The peak levels of the experimental results are at slightly higher frequencies than the estimates: at 3.15 kHz or 4 kHz.

For the experimental results, the sound pressure levels for bands above 3 kHz at 5° are much larger than the suction side NAFNoise estimates. This difference, as well as the others noted above, may be attributed to the resonance effect.

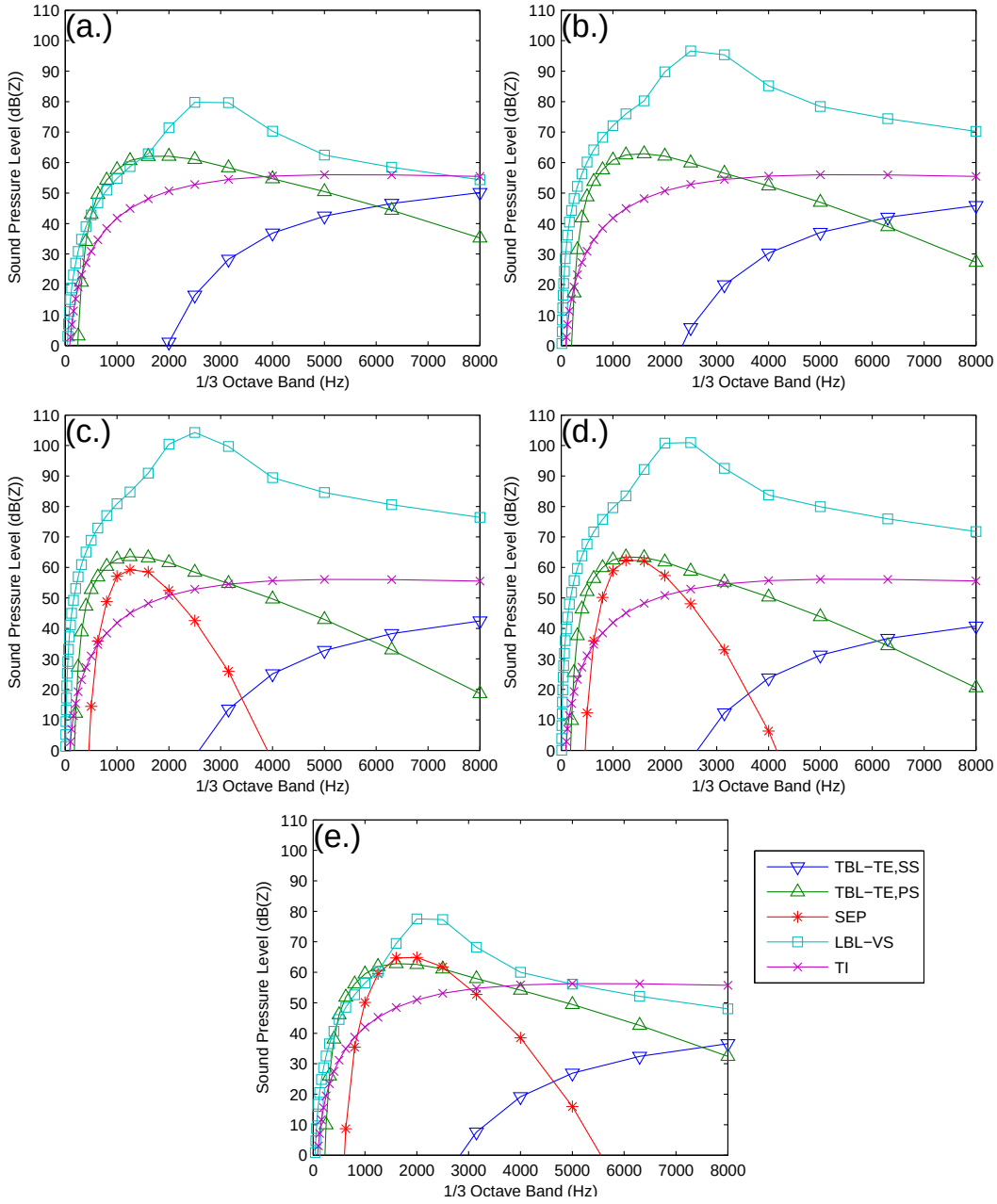

Figure 4.5: NAFNoise estimates at various low angles of attack for SD-7037 airfoil, with LBL-VS noise using suction side boundary layer properties for calculation: a.) 0°, b.) 1°, c.) 2°, d.) 3°. e.) 5°

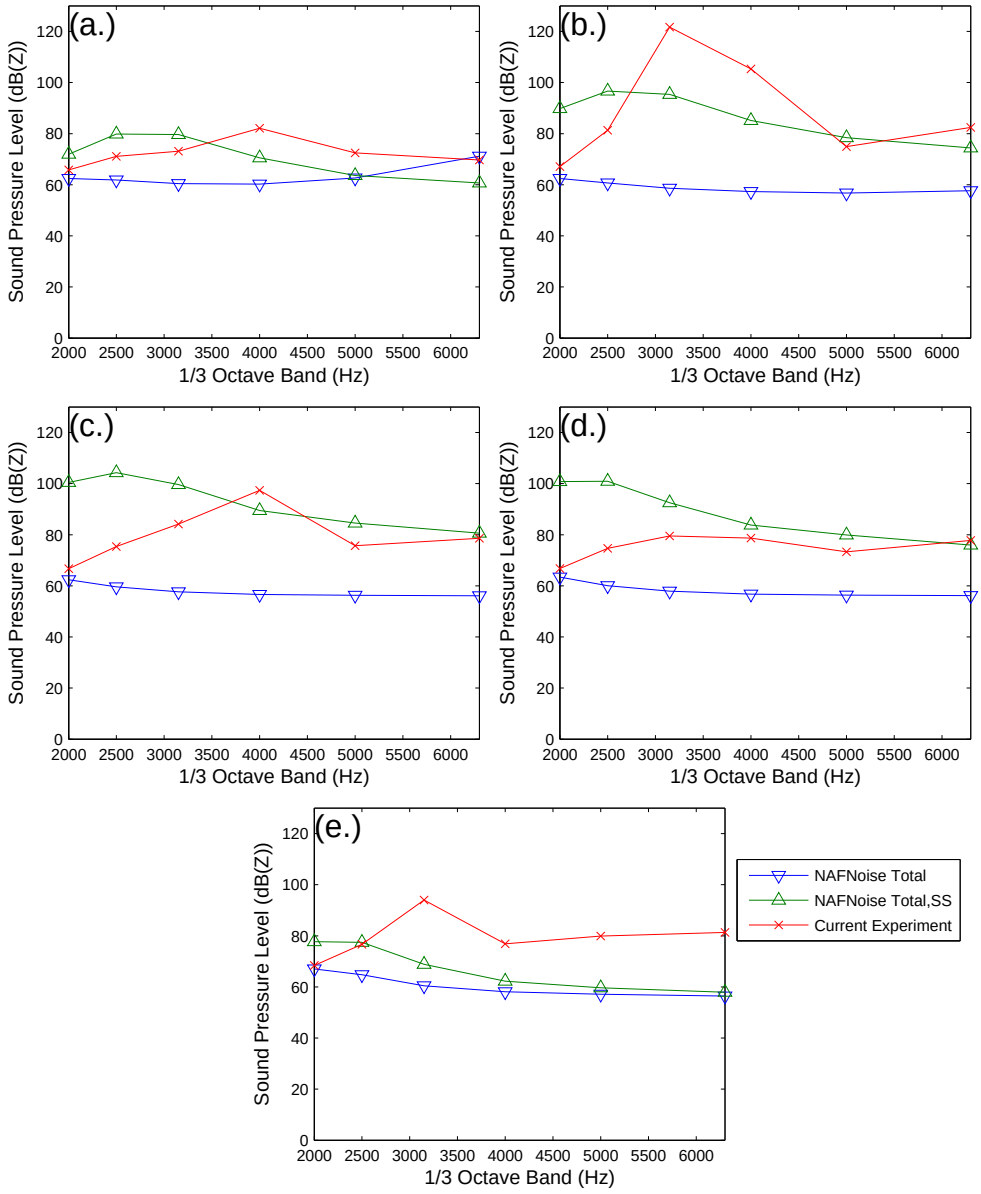

Figure 4.6: Total 1/3 octave sound pressure levels of the NAFNoise estimates (pressure and suction side results) compared with results from current experiment. respective tunnel background subtracted airfoil noise from the experiments of the current study: a.) 0°, b.) 1°, c.) 2°, d.) 3°. e.) 5°.

4.2.2 Narrowband Spectra

Figures 4.7 and 4.8 show the narrowband acoustic spectra for a frequency range between 2 kHz and 7 kHz at various low and high angles of attack. As a reference, the narrowband acoustic spectrum for the wind tunnel background noise is included in the figures.

For low angles of attack between 0° and 5°, the narrowband acoustic spectra are shown in Figure 4.7. Tonal noise are consistently observed at 3.4 kHz, at 4.1 kHz and at 5.5-6 kHz for all the angles of attack shown. Tonal noise exists at other frequencies however they appear randomly with changing angles of attack. In general, the tonal noise at 3.4 kHz and 4.1 kHz have the highest sound pressure levels. This is shown with the 1/3 octave spectra in figure 4.2, where the corresponding 1/3 octave bands at 3.15 kHz and 4.1 kHz consistently have the highest sound pressure levels with the different angles of attack.

The trend observed with changing angles of attack in figure 4.2 closely match the behaviour of the tonal noise at 3.4 kHz and 4.1 kHz. The hump-shaped spectra seen in figure 4.2 can be attributed to the tonal noise contributions and not from a broadband noise source. In low Reynolds number cases, broadband noise is not known to be a main feature of the airfoil acoustic spectra. This can be seen in the results of other studies [21] [26]. It is also possible that the background noise has obscured the broadband noise component, as suggested by Chong and Joseph [25] when analyzing their experimental results.

Figure 4.8 shows the narrowband acoustic spectra for the airfoil at high angles of attack between 10° and 20°. In contrast to figure 4.7, tonal noise has effectively disappeared from the acoustic spectrum. The tonal noise is found at the frequency of 3.4 kHz and 4.1 kHz at around 10 to 15 dB above neighboring frequencies. As discussed previously in section 4.1.2, this is likely due to some resonance effects. However, the low sound pressure levels of the tonal noise do not significantly contribute to the 1/3 octave sound pressure levels at 3.15 kHz and 4 kHz. This was previously shown in section 4.2.1.

The sound pressure levels are seen to have a slight broadband increase with increasing angles of attack. This is most visible between 2.5 kHz and 3 kHz. Similar observations were made in figure 4.3. The increase in the 1/3 octave sound pressure levels in that case can be attributed to broadband noise from stall. It is not due to tonal noise, as in the case with low angles of attack.

The behaviour of the sound pressure level magnitudes and sound frequency can be further examined. Figure 4.9 and 4.10 shows the relationship of sound pressure level magnitudes and sound frequency respectively for the tones at 3.4 kHz and 4.1 kHz at the various angles of attack.

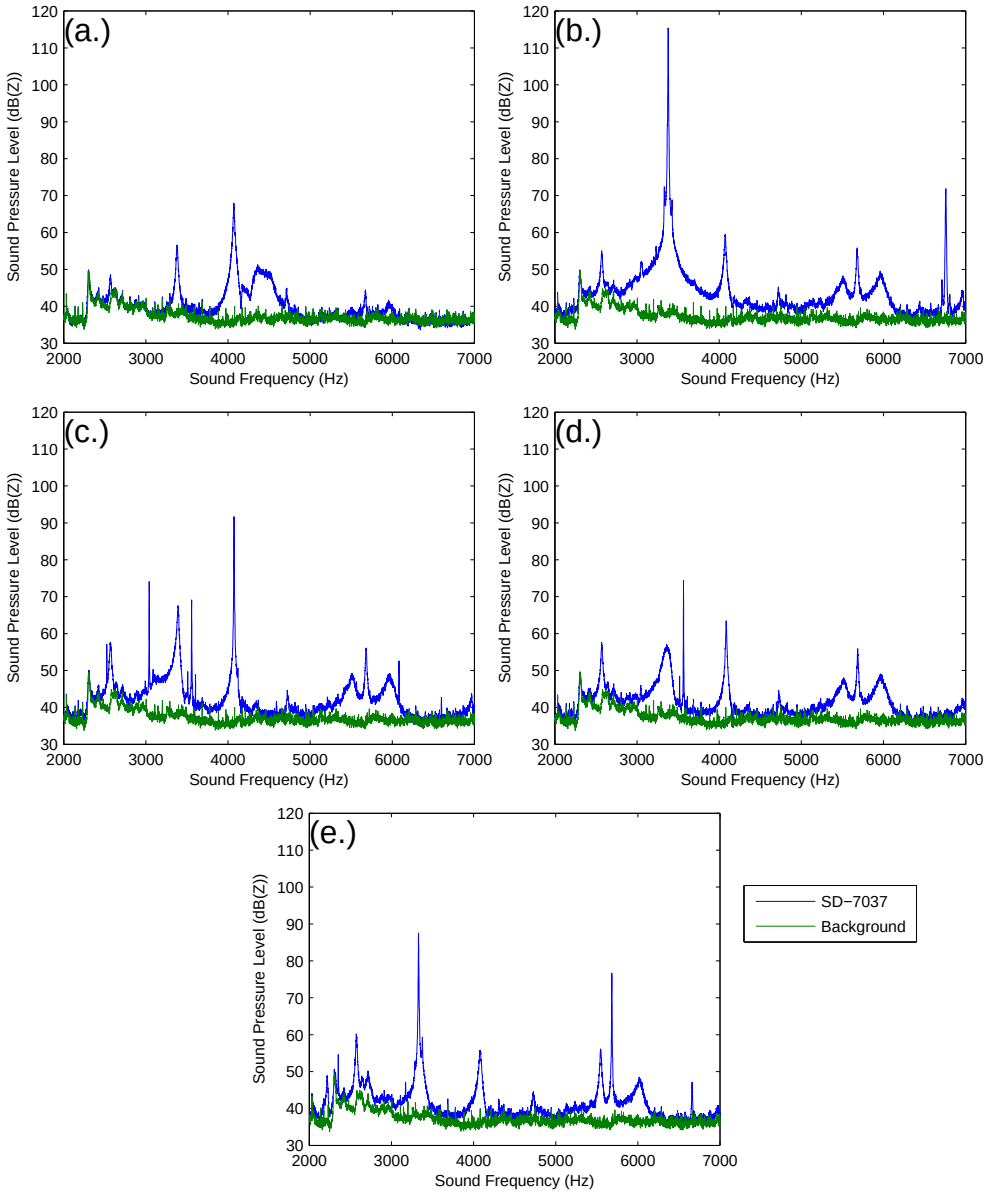

Figure 4.7: Narrowband acoustic spectra of the SD-7037 airfoil at low static angles of attack: a.) 0°, b.) 1°, c.) 2°, d.) 3°, e.) 5°. Tunnel background noise plotted with the acoustic spectra

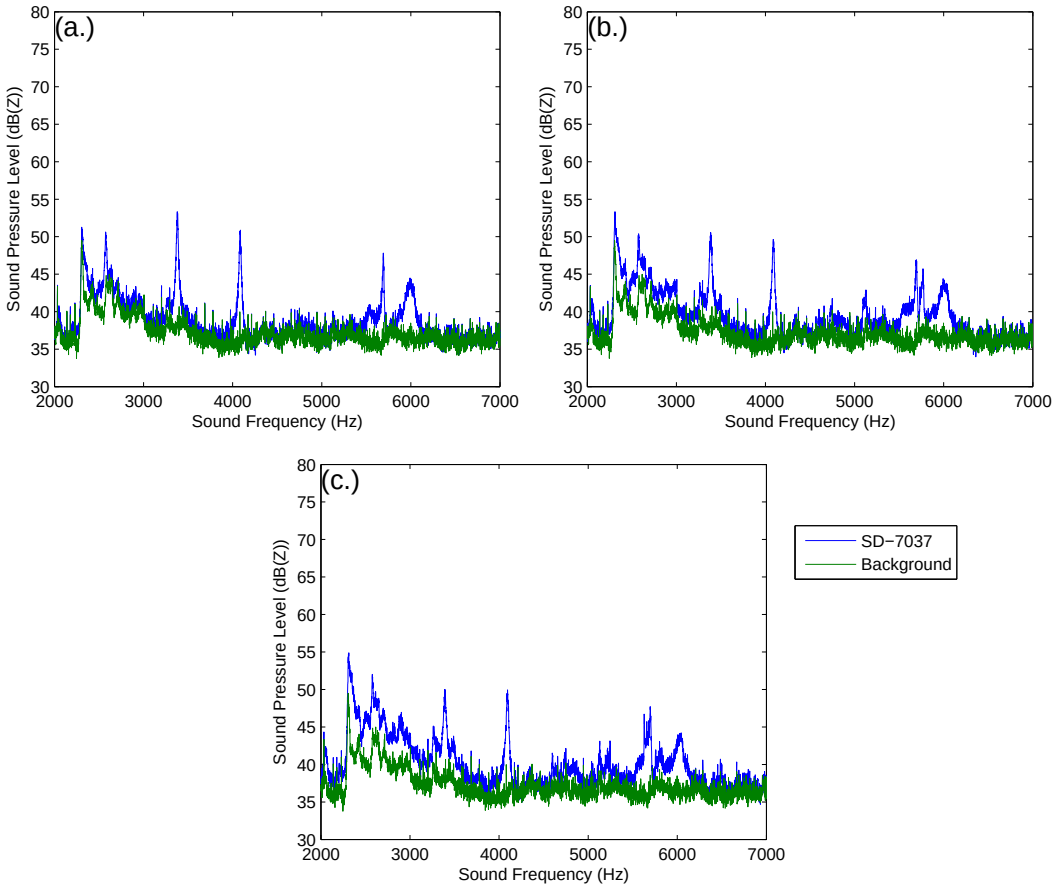

Figure 4.8: Narrowband acoustic spectra of the SD-7037 airfoil at high static angles of attack: a.) 10°, b.) 15°, c.) 20°. Tunnel background noise plotted with the acoustic spectra

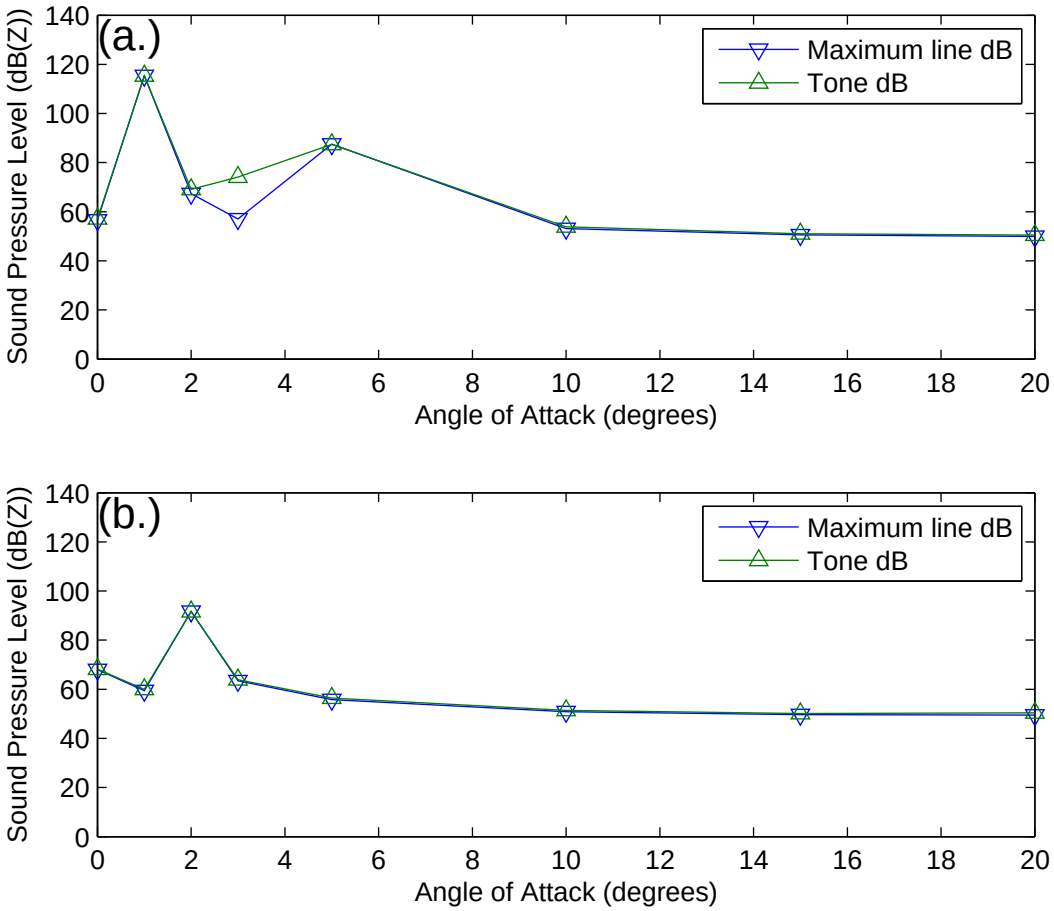

Figure 4.9: Change in tone sound pressure level value vs. angle of attack a.) for 3.4 kHz tone b.) for 4.1 kHz tone.

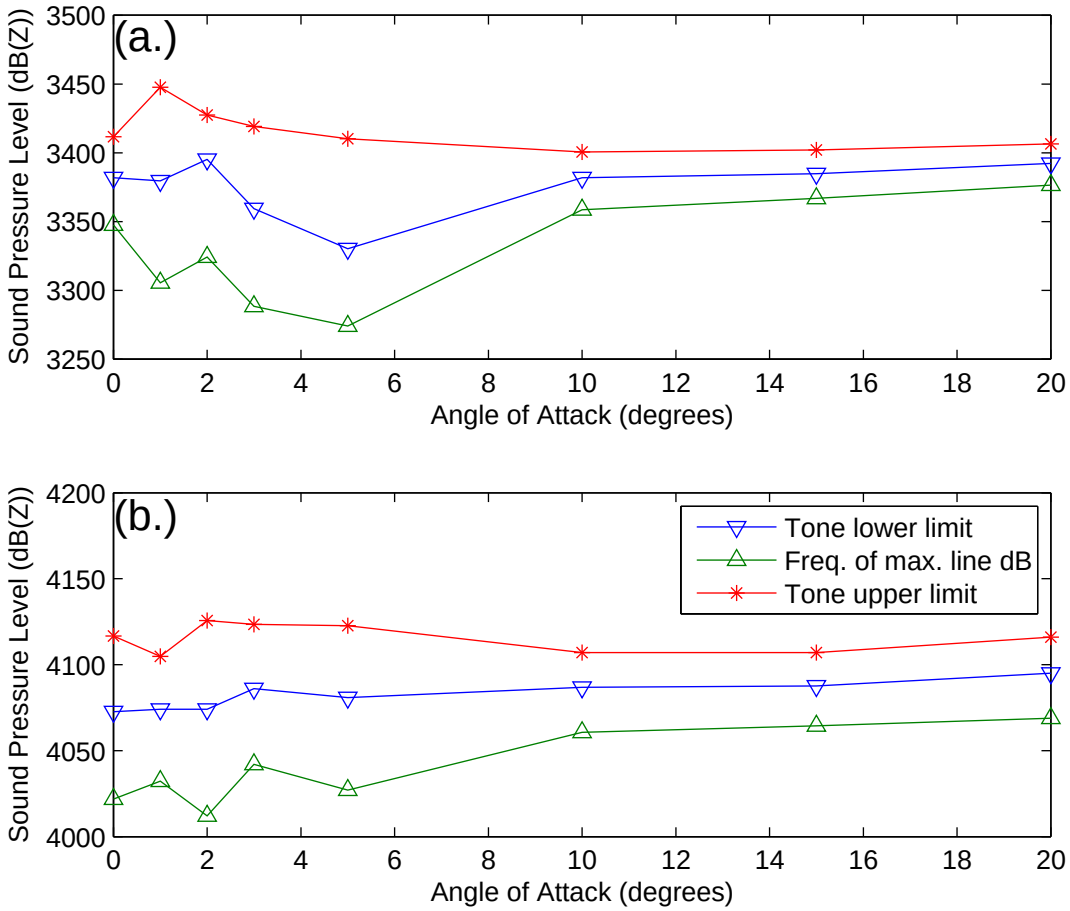

Figure 4.10: Change in tonal frequency vs angle of attack a.) for 3.4 kHz tone b.) for 4.1 kHz tone

In figure 4.9a, the sound pressure levels of the 3.4 kHz tone is shown to reach its peak magnitude of 115 dB at 1°. The levels are greatly reduced at 2°, but increase again at 3° to a second peak at 5°. For higher angles of attack, the sound pressure levels of the tones are below the magnitudes of the lower angles of attack and the change in sound pressure levels remains flat with changing angles of attack.

For the tone at 4.1 kHz, shown in figure 4.9b, the peak magnitude value is found at 2 degrees. Otherwise, tone sound pressure level magnitude is around 60 dB to 70 dB at low angles of attack. At higher angles of attack, the tonal magnitude are more consistent at the 50 dB neighbourhood.

It is expected that the tonal noise would appear, reach a peak value and disappear with increasing angles of attack. This behaviour is due to the development of an increasingly favourable laminar boundary layer condition with a small increase in the angle of attack. With a larger increase in the angle of attack, the onset of turbulent boundary layer conditions would reduce and eliminate the tonal noise generation mechanism. Past studies [11] [14] [92] have outlined regions (seen in figure 2.4) where tone noise is expected to be found given the Reynolds number and the angle of attack.

In this study, with the exception of the low sound pressure level magnitude tones found at higher angles of attack, the trend of the 4.1 kHz tone follows the expected behaviour. The 3.4 kHz tone exhibits a change in trend at 2° after reaching its peak sound pressure level at 1°. The increase in sound pressure level at 3° and 5° may suggest the resonance effect caused a deviation in behaviour at those angles of attack.

For sound frequency, the 3.4 kHz and 4.1 kHz tones appear to remain at a fixed frequency throughout the various angles of attack in figures 4.7 and 4.8. Under resonant-free conditions, the change in the angle of attack alters the properties of the boundary layer. In many LBL-VS noise generation models reviewed, there are key components of the noise generation mechanism which would be affected with a change in the angle of attack. The change in these components can lead to a shift in the frequency of tonal noise. When the tones frequency is found unchanged with changing angles of attack, it suggests the resonance effect has altered its behaviour.

In figure 4.10, the tones are found to vary slightly in frequency with changing angles of attack. For the 3.4 kHz tone, as seen in figure 4.10a, the frequency varies with changing of angle of attack below 5°. The tone's frequency appears to increase slightly with changes in angle of attack up to 2°. Between 2° and 5°, the frequency decreases with increasing angle of attack. At the higher angles of attack ($10° - 20°$), the tone frequency appears to return to the same range as when the airfoil was at 0°; increasing slightly with increasing angle of attack. Overall, the frequency varied by less than 100 Hz throughout the entire

range of changing angles of attack.

For the 4.1 kHz tone, as seen in figure 4.10b, the frequency of the tone was generally found to increase with the increase in angle of attack. The increase is roughly by 30 Hz from 0° to 20°.

Although the values appear small, in reviewing various studies [21] [22] [25] [26], the change in frequency in the current study is found to within typical values. However, the existence of tones at angles of attack of 10° and higher remains an issue.

For further insight, the tone noise behaviour can be estimated by analytical methods such as using the Orr-Sommerfeld equation to calculate the amplification of flow instability. This was conducted in studies by Chong and Joseph [25] [77] and by McAlpine et al. [20]. This could not be conducted as part of the current study but is recommended for future investigations.

Another feature for discussion with the results of the current study is related to the appearance of side peaks in the narrowband acoustic spectra. Desquenes et al. [16] and Probsting et al. [21], have noted the appearance of equi-spaced secondary tonal components around a main and dominant tonal component in the airfoil acoustic spectra. Their studies were reviewed in section 2.1.1.6. It was suggested that amplitude modulation of the main tone to be the cause of this phenomenon.

Although many individual tones appear in the current study, they are not found in equi-spaced intervals nor in similar appearances to those seen in other studies. This would suggest the modulation effect is not present. Examining the results in the time domain, it was found that the tone frequency and magnitudes remains fairly constant with time (further discussed in section 4.4). It does not appear that side peaks are present under current experimental conditions.

Looking at some of the other studies reviewed [22] [26], there are other instances where side peaks are not found in the acoustic spectra. It is possible that their absence is related to a lack of instability in the flow to cause the main tone to modulate. Low Reynolds number or other stable flow condition factors can contribute to the cause.

Side peaks are later observed with the dynamic oscillating case. Further discussion is found in section 4.4.2.

4.3 Modified Trailing Edge Static Cases

In section 4.2, the acoustic spectra of the SD-7037 airfoil for the OTE case were examined with the key features discussed. In this section, the effects of a modified trailing edge on

the acoustic spectra of the airfoil under static flow conditions are examined. The various trailing edge configurations discussed in this section were previously introduced in section 3.1.2.2. They are the ZLA case, FPL case, the NSR case and the WSR case.

In general, the experimental results of the modified trailing edge cases are similar to those found with their OTE case counterparts. Like the OTE case, the narrowband acoustic spectra for the various trailing edge cases contain the tonal noise at 3.4 kHz, tonal noise at 4.1 kHz and other minor tonal noises. Side peaks are also not present in the modified trailing edge acoustic spectra.

While the acoustic spectra are generally found to be similar, the modified trailing edge cases do display different sound pressure levels for the tonal components in some cases. The tone's behaviour with respect to the angle of attack has been altered as well. These modifications are found in the spectra at low angle of attack. At high angle of attack, the results between the modified trailing edge cases and the OTE cases have no distinguishable differences. As such, further analysis and discussions in this section will be limited to low angle of attack cases only.

The ZLA case is first examined. The ZLA case was included in the experiment to determine if the attachment method, i.e. the 2 mm overlap, would create any artefact noise source in the experiment. Initially, it is believed the 2 mm attachment overlap may cause some interference to the LBL-VS noise generation mechanism as the attachments were glued to the pressure side by the trailing edge. Although boundary layer trips are typically more effective at up stream locations, where transition into turbulence at an earlier point would prevent the formations of mechanisms and structures associated with laminar boundary layer and LBL-VS noise, introducing a trip/disruption may still have an impact. However, as the noise generation mechanism was found to be located on the suction side of the airfoil, it is speculated that the effect due to the attachment should be further reduced.

Figure 4.11 shows the 1/3 octave sound pressure levels at various low angles of attack for the ZLA case for the bands between 2 kHz to 6.3 kHz. A comparison can be made with the results of the OTE case, shown previously in figure 4.2. Between the two cases, the ZLA case results have sound pressure levels and spectral profiles closely matching the OTE cases. The maximum sound pressure level for the ZLA case was found to be within roughly 2 dB of the OTE case results.

While the 1/3 octave acoustic spectra profiles have matching counterparts between the two trailing edge configurations, they were found offset by 1° in the angle of attack. For example, the spectral profile for the ZLA case at 2°, where the maximum 1/3 octave band sound pressure level was found, matches with the acoustic spectrum of the OTE case at 1°.

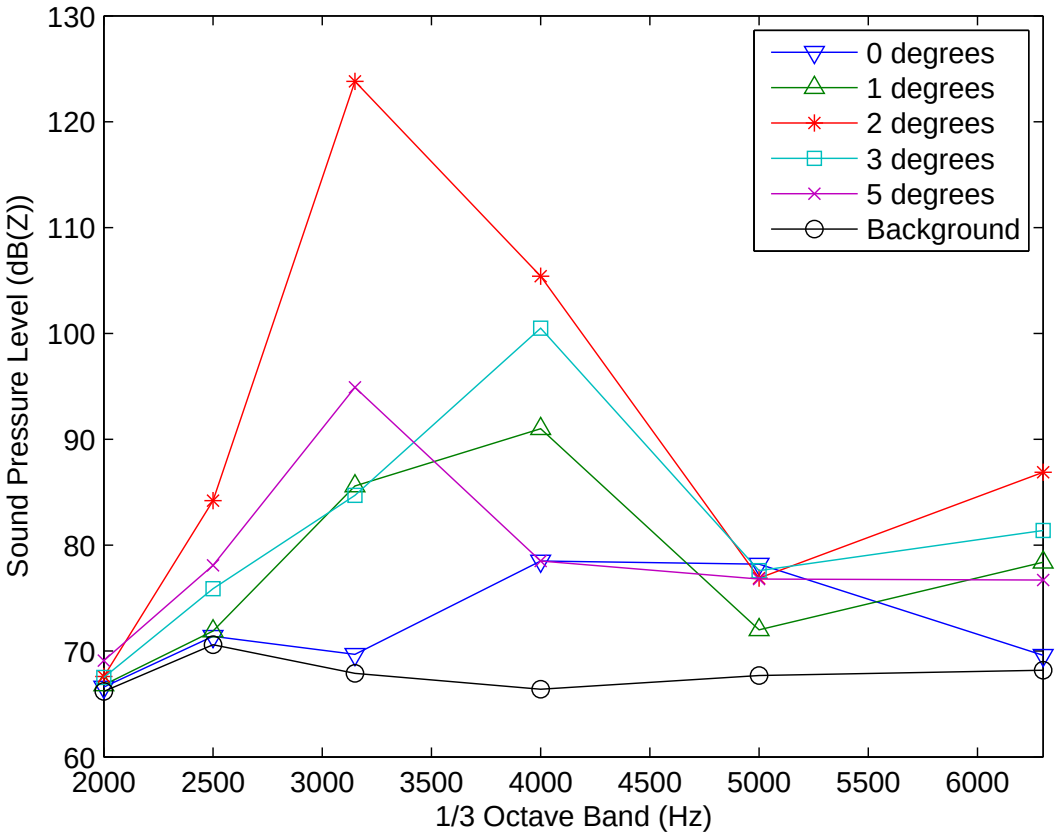

Figure 4.11: 1/3 octave sound pressure levels for the ZLA case at various low angles of attack. Wind tunnel background noise is included in the figure for comparison.

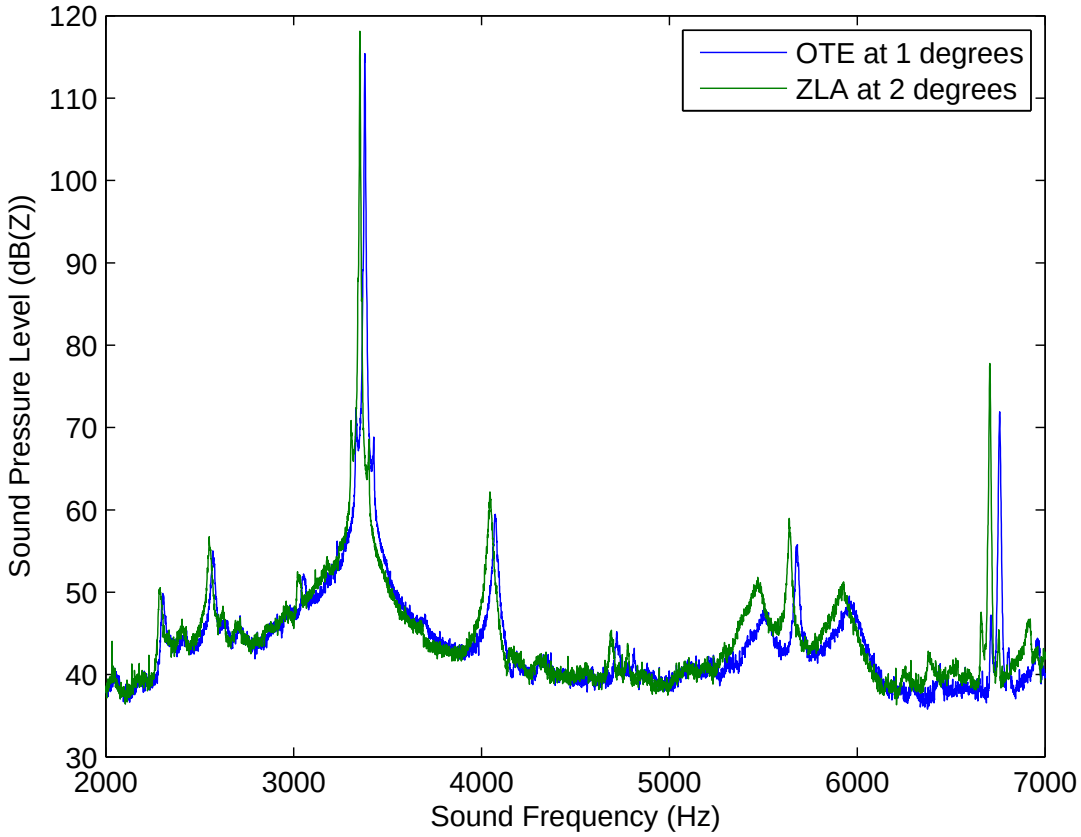

Figure 4.12: Comparison of narrowband acoustic spectra between OTE case at 1° and ZLA case at 2°

It should be noted that the maximum 1/3 octave band sound pressure level for the OTE case was found at 1°. Likewise, the spectral profile of ZLA case at 3° match well with the OTE case at 2°. A disagreement is found at 3.15 kHz band between the ZLA case at 0° and OTE case at 1°, however, the rest of the spectrum is well matched.

Examining the narrowband acoustic spectra for the maximum sound pressure level cases from the ZLA and OTE cases, they were found to be nearly identical. This is shown in figure 4.12.

It is possible there was an error during the experiment in setting the initial angle of the airfoil. Due to alterations made to the wind tunnel shortly after the experiments, the

experiment could not be conducted again for verification. However, as discussed later, the other trailing edge modification cases have introduced broad angle of attack changes to the acoustic spectra. The offset effect has no impact on further analysis. As such, additional consideration is not necessary.

Given the matching acoustic spectra and similar sound pressure levels, the acoustic spectra of the ZLA attachment do not appear to have introduced significant differences compared with the OTE case.

For the FPL case, the 1/3 octave sound pressure levels at various angles of attack are shown in figure 4.13. Again, the results can be compared with the OTE case. The maximum 1/3 octave band sound pressure level is less than 110 dB, which is lower than the maximum sound pressure levels seen for the OTE case.

The lower sound pressure level may be attributed to the lengthening of the chord by the trailing edge extension. The decrease in sound pressure level is speculated that the transition into turbulence is further promoted by the increased length or altered profile. This speculation should be further investigated by more detailed examination of the boundary layer measurements, which is not in the scope of the current study.

With the introduction of the trailing edge extension, the presence of the tonal noise is extended at low angles of attack with compared with the OTE case. Sound pressure levels comparable to the peak value are seen over a wider range of angles of attack: at 4.1 kHz band at 1° and at 3.15 kHz band from 3° to 5°. It is possible that the increased length from the trailing edge modification has extended the tonal noise for further angles of attack because of some resonance effect. The extended chord length is still below the threshold where Parker β resonance is seen. However, it is possible another type of resonance effect is the cause.

The FPL case is also seen to have a broadband increase in sound pressure level. This is best shown in a comparison between the FPL and OTE narrowband acoustic spectra in figure 4.14. As speculated earlier, the lengthening of the chord and alteration of the profile should promote a turbulent regime. Subsequently, broadband noise, which is associated with TBL-TE noise, should increase as well.

The 1/3 octave band results for the two serrated cases, NSR and WSR, are presented in figure 4.15 and figure 4.16 respectively. In general, it was found that the results of the two serrated cases are similar. The aspect ratio of both serrations used in this study can be considered to be relatively wide when comparing them to the other serration aspect ratios that were examined in past studies [72] [81]. Examining narrower serrations was not possible in the current study due to limitations in manufacturing teeth of a physical scale

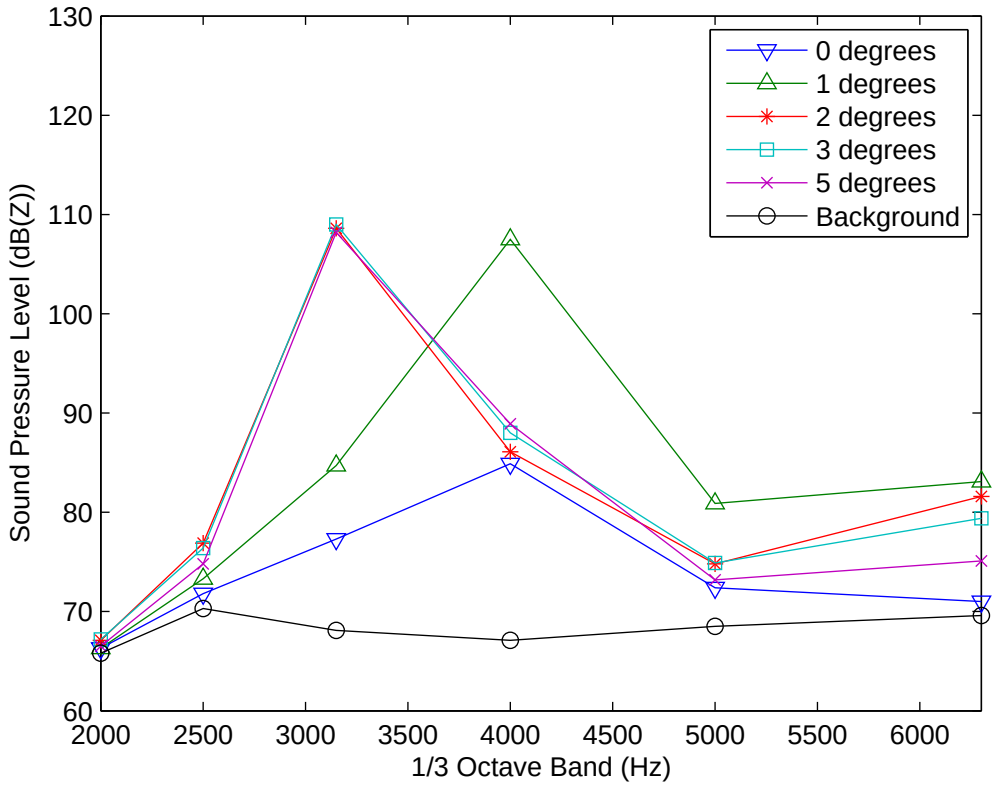

Figure 4.13: 1/3 octave sound pressure levels for the FPL case at various low angles of attack. Wind tunnel background noise is included in the figure for comparison.

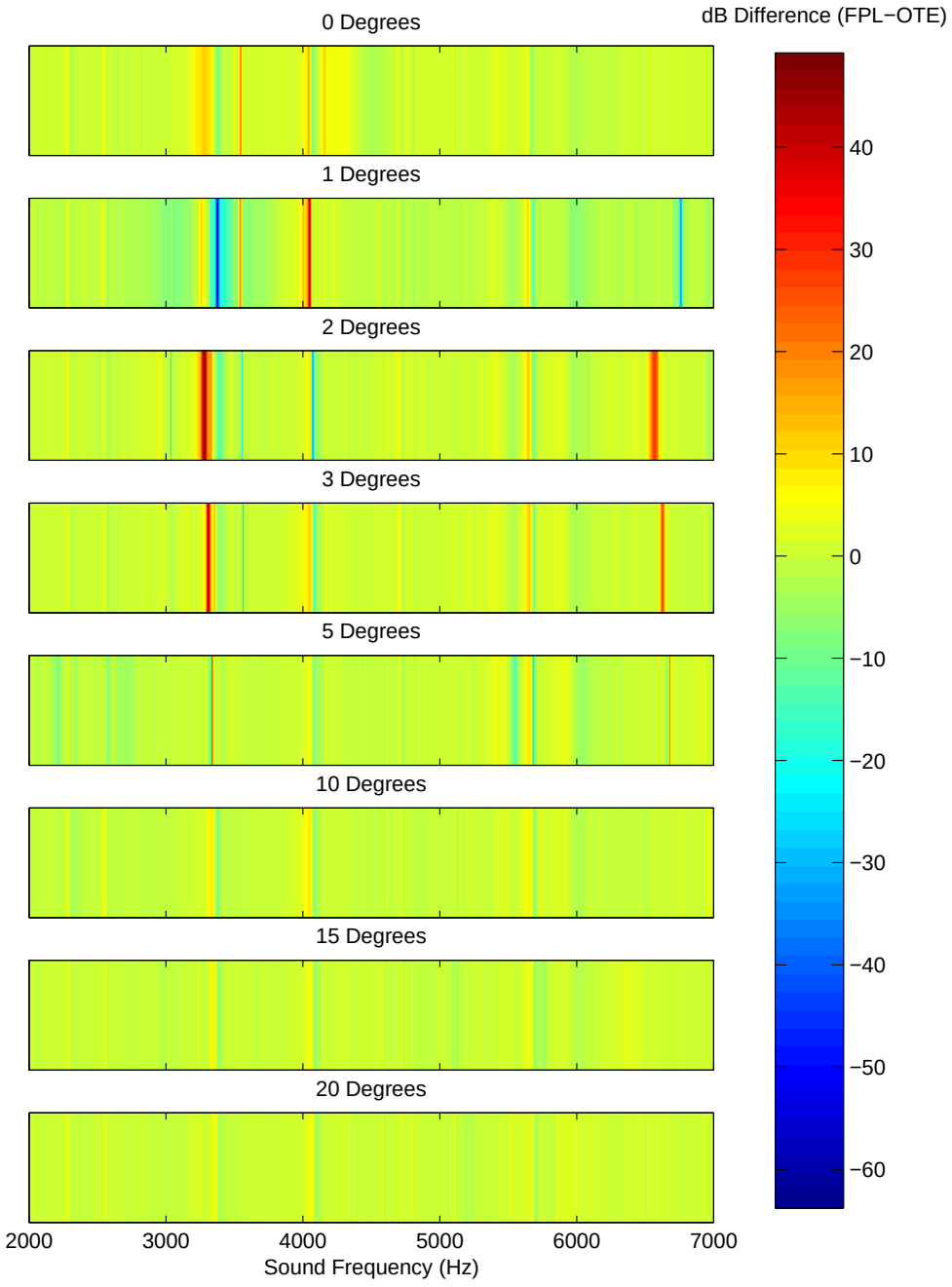

Figure 4.14: Sound pressure level difference between FPL case and OTE case

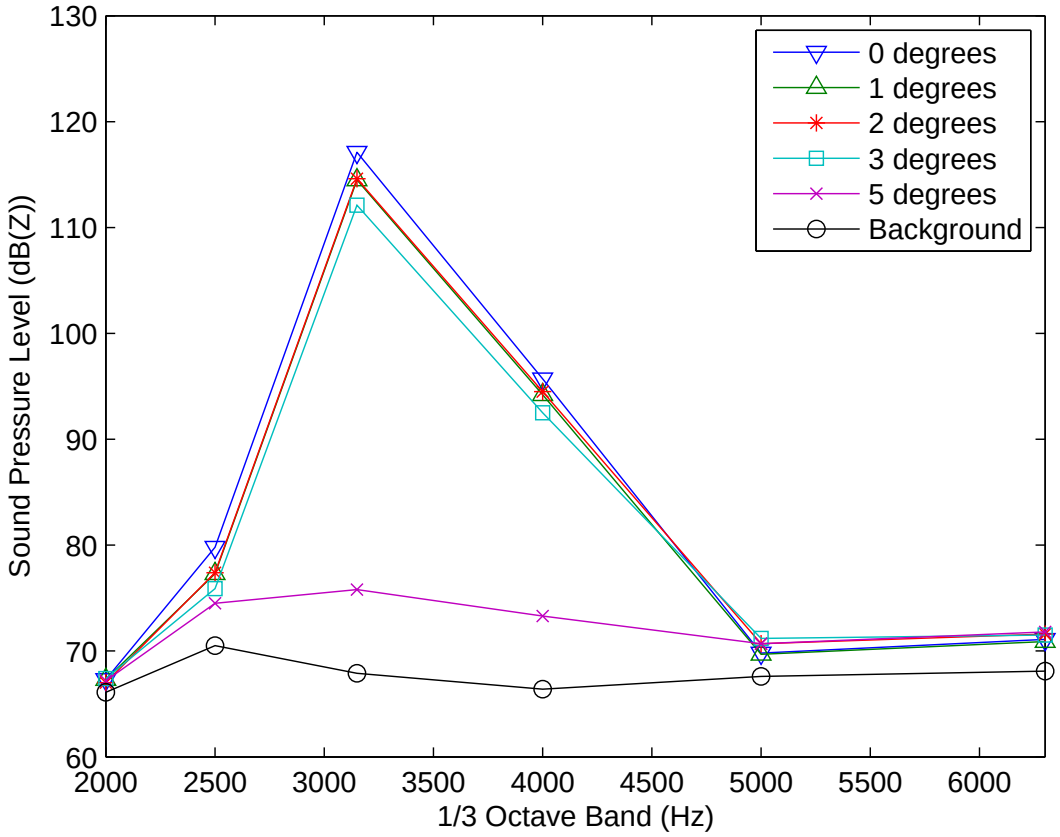

Figure 4.15: 1/3 octave sound pressure levels for the NSR case at various low angles of attack. Wind tunnel background noise is included in the figure for comparison.

proportional to the current airfoil. With both relatively wide aspect ratios, there may be insufficient contrast in the results to see a difference.

Like the FPL case, the maximum sound pressure level for the serrated case are lower than maximum sound pressure levels for the OTE case. The serrated case reduced the maximum sound pressure level by 7.2 dB. This is a smaller reduction than when the FPL case was compared with the OTE case. Like the FPL case, both the NSR case and the WSR case have tonal noise persisting at other low angles of attack. Sound pressure levels greater than 110 dB were observed from 0° to 3° at the 3.15 kHz band; leading to the mixed effect of decreasing sound pressure level at 1° and increasing sound pressure level at

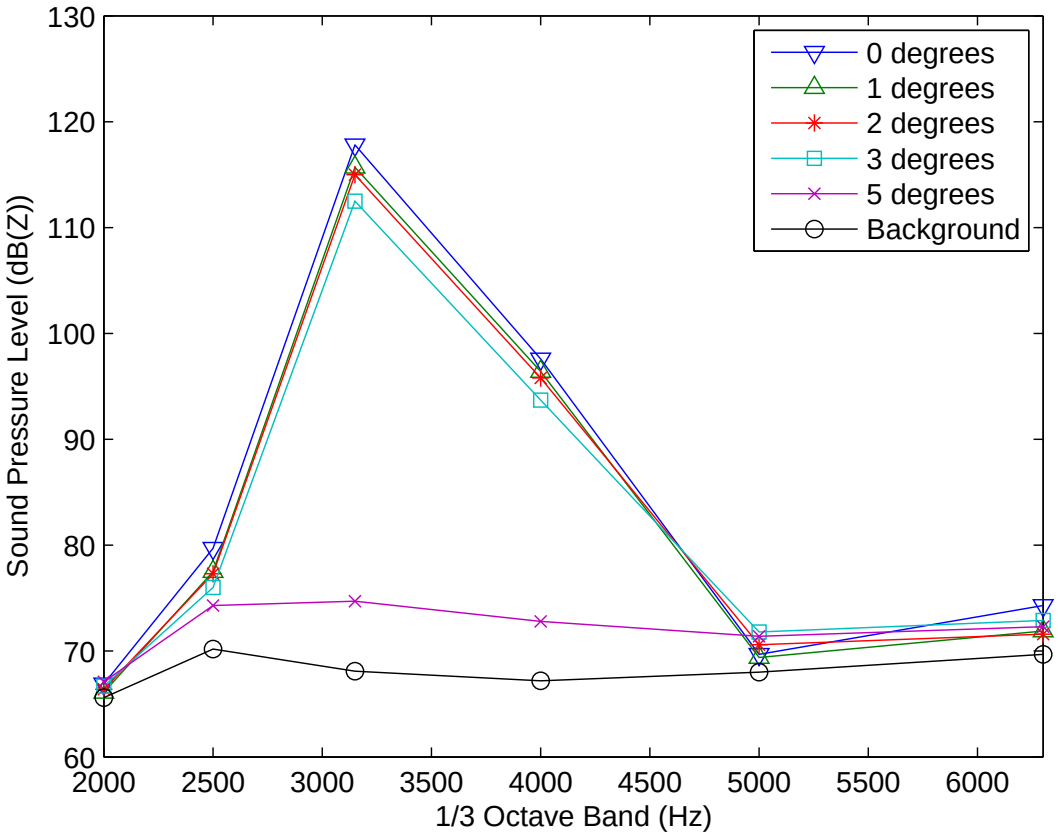

Figure 4.16: 1/3 octave sound pressure levels for the WSR case at various low angles of attack. Wind tunnel background noise is included in the figure for comparison

the other angles of attack.

Unlike the FPL case, the serrated cases have reduced the 1/3 octave sound pressure levels at the 6.3 kHz band at low angles of attack cases. The ZLA cases or the FPL cases have comparable results with the OTE case. The reduction can therefore be attributed to the serrated pattern. The 6.3 kHz band sound pressure levels were reduced by up to 11.5 dB.

The effects of serrations are further illustrated in figure 4.17, where a comparison between narrowband acoustic spectra for the NSR case and the OTE case can be found. The WSR/OTE level differences are closely similar the NSR/OTE comparison. As such, they will not be presented. Aside from the tonal noise persisting at 3.4 kHz from 0° to 3°, it was observed that broadband sound pressure levels are not reduced when compared with the OTE case through most of the frequency spectrum shown. The sound pressure level reduction seen in the 1/3 octave results is attributed to the serrations effect on tonal noise. In figure 4.17, multiple narrowband reductions are found throughout the spectrum shown. These results show many tones, either prominent or minor, to have been reduced.

The effect of serrations observed in the current study may best be explained by Chong and Joseph [77], who had found reduction of tonal noise with interference to the laminar separation bubble found near the trailing edge. They suggest this interference affects the feedback mechanism of the LBL-VS noise mechanism, and subsequently reduced or eliminated the tonal noise. This reduction mechanism is in contrast to those theorized by other studies [72] [73] [81] , where broadband noise reductions were observed. Given that tonal noise is seen to have been reduced in the current study, the explanation of Chong and Joseph [77] is the most appropriate.

4.4 Airfoil Self-Noise under OTE Dynamic Case

In section 4.2, the behaviour of the airfoil noise for the OTE configuration under static conditions was examined. In this section, the behaviour of the airfoil under dynamic pitching oscillation is discussed with comparison to its counterparts in the static case. The details for dynamic case experiments can be found in section 3.1.3 or in the thesis of Gharali [6].

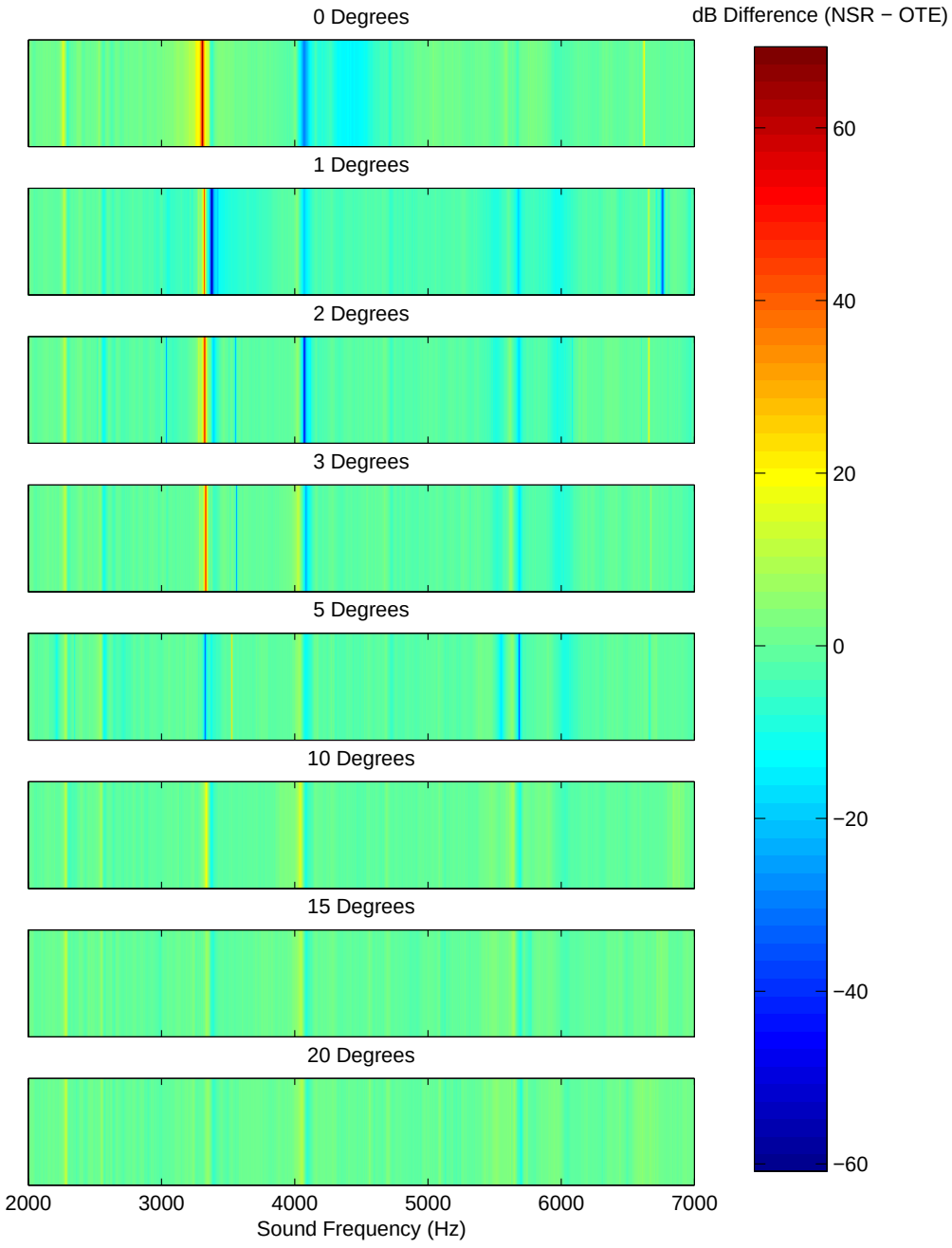

Figure 4.17: Sound pressure level difference between NSR case and OTE case

Table 4.1: 1/3 octave sound pressure levels for OTE dynamic case. 1/3 octave sound pressure levels for static angles of attack at 1 degrees, at 15 degrees and the wind tunnel background noise levels are included for comparison

	2.5 kHz	3.15 kHz	4 kHz	5kHz	6.3 kHz
OTE Dynamic Case	76.9	88.2	85.2	72.2	72.8
Static Low Angle of Attack (1)	81.3	121.7	105.3	74.9	82.4
Static High Angle of Attack (15)	74.1	71.7	69.5	70.4	71.5
Wind Tunnel Background Noise	70.2	68.0	67.0	68.1	69.0

4.4.1 Acoustic Spectra

Like the analysis conducted for the static cases in section 4.2, the results of the OTE case under dynamic conditions are examined in 1/3 octave and narrowband acoustic spectra. Table 4.1 shows the 1/3 octave sound pressure level for selected bands of the OTE dynamic case. The sound pressure level profile, i.e. the level of each band relative to each other, is similar to the profile seen for the static low angle of attack results observed in figure 4.2. As such, the information will not be plotted into figure form to illustrate the spectrum profile. Instead, the information is presented in numerical form. For comparison, the 1/3 octave band sound pressure levels for the wind tunnel background noise and the static case results representing low and high angles of attack are included in table 4.1.

As discussed, the 1/3 octave spectrum profile for the dynamic case is similar to the profile seen for the static case at low angles of attack. Like the static low angle of attack cases, the 1/3 octave bands centered at 3.15 kHz and 4 kHz for the dynamic case have the highest levels. The sound pressure level of the neighbouring bands have similar sound pressure level to each other, but the magnitudes are much lower compared with 3.15 kHz and 4.1 kHz. For the OTE dynamic case, the neighbouring bands of 2.5 kHz, 5 kHz, and 6.3 kHz have sound pressure level values between 70-80 dB. The 3.15 kHz and 4 kHz band are roughly 90 dB.

Comparing with the peak levels seen from the static cases, which were observed at 1° angle of attack, the sound pressure levels for the dynamic case are lower by roughly 20-30 dB at the 3.15 kHz and 4 kHz bands. For the other band levels seen in table 4.2, the dynamic case sound pressure levels are roughly 10-20 dB lower than the maximum observed for the low angle static cases. However, the1/3 octave band sound pressure levels of the dynamic case are similar when compared with the other low angle of attack static

cases.

Comparing with cases of high static angles of attack, the sound pressure levels of most bands in the dynamic case also have similar levels. The exceptions are found for 3.15 kHz and the 4 kHz band, where levels are elevated as seen for the profiles of static low angle of attack cases. This can be seen from a comparison of the values in table 4.1. Note from figure 4.3, the 1/3 octave sound pressure levels for all cases at high angles of attack have similar values.

A further discussion regarding the OTE dynamic case spectrum profile can be aided by examining the narrowband acoustic spectrum. The results are presented in figure 4.18. Once again, the wind tunnel background spectrum, 1° and 15° spectra are included for comparison.

From the narrowband acoustic spectrum, it can be seen that there are two prominent and elevated levels centered at 3.3 kHz and 4.1 kHz. These levels match the notable tones found in the static case. The sound pressure levels observed are much lower than the peak values seen at 1° angle of attack. The same observation was seen previously with the 1/3 octave spectra. The elevated levels appear tonal in nature but spread over a broader range of frequencies comparing with its static counterparts. Given the angle of attack for the airfoil changes from $0° - 22°$ during the dynamic case, it can be reasoned that the appearance of the spectrum is an average of spectra at low angles; where tonal noise are prominent, and at high angles, where tonal components are subdued.

As tonal noise has sound pressure levels that are much higher in magnitude than the sound pressure levels of noise in the turbulent and stall regimes, the dynamic case spectrum resembles the low angles of attack.

Examining frequency ranges for the other 1/3 octave bands, at frequencies between 2 kHz and 3.15 kHz, the dynamic case narrowband spectra does not appear to have additional tones comparing with the static acoustic spectra. The narrowband spectrum of the dynamic case shows a broadband slight elevation, which may explain the slightly higher values seen from table 4.1. At higher frequencies (above the upper limit of the 1/3 octave band at 4 kHz is roughly 4.5 kHz), the dynamic case does not have the other tones that are seen at the various static angles of attack. This can explain why the 1/3 octave band levels have lower values for the dynamic case at this frequency range compared with the static cases.

The narrowband acoustic spectrum for the dynamic case also contains one characteristic not found in the static cases. As seen in figure 4.18, the acoustic spectrum contains many small tonal components/side peaks evenly spaced between 3 kHz and 4.5 kHz. The side peaks are spaced at an interval of 25 Hz. From literature, the cause of the sidepeaks have been suggested to be due to amplitude modulation of the vortex being shed from the

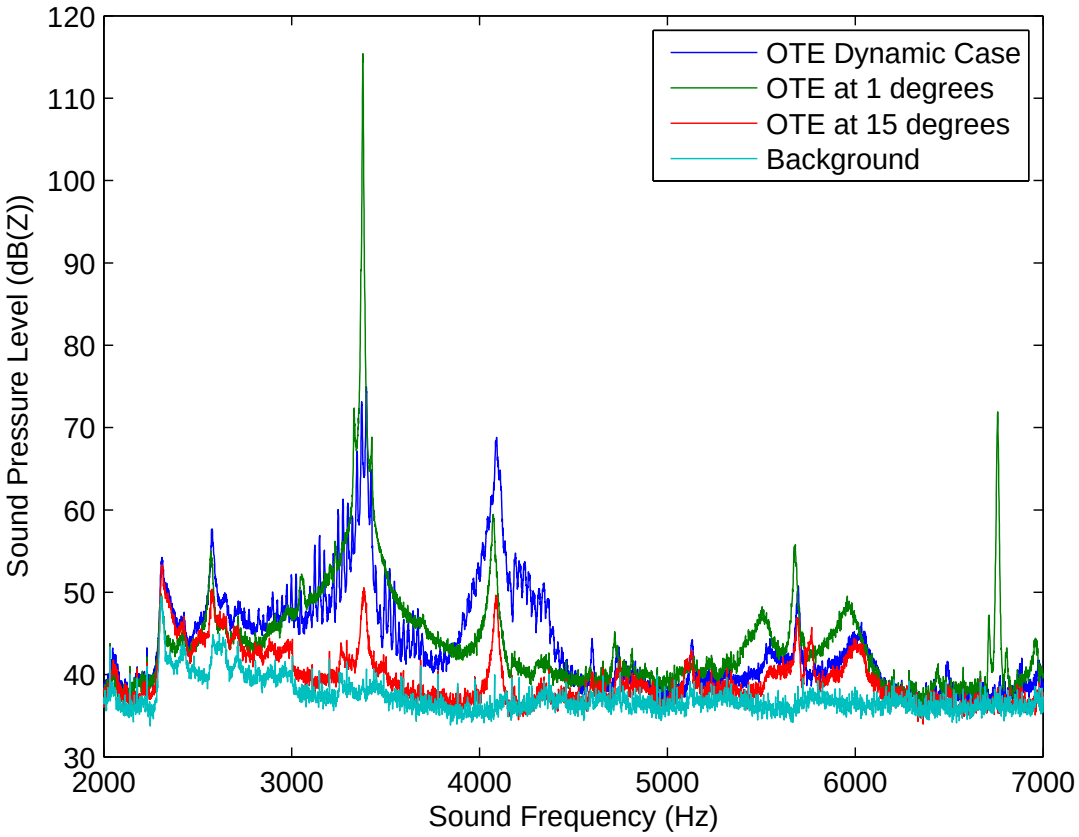

Figure 4.18: Narrowband acoustic spectrum for OTE dynamic case. The OTE static case at 1°, at 15° and wind tunnel background noise are included for comparison.

airfoil surface; observed in studies such as [16] [17] [21]. However, for those studies, the side peaks were observed under static conditions. In the current study, the side peaks were only observed here in the dynamic case and not for the static case.

The explanation for the results observed may involve the oscillation of the airfoil as the airfoil pitching frequency is set at 25 Hz for the current experiment. Probsting et al. [21] investigated the phenomenon using wavelet analysis to examine the change in the frequency spectrum with respect to the time domain. For the current study, wavelet analysis was conducted for the dynamic case. The results are further discussion in section 4.4.2.

Indeed, during the experiment, the airfoil under dynamic case conditions emits a noise that is very different than that of the static case. From a qualitative observation during the experiment, the tone appears noticeably to be intermittent. Given that in section 4.2, it was observed that tonal noise was prominent only at the low angles of attack, the intermittent appearance may be related to the changing angles of attack from the oscillation. This further supports a need to examine the dynamic case results in the time domain.

4.4.2 Time Dependent Analysis

To begin with the analysis of the dynamic case signal in the time domain, the recorded dynamic pressure signal is plotted with respect to time. This is shown in figure 4.19. For comparison, the waveform for OTE case at static angles of attack at 1° and background noise is shown in the figure. By inspection, the dynamic case waveform contains a periodic component that is not observed in the static case or the background noise. The component has a period of 0.08 s, matching the 25 Hz oscillation rate of the pitching airfoil. Indeed, the oscillation of the airfoil would cause a large pressure variation. As such, it is reasonable that a cyclical component is observed in the signal.

To further assess the occurance of phased high frequency components, a wavelet analysis was conducted to examine the signal in the time domain. The details of the technique are well explained in [91] and was previously employed by Probsting et al. [21]. The signal comparison is shown in one second interval of the noise measurements. Although there are minor variations between the different time intervals of the signal, the results do not vary significantly and typical results are seen in the following figures.

While the range of the spectrum most relevant to the discussion from the previous section is located between 2-5 kHz, some notable observations are found in other frequencies. Figure 4.20 shows the wavelet analysis results at pseudo-frequency from 0-200 Hz. In the figure, there are notable wavelet contours located at pseudo frequency of 25 Hz. This corresponds with the airfoil oscillation as discussed previously.

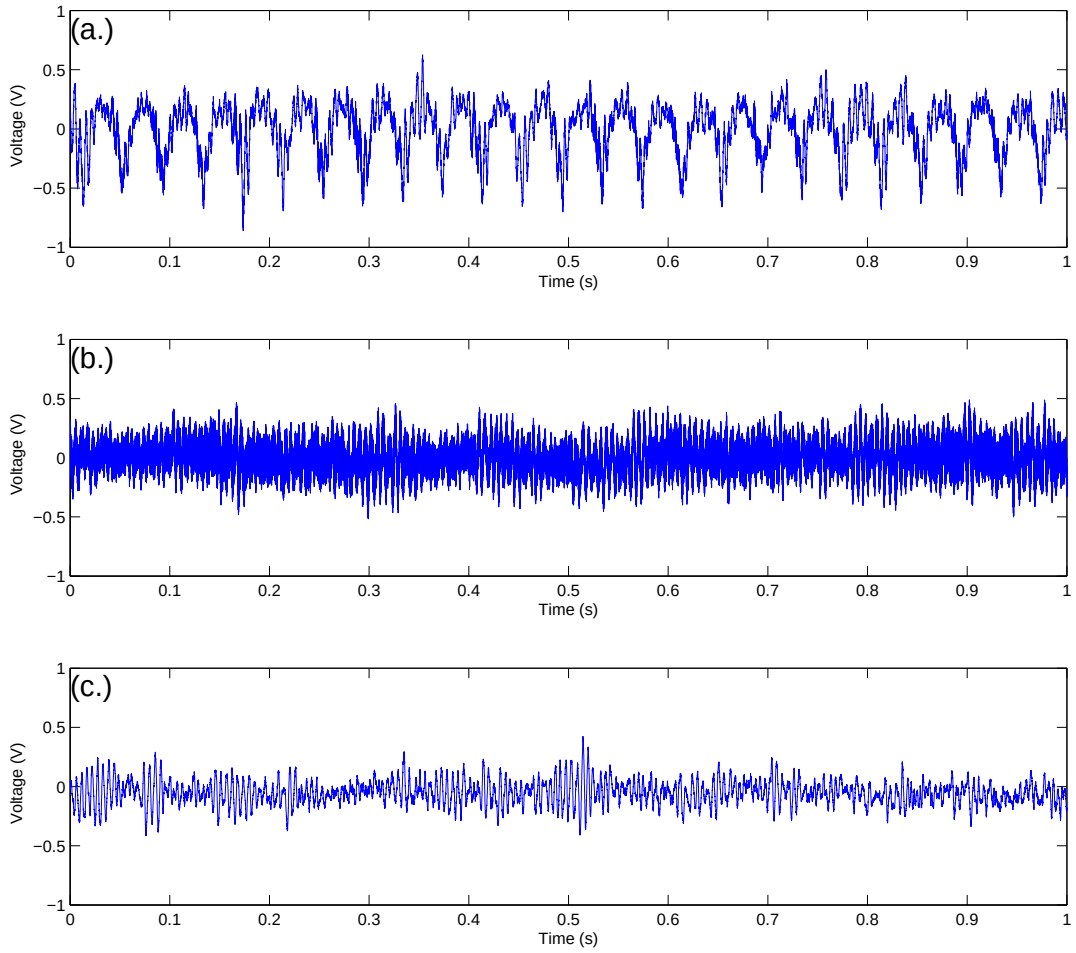

Figure 4.19: Microphone voltage signal from OTE case noise measurements. a.) Dynamic case b.) Static case at 1° c.) Wind tunnel background noise

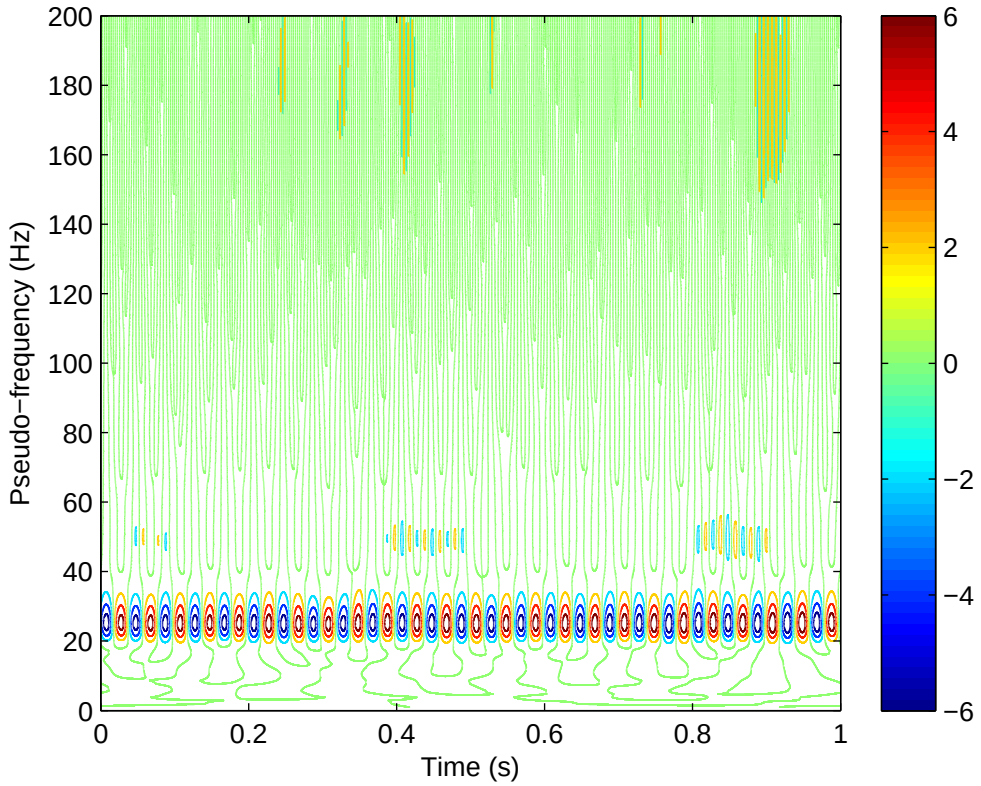

Figure 4.20: Typical results of wavelet analysis of OTE noise measurements over 1 second, pseudo frequency from 0-200 Hz. Contour colorbar included to give a qualitative sense of relative magnitudes only

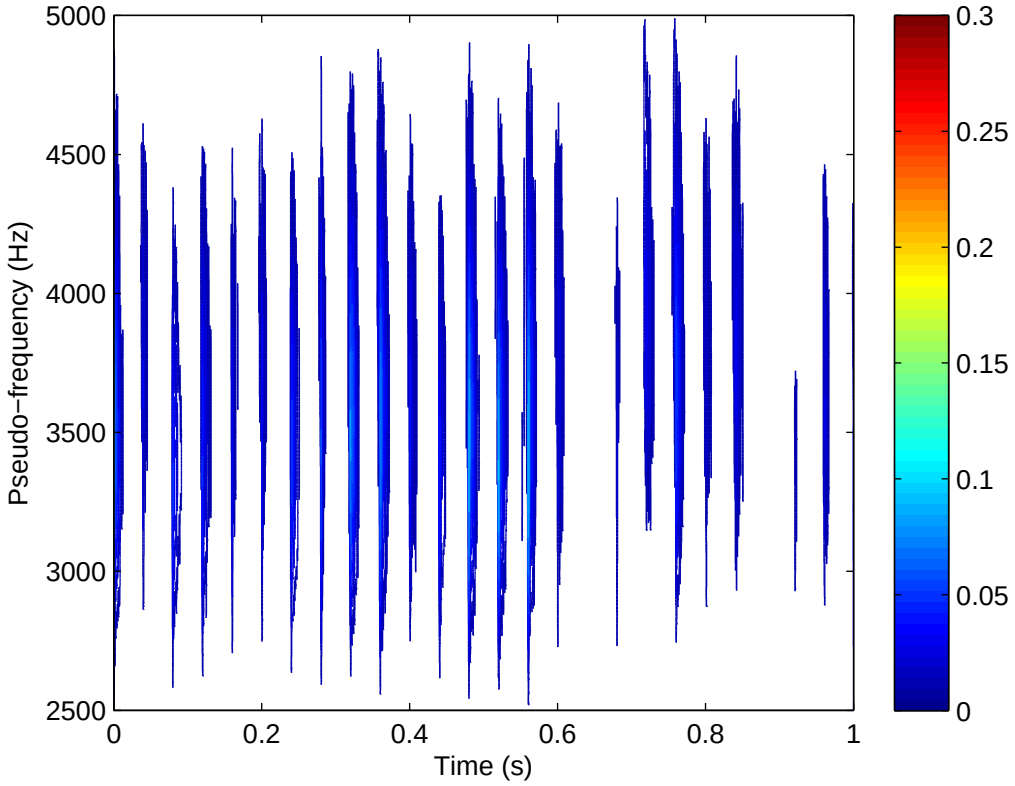

Figure 4.21: Wavelet analysis of the microphone signal for OTE dynamic case over 1 second at pseudo frequencies of 2500 to 5000 Hz

Figure 4.21 shows the wavelet contours at pseudo frequency range of 2.5 kHz to 5 kHz. The contours in the figure show the regions of high wavelet coefficient. These contour regions are consistently centered between 3.4 kHz to 4.1 kHz; corresponding to the two prominent tonal noise frequencies observed in all the narrowband acoustic spectra shown previously. These regions are found spaced throughout at regular intervals of 25 Hz. This suggests the occurance is related with the oscillation and that peaks corresponds to a phase of the cycle.

From the results of section 4.2, the tonal noise in this frequency range corresponds to airfoil generated tonal noise at low angles of attack. It can be concluded that the airfoil is undergoing the same process during the time of high wavelet coefficients. The regions of lower value wavelet coefficient present moments when corresponding pseudo frequency

is at a low magnitude. These regions represent moments when the airfoil is not emitting tones at notable levels and should correspond to the phase in the cycle when the airfoil's angle of attack is sufficiently high that turbulent boundary layer or stall conditions are found.

The spacing of the high wavelet coefficient contour regions at 25 Hz results in the appearance of side peaks at the 25 Hz interval in figure 4.18. The change in contours seen in wavelet analysis represents change in correlation between the Morlet wavelet and the signal. This correlation is related to the magnitude of the acoustic component at that particular frequency. Variation of the contours is an indication of amplitude modulation. This conclusion regarding the coherent pattern would be similar to the observations of Probsting et al. [21] in relation to this pattern and the tonal noise.

It should be noted that dynamic stall has altered the fluid flow at various phases of the oscillation cycle compared with their static angle of attack counterparts. Most notably, the existence of large scale coherent vortices at high angle of attack is much different than the fluid at static (stall) angles of attack. However, at low angles of attack, the effect of dynamic stall phenomenon is not significant. The flow phenomenon associated with LBL-VS noise still exists and hence contributes to the noise generated.

In the current study, a wavelet analysis was also conducted on the measured audio signal for various static cases at OTE configuration. Figure 4.22 shows a typical one second wavelet analysis for OTE case at 1° static angle of attack.

The results at 1° is typical for static angle of attack cases. With changing angles of attack, the frequencies at which the high wavelet coefficient regions are found tend to shift to lower frequencies with increasing angle of attack (similar to observations seen with the NAFNoise predictions). The change in magnitude of the contours with the changing angle of attack follows the same trend as those seen previously in figure 4.2. As such, the results at other angles of attack are not shown.

Wavelet contours appear more consistent with high amplitude regions appearing intermittently. This is opposed to the equi-spaced 25 Hz interval observed for the dynamic case. Accordingly, the tone observed for the static case is characterized as continuous in nature in contrast to the intermittent characteristics noted for the dynamic case.

4.5 Modified Trailing Edge Dynamic Cases

In this section, the results for the different trailing edge configurations under dynamic conditions are presented. Like the analysis conducted for the OTE case in the previous

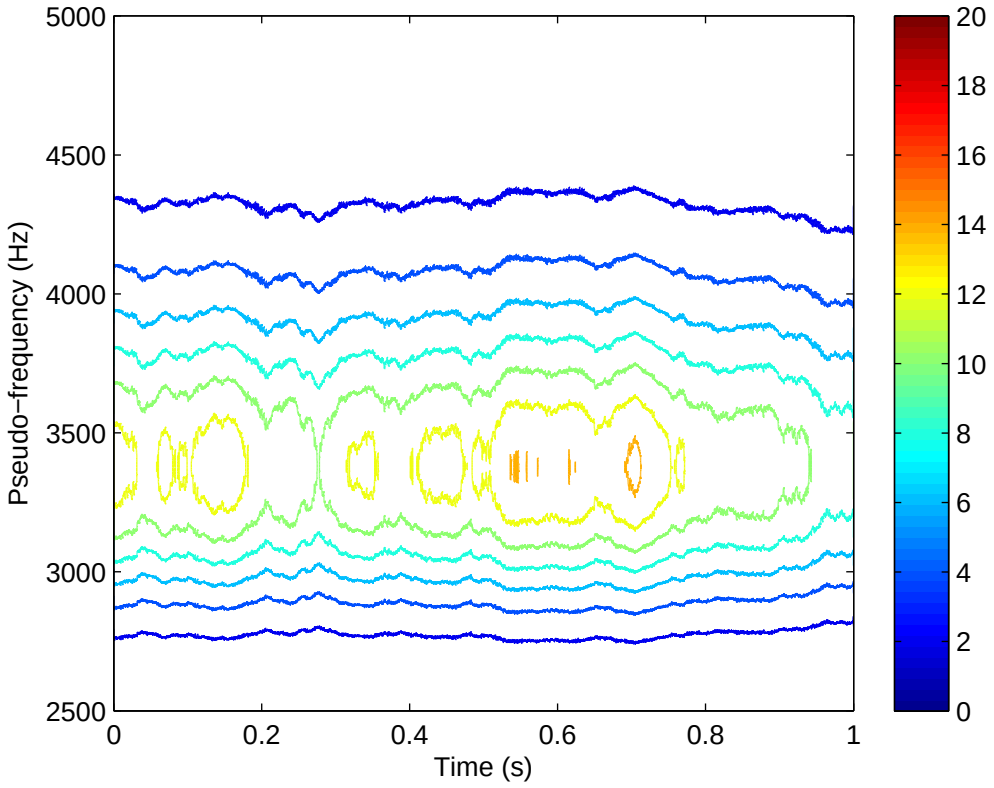

Figure 4.22: Wavelet analysis of the microphone signal for OTE static case at 1° over 1 second at pseudo frequencies of 2500 to 5000 Hz

Table 4.2: 1/3 octave band sound pressure levels between 2.5 kHz to 6.3 kHz for various trailing edge configurations

	2.5 kHz	3.15 kHz	4 kHz	5kHz	6.3 kHz
ZLA Dynamic Case	77.8	87.0	88.6	74.6	73.2
NSR Dynamic Case	76.0	88.7	75.6	71.6	72.0
WSR Dynamic Case	76.0	98.5	81.3	71.8	72.7
FPL Dynamic Case	77.8	92.6	83.4	72.4	72.9

section, the sound measurements for each case are examined in 1/3 octave bands, narrowband acoustic spectra and compared with wavelets in order for the changes in acoustic behaviour to be assessed.

The narrowband time average acoustic spectra are found in figures 4.23 to 4.26 for the ZLA, NSR, WSR and FPL cases. As references, the narrowband acoustic spectrum for OTE dynamic case and the wind tunnel background noise are plotted with each figure. The 1/3 octave spectra levels for bands centering at 2.5 kHz to 5 kHz are also presented to aid in the discussion of the narrowband acoustic spectra. The trend for 1/3 octave spectra levels for each trailing edge configuration case is similar to the OTE case as seen previously in section 4.4.1. The values can be found in table 4.2.

The ZLA case results are shown in figure 4.23. Like the static case, comparing with the OTE case, it was found that the ZLA configuration (i.e. the existence of the overlap) does not have a significant effect. For the frequency range shown, the ZLA case mostly follows the spectrum of OTE case. One notable exception was found in the frequency range after 4.1 kHz; where the broad frequency tonal component is found to have slightly increased levels. Comparing the 1/3 octave band sound pressure leves, the 4 kHz band increased by about 3 dB for the ZLA case comparing with the OTE case.

The sound pressure levels near the tone at 3.4 kHz and for the rest of the spectrum are nearly identical to the OTE case. For the 1/3 octave bands other than 4 kHz in table 4.2, the sound pressure levels for the ZLA case and the OTE case are within 1.2 dB of each other.

For the serrated cases, the narrowband spectrum of the NSR case and the WSR case are shown in figure 4.24 and 4.25 respectively. For 4.1 kHz tone, the serrated cases both display reductions in sound pressure level compared with the OTE case. The 1/3 octave band at 4 kHz for the NSR case shows nearly a 10 dB difference with the OTE case. The WSR case shows a 3.9 dB reduction compared with the OTE case.

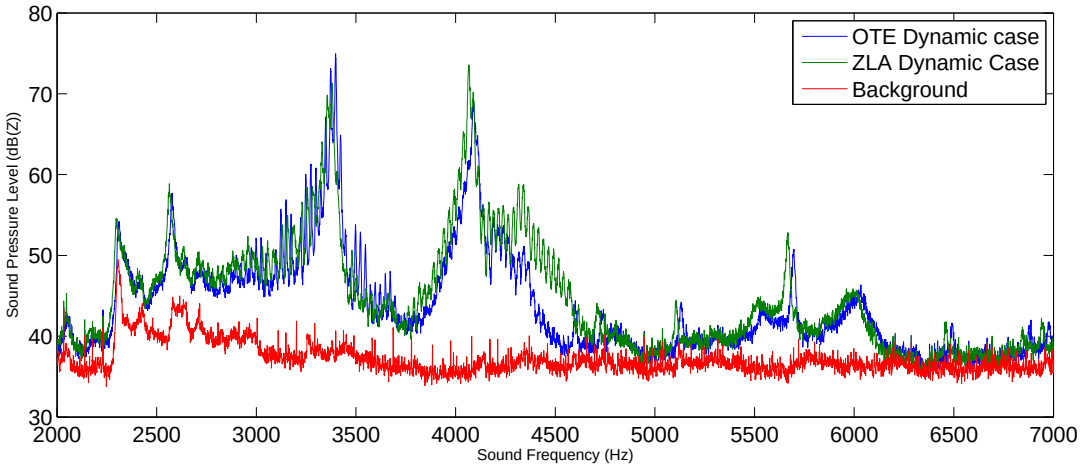

Figure 4.23: Narrowband acoustic spectrum of the ZLA dynamic case

At the 3.4 kHz tone, the NSR case displays similar sound pressure levels as the OTE case. The peak sound pressure level is at similar levels and is a slight reduction in the levels at surrounding frequencies. The WSR case displays slightly elevated sound pressure levels comparing with the OTE case; with greater side peak levels and a higher peak tonal value. In terms of 1/3 octave band levels, there is a difference of 0.5 dB between the NSR case and the OTE case.There is an increase of 10.3 dB for the WSR case.

The FPL case can be seen in figure 4.26. For the 4.1 kHz tone, there is a slight decrease in levels but not to the degree seen for the serrated cases. Peak tonal sound pressure level remains similar to the OTE case. For the 3.4 kHz tone, there is a broadband increase roughly 500 Hz below the tone's peak level. Overall, the 1/3 octave levels increased by 4.4 dB for the 3.15 kHz band. There is a decrease of 5.2 dB for the 4 kHz band.

The behaviour of the narrowband acoustic spectra can be explained with the results of the wavelet analysis. The typical wavelet analysis results within a one second time span between the pseudo frequency of 2.5 kHz and 5 kHz are found in figure 4.27, 4.28, 4.29 and 4.30 for the NSR, WSR FPL and ZLA cases respectively.

The noise measurements recorded for the various trailing edge configurations show results that exhibit the same features as the OTE case. Like the OTE case, each of the trailing edge configuration displays a noted pattern at a pseudo frequency of 25 Hz. Indeed, this 25 Hz pattern is attributed to the pressure fluctuations created by the periodic oscillation of the airfoil. The addition of the trailing edge modification was not expected to alter this behaviour. As the results are similar to those seen previously in figure 4.20,

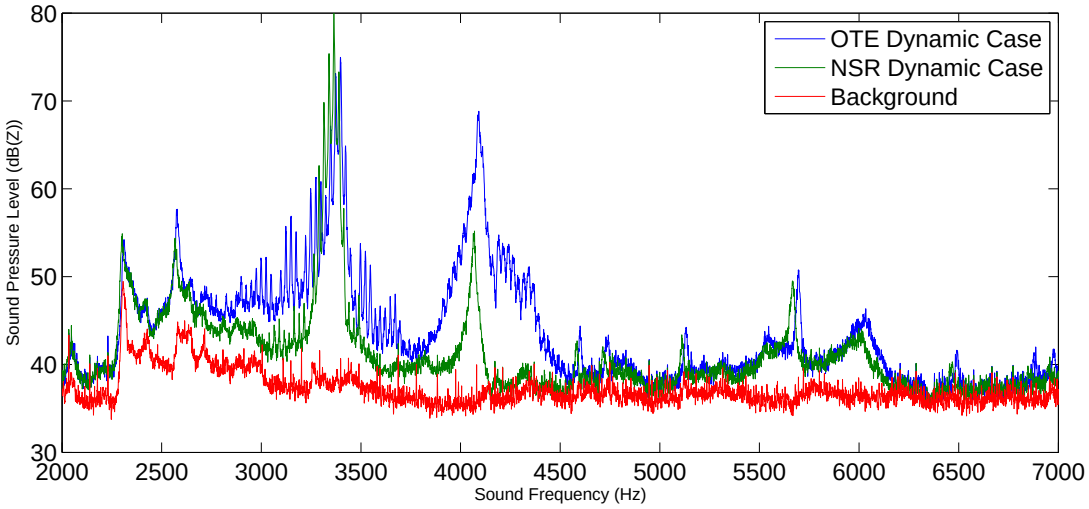

Figure 4.24: Narrowband acoustic spectrum of the NSR dynamic case

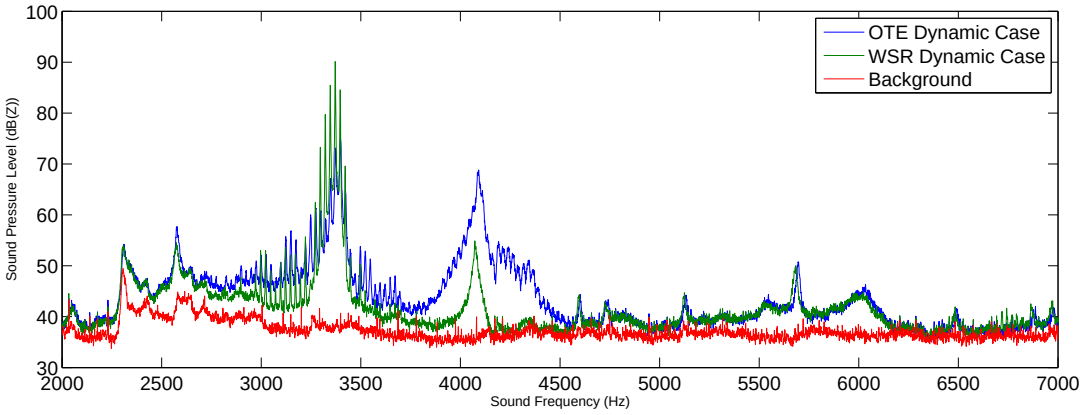

Figure 4.25: Narrowband acoustic spectrum of the WSR dynamic case

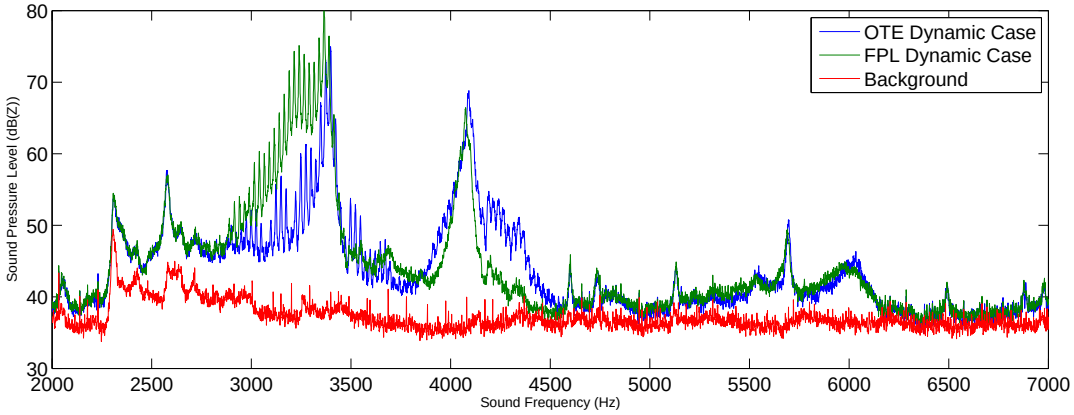

Figure 4.26: Narrowband acoustic spectrum of the FPL dynamic case

they will not be presented again.

At the pseudo frequencies where prominent tonal noise is observed (2.5 kHz to 5 kHz), wavelet contours are also found to occur periodically at the rate of 25 Hz. Again, given the explanation of this behaviour as discussed previously in section 4.4.1 and the presence of side peaks in figures 4.23 to 4.26, their presence is expected.

In general, for the wavelet coefficient contour patterns of the different trailing edge extension cases, their peak values were primarily found to center over the frequency of 3.4 kHz only. It is in contrast with the OTE case, the range of frequencies are found to be centered between the frequencies of the two prominent tones observed in the narrowband spectra: 3.4 kHz and 4.1 kHz. For example, in figure 4.21, the region of wavelet coefficient greater than 0.01 varies from 1000 Hz to 2000 Hz in span. For the WSR case shown in figure 4.28, the span is more frequently at 1500 Hz in width for the wavelet coefficient values greater than 0.01.

As well, the wavelet analysis shows the extent of the wavelet coefficient contours in the frequency domain to have been altered by the trailing edge extension. Both of these changes reduce the occurance of high wavelet coefficient values at 4.1 kHz. As such, when examining the narrowband acoustic spectra, the 4.1 kHz tone is decreased for all trailing edge attachment cases. Conversely, an increase was seen for the ZLA case due to higher rate of occurance of higher wavelet coefficient values at 4.1 kHz.

Further examining each individual case, it can be seen that the addition of the NSR pattern did not increase the magnitude of the wavelet coefficient, as the maximum wavelet coefficient seen in figure 4.27 is of similar value to the OTE case in figure 4.21. The

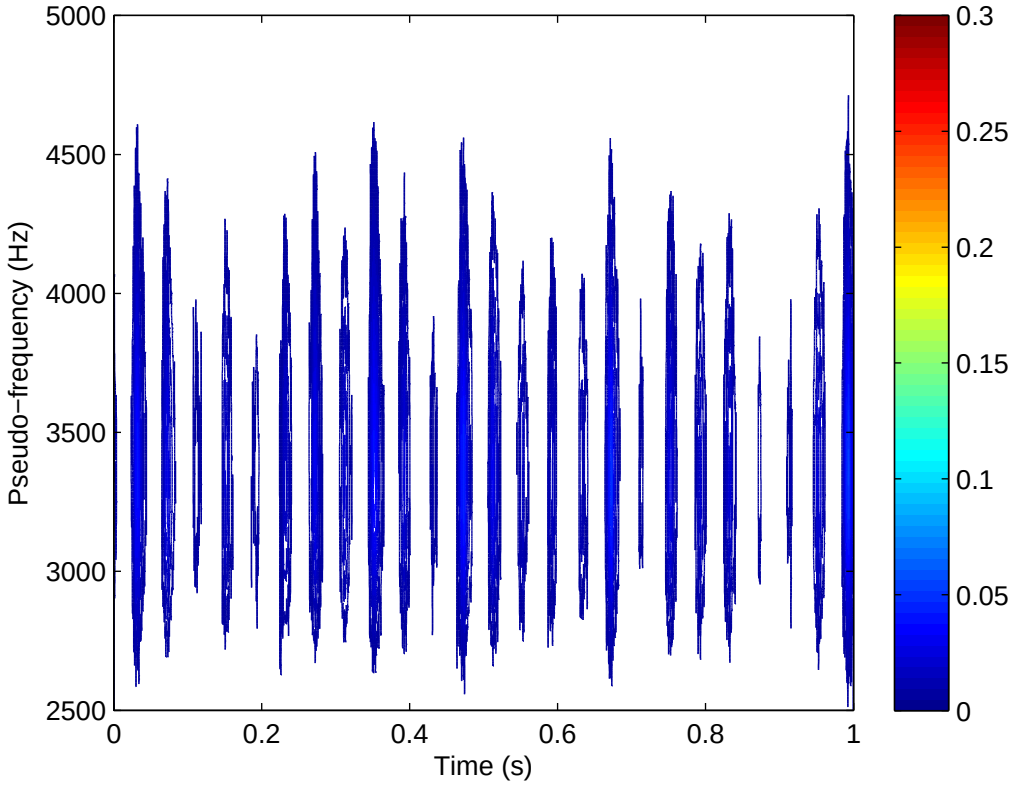

Figure 4.27: Wavelet analysis of the microphone signal for the NSR dynamic case

frequency extent of each wavelet also appears to vary periodically. For the OTE case seen in figure 4.21, the extent of the contours varies from 1000 Hz to 2000 Hz and occurs in a intermittent manner. For the NSR case, the contours seem to alternate from a wide spread frequency range to a narrow spread frequency at a rate of 2-3 cycles per second.

For the FPL and WSR case, there are much higher wavelet coefficients found throughout the spectra when compared with the OTE case. This corresponds with a greater magnitude of sound pressure levels as seen with the narrowband spectra results. In particular, the higher wavelet coefficient contours centered at 3.4 kHz corresponds with the increased sound pressure levels observed in the narrowband acoustic spectra near that frequency.

The contours of the WSR case and FPL case have a more consistent frequency span compared with the NSR case and the OTE case. For each cycle, it is more consistent for the WSR case or the FPL case to have a notable contour region present at 4.1 kHz

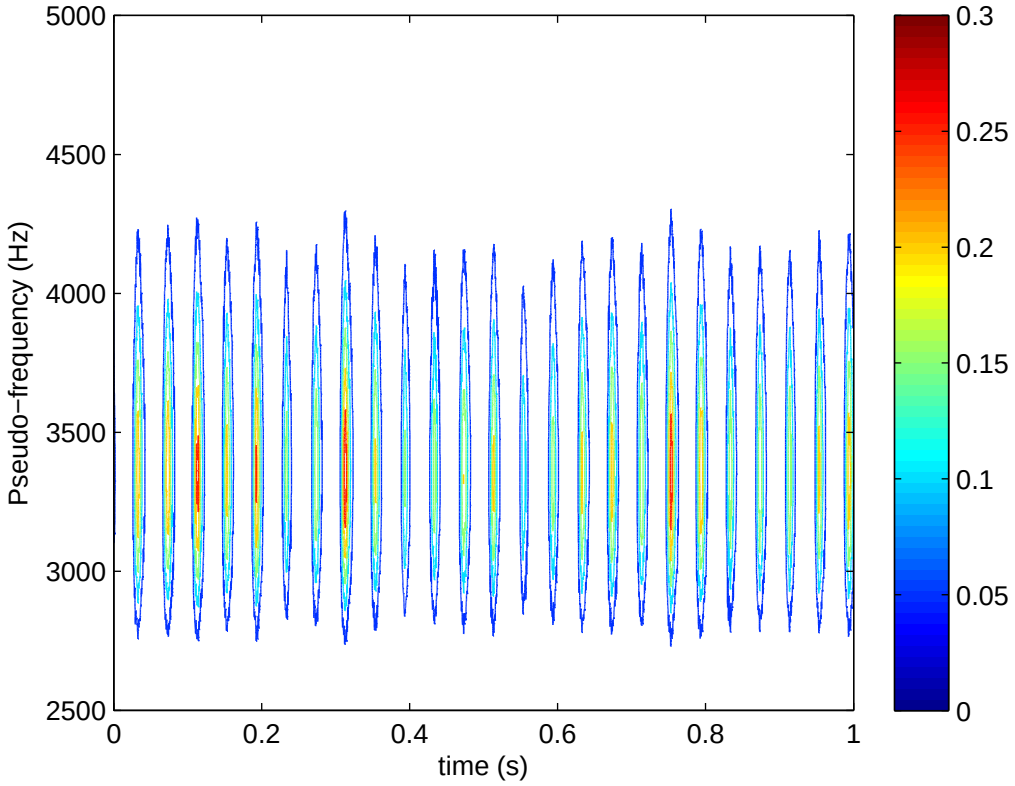

Figure 4.28: Wavelet analysis of the microphone signal for the WSR dynamic case

(comparing with the OTE case). Given that the contours do not center near 4.1 kHz, the WSR and FPL cases have reduced sound pressure level values compare with the OTE case at this frequency. The more frequent appearance of high contour levels at 4.1 kHz would explain the higher levels observed at the WSR case when compared with the NSR case. The FPL case has increased contour levels compare with the WSR case and NSR case. The increased contour levels undo the reduction effect of having the carrier frequency away from the 4.1 kHz. Hence, the 4.1 kHz tone for the FPL case has less reduction compared with the NSR case or the WSR case.

The ZLA results has similar contour levels compare with the OTE result. The presence of more wavelets contours with the span reaching to the frequency of 4.1 kHz contributes to the higher sound pressure level observed at that frequency in figure 4.23.

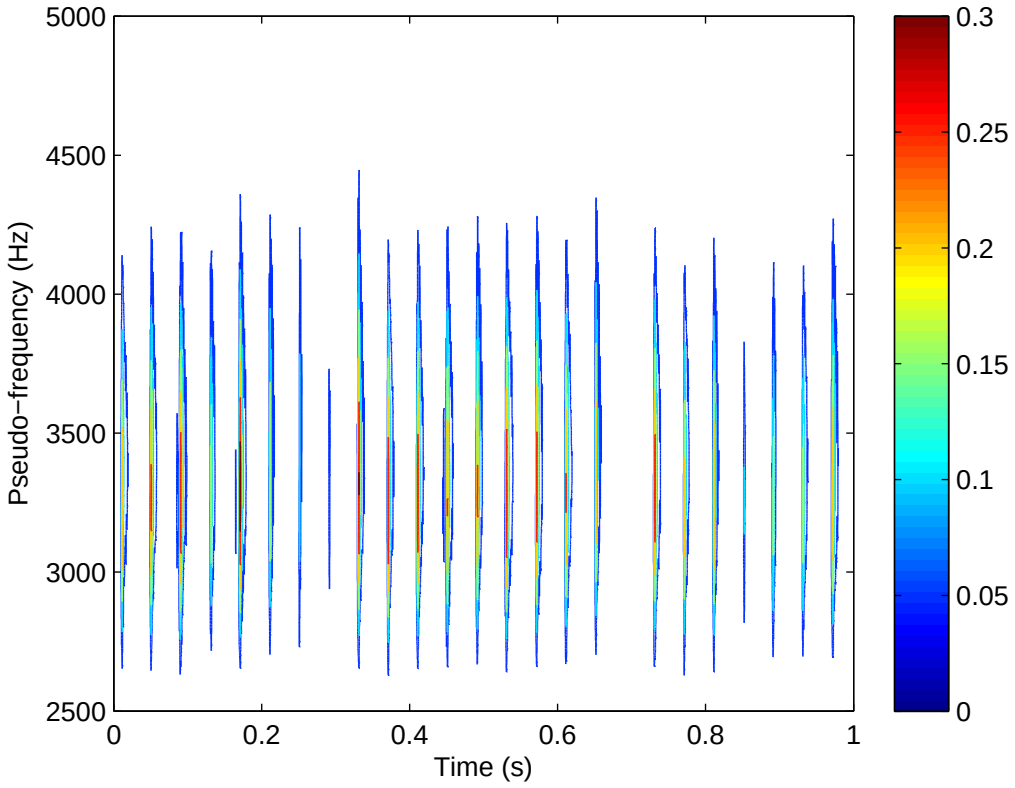

Figure 4.29: Wavelet analysis of the microphone signal for the FPL dynamic case

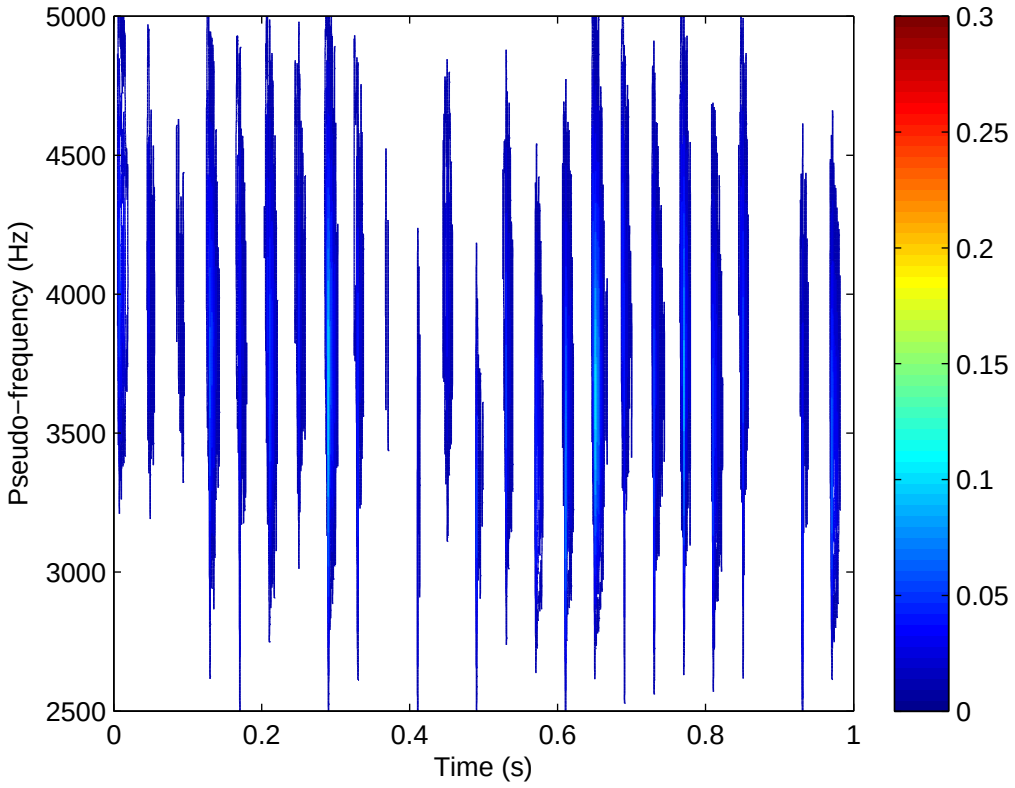

Figure 4.30: Wavelet analysis of the microphone signal for the ZLA dynamic case

4.6 Summary

In the current study, tonal noise caused by the LBL-VS noise generation mechanism has been examined under dynamic oscillation and at various static angles of attack for the the SD-7037 airfoil profile (at $Re_c = 4.0 \times 10^4$). Different from many past studies, there is evidence in the current experimental results to show LBL-VS noise to be generated from a mechanism located on the suction side of the airfoil. From other studies with similar findings [27] [29], the cause can be attributed to critical noise generation mechanisms being found on the suction side in the low Reynolds number regime ($Re_c < 10^5$).

The airfoil self-noise estimates calculated from the BPM model was initially found to be in poor arrangement with the experimental results. On inspection, the BPM model uses pressure side parameters to predict LBL-VS noise. By using suction side parameters, the BPM model yielded a better estimate for LBL-VS noise; better matching the results and trends with respect to the angle of attack observed in the experiments.

The dynamic case examined the SD-7037 airfoil profile under oscillation from 0° to 22° with a reduced frequency $k = 0.08$. This condition was previously studied aerodynamically by Gharali [6]. The tonal noise was found to be reduced compared with the static case results at low angles of attack. Examining the signal in the frequency and time domain has found that tonal noise occur at certain phases of the oscillation cycle. As well, side peaks were found in the dynamic case narrowband acoustic spectrum. The peak spacing corresponds to the oscillation frequency; suggesting the pressure fluctuation of the oscillation to contribute to the amplitude modulation in the main tone signal in this case.

Trailing edge sawtooth serrations had mixed effects on the tonal noise generated from the SD-7037 airfoil profile. For the static case, prominent tones were found to persist with small angles of attack, reducing the largest observed sound pressure level but increasing the sound pressure level in some instances when compared to the unmodified trailing edge counterpart. For the dynamic case, moderate reduction can be seen for the tonal components in the acoustic spectrum. Serrations of aspect ratio $\lambda/h = 0.67$ (NSR case) were found to be effective. This serration aspect ratio is similar to those found effective in other studies [77] [79]. The serrations with a wider aspect ratio of $\lambda/h = 1.33$ (WSR case) were found to be detrimental.

Chapter 5

Outdoor Noise Measurements

In this chapter, the results of acoustic measurements conducted with the Wenvor wind turbine at the Wind Energy Group outdoor wind turbine test site are discussed. The measurement campaign explores wind turbine noise emitted from an unmodified original trailing edge. The results shown here can assess the feasibility of future studies of aeroacoustic devices with the outdoor test site. The setup related to this experiment was discussed in section 3.2: Outdoor Experiments. This chapter is organized as follows:

- Characterization of the wind turbine test site background noise as a pre-analysis consideration (Section 5.1)
- Discussion and analysis of wind turbine noise experiments results (Section 5.2)
- Assessment of the test site feasibility for future acoustic measurement and recommendations (Section 5.3)

5.1 Background Noise Measurements

Before the analysis of the collected wind turbine noise data, the background noise characteristics of the test site should be fully understood. Some features of the test site background noise have already been identified and discussed qualitatively in section 3.2.1.1. The current section will focus on the quantitative findings related to the background noise of the test site as measured during the experiments.

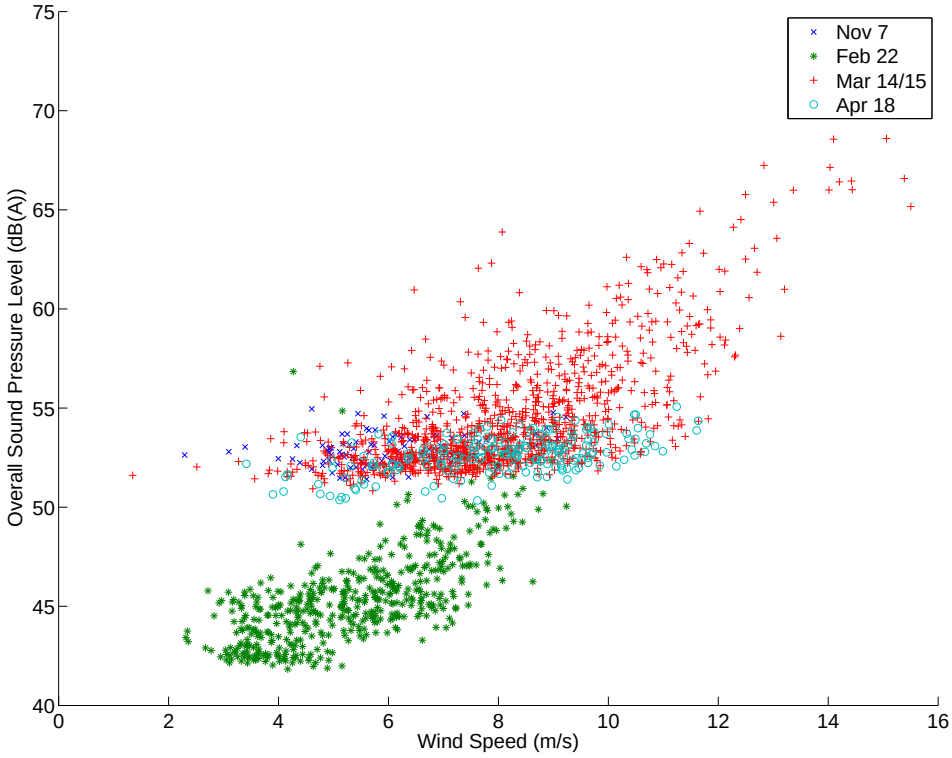

Figure 5.1: OASPL of background noise vs. windspeed as measured by the 20m RMY anemometer.

5.1.1 Overall Sound Pressure Levels

Figure 5.1 shows the 10 second averaged A-weighted overall sound pressure level (OASPL) of the background noise with respect to the average wind speeds measured by the 20m RMY anemometer. The background noise (1928 data points) used in the following discussion was collected during 4 separate days of experiments on site. The data points associated with each day are denoted by different marker types and colors in the figure.

From figure 5.1, the OASPL is seen to increase with increasing wind speed. This behaviour is well observed in past literature [33] [54]. The background noise data is divided into two separate groups. The results from November 7, March 14/15 and April 18 are similar to each other with only minor variations. The results from February 22 are found

to have OASPL at nearly 10 dB lower than the other results for a given wind speed. In comparison, the sound pressure level values from February 22 are comparable with those seen in the NREL studies [54] [55] [56] [57] [58] [59]. Reviewing the audio recordings from the experiments, it was found that the noise from the nearby bio-gas power plant was quieter on February 22; resulting in a quieter overall background noise during that day.

In terms of variability, the results of all days excluding Feb 22 are examined with respect to upstream wind directions. The box plots of integer wind speed bins values for various upstream wind direction intervals are shown in figure 5.2. The directions of $260° - 275°$, $275° - 305°$, $305° - 320°$ and $320°+$ are presented in figures 5.2a, b, c and d respectively.

While only the directions from $275° - 305°$ are considered valid in a setup conforming to the IEC standard [8] (i.e. within $\pm 15°$ of the microphone orientation), during the experiment, numerous datapoints have been found to be outside this interval. At the same time, as further discussed in section 5.2.1, the wind turbine is mostly yawed in this orientation. In the design of the experimental setup, the microphone measurement positions were determined based on turbine yaw orientation; with the assumption that upstream wind direction will mostly be aligned with the turbine. The current experiment is considering data points with upstream wind directions outside the interval conforming with the IEC standard [8]. If there are any differences, they should be identified.

For the upwind directions of $275° - 305°$, as shown in figure 5.2b, the range of values within an integer wind speed bin is roughly 8 dB on average. This range of values is similar to those seen in other studies [54] [55] [56] [57] [58] [59].

As the upstream wind direction become more misaligned with the microphone orientation, the variability tends to decrease. For the directions of $260° - 275°$ and $> 320°$, with box plot results shown in figure 5.2a and d respectively, the range of values within an integer wind speed bin is less than 5 dB on average. The $305° - 320°$ direction, with box plot results shown in figure 5.2c is also seen to have slightly reduced variability compared to $275° - 305°$. The reduction in variability with greater misalignment of wind direction and microphone orientation may be related with directivity of sound.

The average OASPL values within integer wind bins are also different when comparing with respect to wind direction. Figure 5.3 shows the average OASPL values of results from days excluding February 22 when binned with respect to integer wind speeds and upstream wind direction intervals. The results from the directions of $260° - 275°$, $305° - 320°$ and $> 320°$ are presented in sub-figures a, b, and c respectively. These intervals are compared with data in the direction of $275° - 305°$ (range conforming to setup from IEC standard [8]). The values are derived from bootstrap sampling. The 95% confidence interval of the average values are also presented in the figures. A summary of sample sizes for each integer

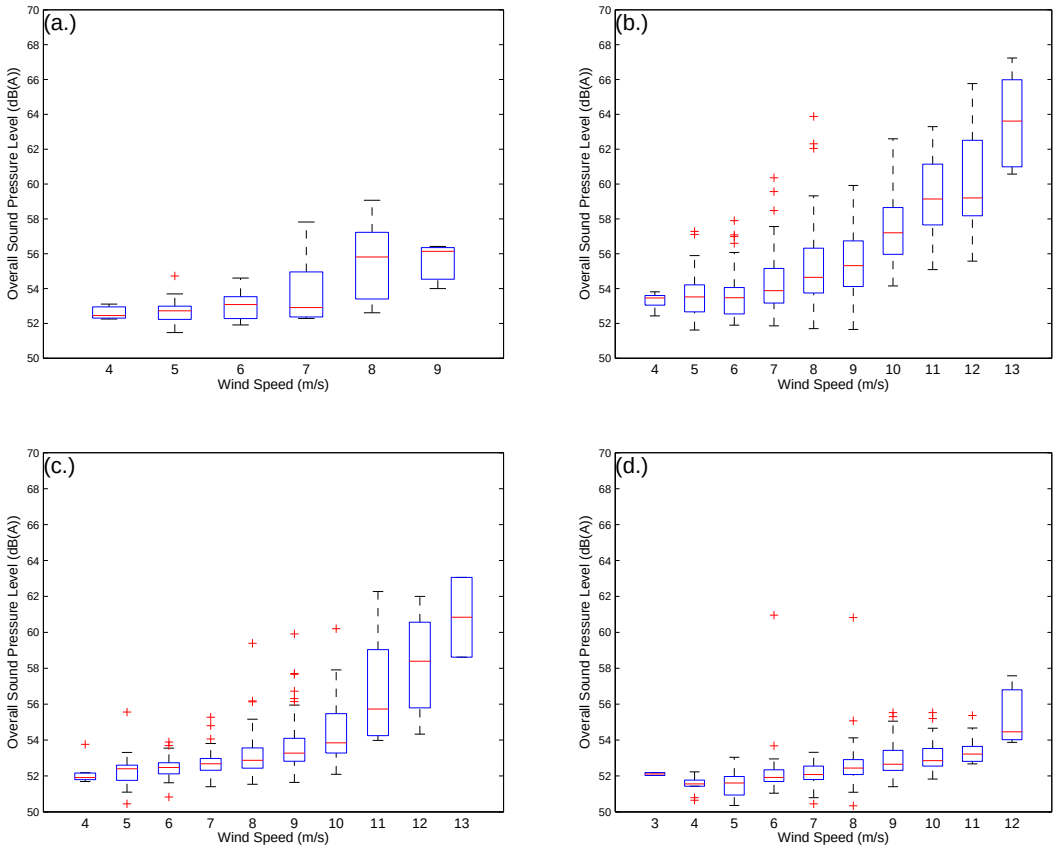

Figure 5.2: Box plot of background noise OASPL values at different integer wind speed bins with respect to upstream wind direction. a.) $260° - 275°$ b.)$275° - 305°$ c.)$305° - 320°$ c.) $> 320°$

Table 5.1: Sample size of the background noise datapoints in bins of wind directions and wind speeds from 4 m/s to 13 m/s

20m RMY Wind Speed	**4 m/s**	**5 m/s**	**6 m/s**	**7 m/s**	**8 m/s**	**9 m/s**	**10 m/s**	**11 m/s**	**12 m/s**	**13 m/s**
260° – 275° (Sample Size)	3	12	13	7	6	3	N/A	N/A	N/A	N/A
275° – 305° (Sample Size)	5	18	64	87	103	108	61	33	22	6
305° – 320° (Sample Size)	7	31	61	119	104	80	46	29	8	2
> 320° (Sample Size)	10	25	44	55	75	71	41	15	3	N/A

wind speed bin of the different intervals can be found in table 5.1.

In figure 5.3a, the binned values for the direction of $260° - 275°$ are similar to their counterparts for the direction of $275° - 305°$. Indeed, there is generally less than 1 dB difference between the binned values. The differences were not found to be significant.

For angles between $305° - 320°$, the binned OASPL values in figure 5.2b are 1-2 dB lower than their counterparts in the direction of $275° - 305°$. Again, this can be attributed to directivity. The differences between the average values in the bins are significant; with the confidence interval for the differences in bin values typically ranging from 1-3 dB for the same integer wind speed. The values from $305° - 320°$ are consistently lower. However, the values from $305° - 320°$ still increase with windspeed in a similar manner to those from the $275° - 305°$ direction.

For angles $> 320°$, as shown in figure 5.2c, there is a notable difference between the results. Compared binned average values, the differences are found to be on average 3 dB apart, with the confidence interval in the differences typically spanning from 2-4 dB. At higher wind speeds, the trend for $> 320°$ direction appears to diverge from those in the direction of $275° - 305°$; exhibiting a more linear relationship in constrast to the exponential increase.

Given these results, it appears that datapoints from wind direction range of $260° - 275°$ and $305° - 320°$ have similarities with the datapoints from $275° - 305°$. The addition of data from these direction intervals would not significantly increase the variability or cause a large change in average values of binned wind speeds. Regarding to their use in the analysis of the current study, the decision is coupled with considerations needed to be

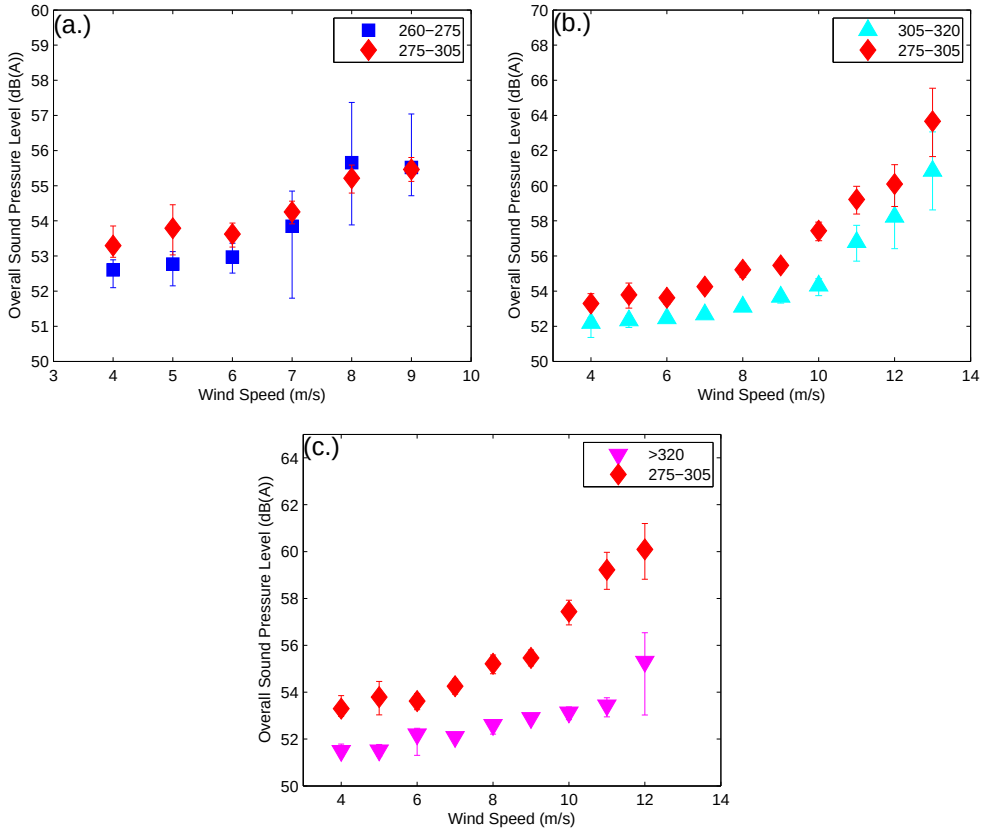

Figure 5.3: Average values of background noise OASPL in different integer wind speed bins with respect to upstream wind direction. Bars indicating 95% confidence interval of the mean value as derived from bootstrap sampling. a.) $260° - 275°$ b.) $305° - 320°$ c.) $> 320°$. Values are compared with the directions of $275° - 305°$.

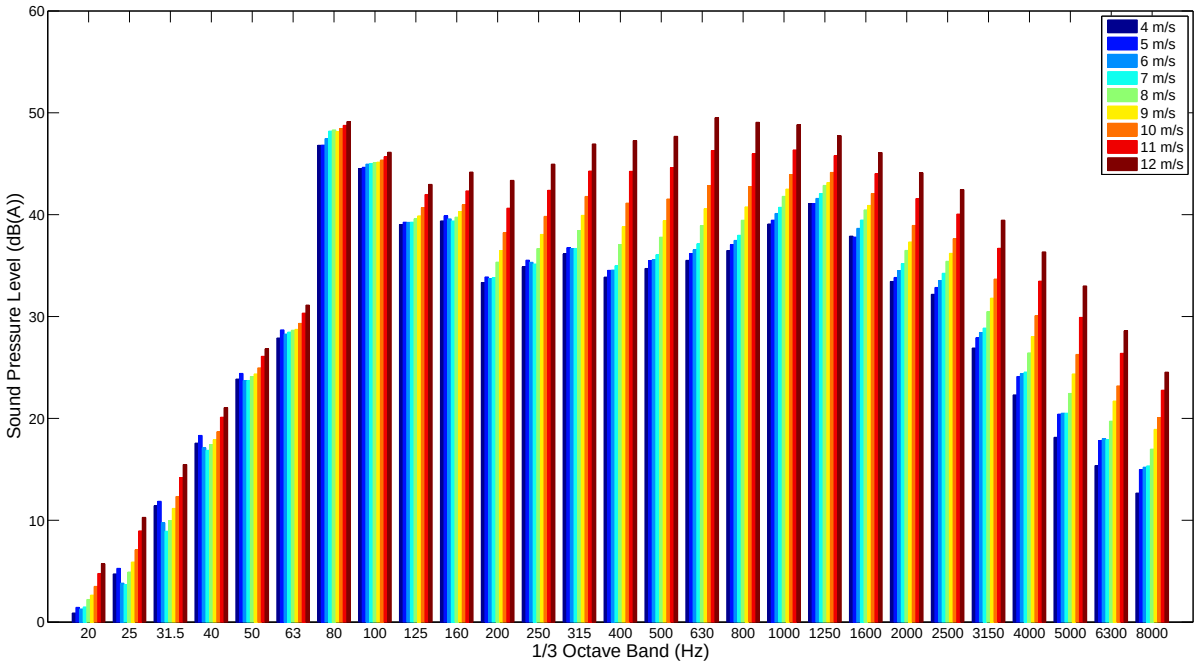

Figure 5.4: 1/3 octave band acoustic spectra of the background noise at various wind speed bins

made for wind turbine noise measurements. A further discussion can be found in section 5.2.1.

5.1.2 Frequency Spectrum

The existing noise sources at the Wind Energy Group test site can be further understood by examining the frequency spectrum of the background noise data. Figure 5.4 shows the 1/3 octave sound pressure level spectra (from 20 Hz to 8,000 Hz) of the background noise at various wind speed bins. Like the OASPL results, the A-weighted acoustic spectra results are presented. As such, 1/3 octave bands are attenuated at the low end of the frequency spectrum.

From figure 5.4, the acoustic spectra of the background noise appears to have two peaks; found near the 80 Hz band and the 1000 Hz band. The 1000 Hz band peak corresponds with the broadband ambient noise. The peak at 80 Hz is associated with the low frequency

noise associated with the equipment of the bio-gas power plant. Despite the attenuation of the A-weighting at the low end of the frequency spectrum, high sound pressure level values are still found between the bands of 80Hz to 160 Hz.

While it is also possible to attribute high sound pressure levels in this frequency range to wind induced microphone noise (Wind induced noise to be found in low/mid frequency range from 63 Hz to 400 Hz [33]), a review of the audio recordings from experiments suggests the high levels to be attributed to low frequency machinery noise is prominent on site.

With respect to increasing wind speeds, the acoustic spectrum is found to retain the same profile throughout the various wind speeds observed. For 1/3 octave bands of 500 Hz or greater, the sound pressure level values are generally seen to increase non-linearly with steady increase of wind speed. At frequencies below 400 Hz, there is relatively flat response to changing wind speed when the wind speed is below 8 m/s. This is likely due to the ambient environmental noise (from the bio-gas power plant and other sources) obscuring the contribution of the wind noise. As the wind flow noise becomes more prominent with increasing wind speed, the sound pressure level would increase with increasing wind speed.

With regards to tonal noise, it was not apparent that a significant tonal noise was present on site during the experiments. While examining the narrowband acoustic spectrum was not included as part of the scope in the original experimental plan, several unplanned fast fourier transform (FFT)/ narrowband frequency spectra were measured for some wind speeds during the experiments. Selected results from March 14/15 are shown in figure 5.5. For the results at 7.55 m/s and below 2500 Hz, minor distinct tones can seen throughout the spectra. With higher wind speeds, the tones appears to be obscured.

The presence of the tones in the background noise on site is not found to be an issue in the analysis of the wind turbine noise spectral profile. It was found that the background tones are either obscured by the turbine noise or are clearly distinguisable from the wind turbine noise signature. This is further discussed in section 5.2.3.

5.1.3 Impact on Analysis

Given the presence of prominent noise sources from the bio-gas power plant at the test site, there is a concern that the signal of the wind turbine noise may not be able to be resolved in the measurements from the background noise, i.e. weak signal to noise ratio (SNR). The high levels of background noise have made it difficult to resolve the wind turbine contributions when comparing OASPL values. For the current study and the future study of the noise reduction properties of serrations at the test site, the wind turbine noise levels

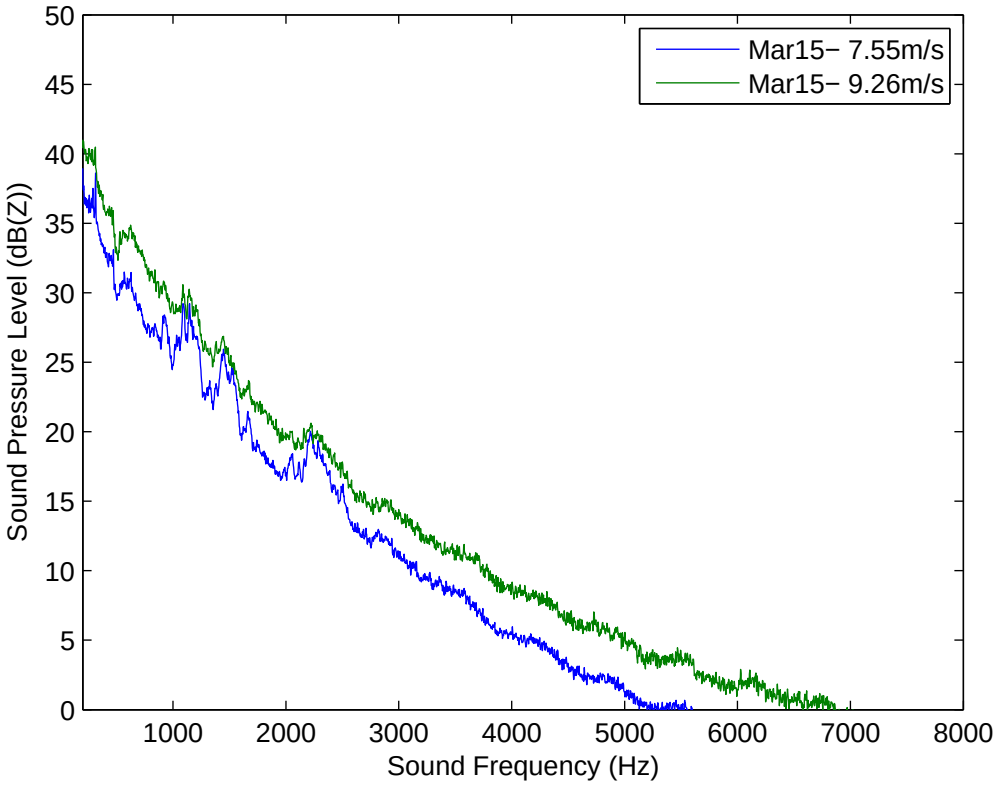

Figure 5.5: Narrowband acoustic spectra of wind turbine test site background noise on March 14/15. Average wind speed during measurement at 7.55 m/s (blue) and 9.26 m/s (green)

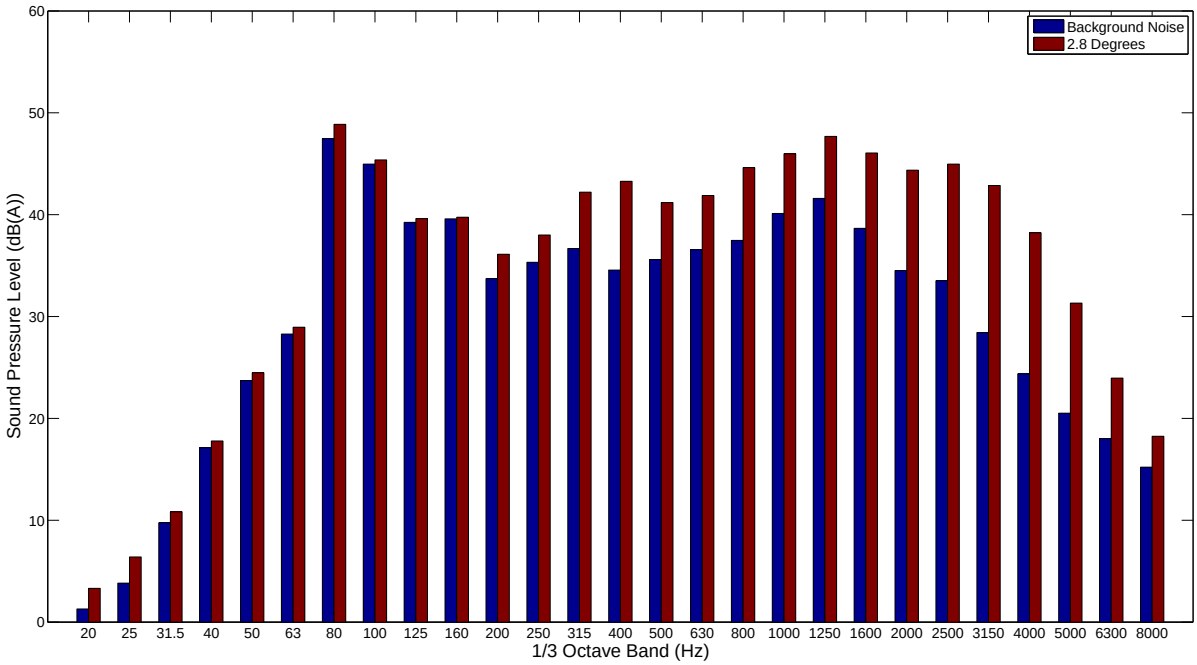

Figure 5.6: 1/3 octave band acoustic spectra of the background noise from the 6 m/s integer wind speed bin, compared with wind turbine noise at normal operation (blade pitch angle of 2.8°). Data from this graph came from all days except February 22

must be well above the background noise levels in order for it to be discernable from the measurement of the combined noise.

To examine this issue, the background noise levels are compared to the turbine noise results. Figure 5.6 shows the 1/3 octave spectrum of the background noise and the wind turbine at the wind speed bin of 6 m/s. As the wind speed increases, the difference between the background noise and wind turbine noise becomes less (discussed further in section 5.2.2). However, the basic relationship shown in figure 5.6 represents a typical relationship throughout the various wind speeds.

While there may not be large differences in OASPL levels between the background noise and wind turbine noise measurements, it was found that at a certain part of the frequency spectrum, there are greater differences between the two measurements. At frequencies below 200 Hz, the background noise and the wind turbine noise measurements have similar sound pressure levels. Given the high levels of noise from the bio-gas power plant, a low

difference is to be expected.

At higher frequencies, the wind turbine noise is found well above the background noise, with broadband noise prominently found greater than 500 Hz. There are also greater differences in the sound pressure levels when compared with the background noise; allowing for a much stronger SNR.

As such, it can be beneficial to assess the wind turbine noise in specific 1/3 octave bands where it is prominent.

5.2 Wind Turbine Noise

This section presents the experimental results of the Wenvor wind turbine noise. During the experiments, the wind turbine noise is combined with background noise contributions when the sound pressure levels were measured. The following discussion will examine the factors affecting the combined noise measurements and to evaluate the wind turbine noise emissions by subtracting the background noise contributions from the combined noise measurements.

5.2.1 General Assessment

Like the test site background noise results discussed in section 5.1, the combined noise measurements of the wind turbine and the background can vary with respect to different parameters on site. With the background noise, as seen in section 5.1.1, the wind speed and the upstream wind direction had an impact on the measured sound pressure levels. In the case of sound pressure levels contributions from the wind turbine, it can be affected by the same factors as well as other factors related to rotor aerodynamics.

Figure 5.7 shows the OASPL of the combined noise on site with respect to the wind speed measured from the 20m RMY anemometer for the different days of experiments. In total, there are 2827 data points shown in the figure. The results are comparable to the background noise results shown previously in figure 5.1.

Like the background noise, the combined noise increases with increasing wind speeds. The rate of increase of OASPL with wind speed for the combined noise is similar to the background noise results. However, the OASPL of the combined noise results are greater than their background noise counterparts due to the addition of the wind turbine noise contributions. Indeed, the airfoil self-noise increases with increasing freestream velocity

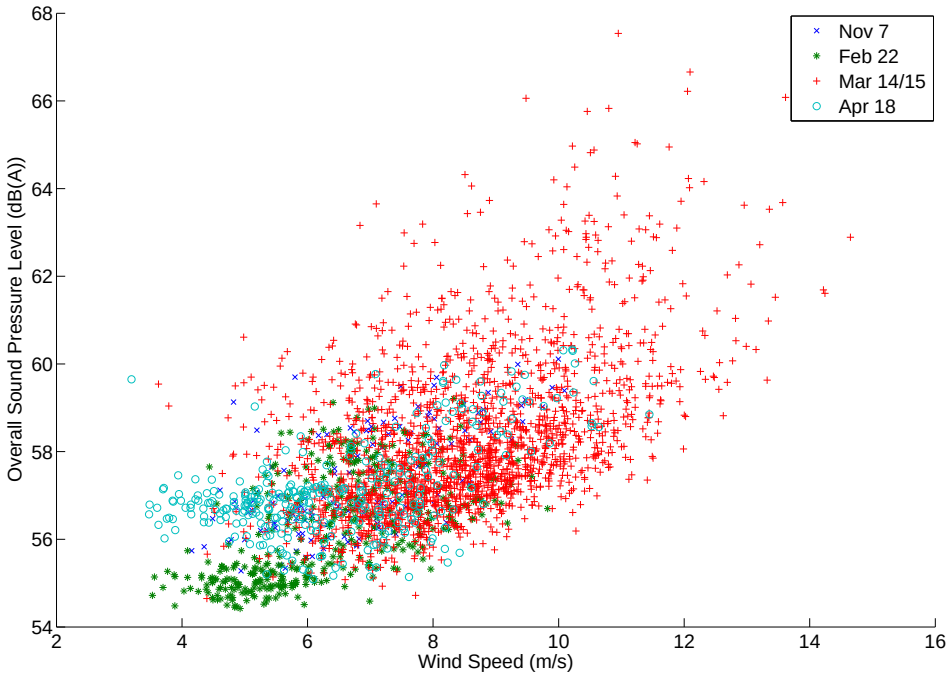

Figure 5.7: OASPL vs. 20 RMY wind speed for combined (wind turbine and background) noise measurements

(U_∞) to the airfoil, which is partially affected by the wind speed on site. As such, the combined noise is expected to behave in this manner.

Unlike the background noise, the OASPL of the combined noise from February 22 are found to be similar to levels seen in the other days of experiments. From figure 5.1, the background noise from Feb 22 are seen to be roughly 10 dB lower than their combined noise sound pressure levels counterparts. Due to the negligible contributions of the background noise, as evident from the large sound pressure level differences, the OASPL values for February 22 reflect mostly the wind turbine noise contributions.

For the effects of upstream wind directions, the combined noise data is seen to behave similarly to the background noise results. Figures 5.8 and 5.9 presents the box plot and average values of each integer wind speed bins at the upstream wind direction intervals previously defined in section 5.1.1. These figures are directly comparable with the background noise results shown in figure 5.2 and 5.3. A summary of the sample size in each

Table 5.2: Sample size of the combined noise datapoints in bins of wind directions and wind speeds from 4 m/s to 13 m/s

20m RMY Wind Speed	**4 m/s**	**5 m/s**	**6 m/s**	**7 m/s**	**8 m/s**	**9 m/s**	**10 m/s**	**11 m/s**	**12 m/s**	**13 m/s**
260° – 275° (Sample Size)	21	40	48	24	24	6	6	N/A	N/A	N/A
275° – 305° (Sample Size)	13	48	93	170	191	152	89	53	6	N/A
305° – 320° (Sample Size)	N/A	21	70	186	247	256	155	87	30	11
> 320° (Sample Size)	N/A	N/A	11	46	64	54	41	24	N/A	N/A

bin, comparable to table 5.1, is shown in table 5.2.

From these figures, it can be seen that the observations made for backgound noise results still hold for the combined noise results. In terms of variability, from figure 5.8, the range of values within each bin is found to be greatest between 275° – 305°, as shown in sub figure b. On average, there is a 7 dB range within each wind speed bin. The bin from the other wind direction intervals behave similarly to their background noise counterparts. The bins from the wind directions of 260° – 275° (in sub figure a) and > 320° (in sub figure d) have less variability. The bins from the direction of 305° – 320°, as shown in sub-figure c, behave similarly to the directions of 275° – 305°.

For the average values, in figure 5.9a, the values of bins from the direction of 260° – 275° values are found to be closely similar to those from the direction of 275° – 305°. In figure 5.9b, the values form the direction of 305° – 320° are found to be consistently lower than their counterpart from the direction of 275° – 305°; with an average difference of 1.6 dB. However, the values for both intervals change with wind speed at a roughly similar trend. Figure 5.9c shows a slightly larger difference between the average values in bins between the directions of > 320° and 275° – 305°. There is also a divergence of values at higher wind speed bins. All of these observations are similar to those made for the background noise results in section 5.1.1.

In examining the directional effects of the combined noise measurements, the effects of the wind turbine yaw direction should be considered as well. Table 5.3 shows the sample size of combined noise measurements for the various wind turbine yaw direction intervals. Comparing to the distribution of samples in the various directional intervals with the upstream wind directions results in table 5.2, it can be seen that the yaw direction data

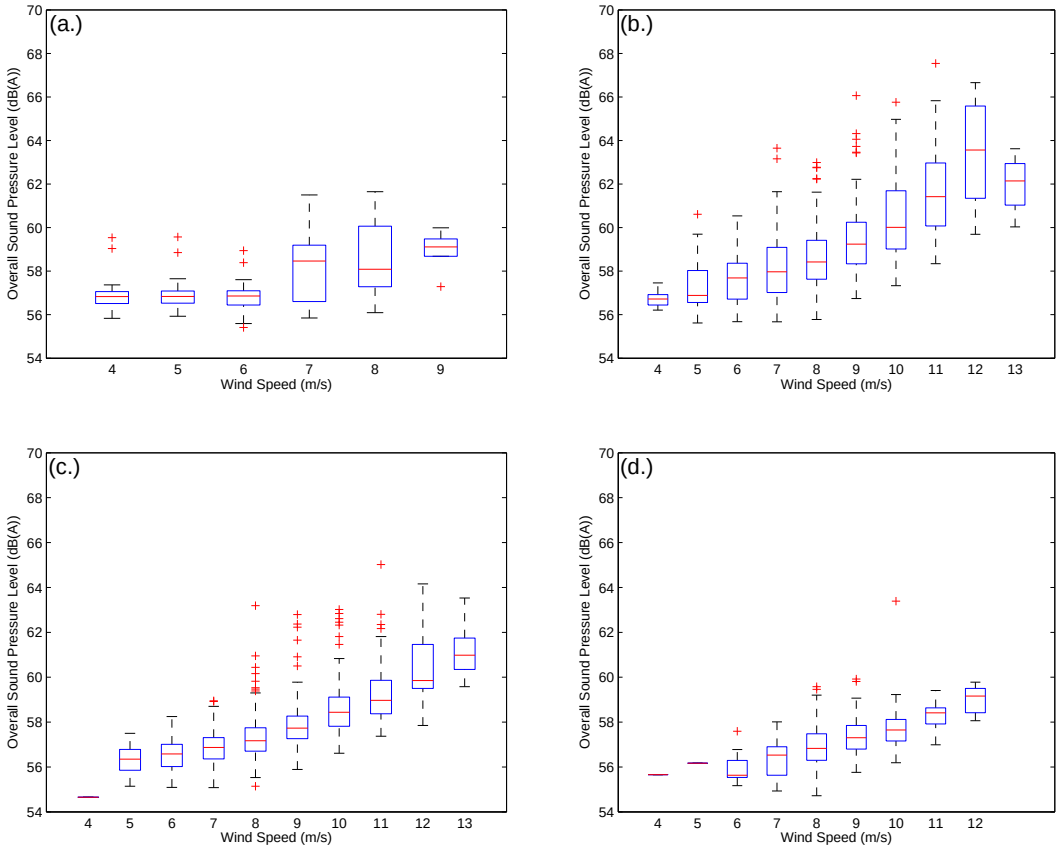

Figure 5.8: Box plot of the combined noise OASPL values at different integer wind speed bins with respect to upstream wind direction. a.) $260° - 275°$ b.) $275° - 305°$ c.) $305° - 320°$ d.) $> 320°$

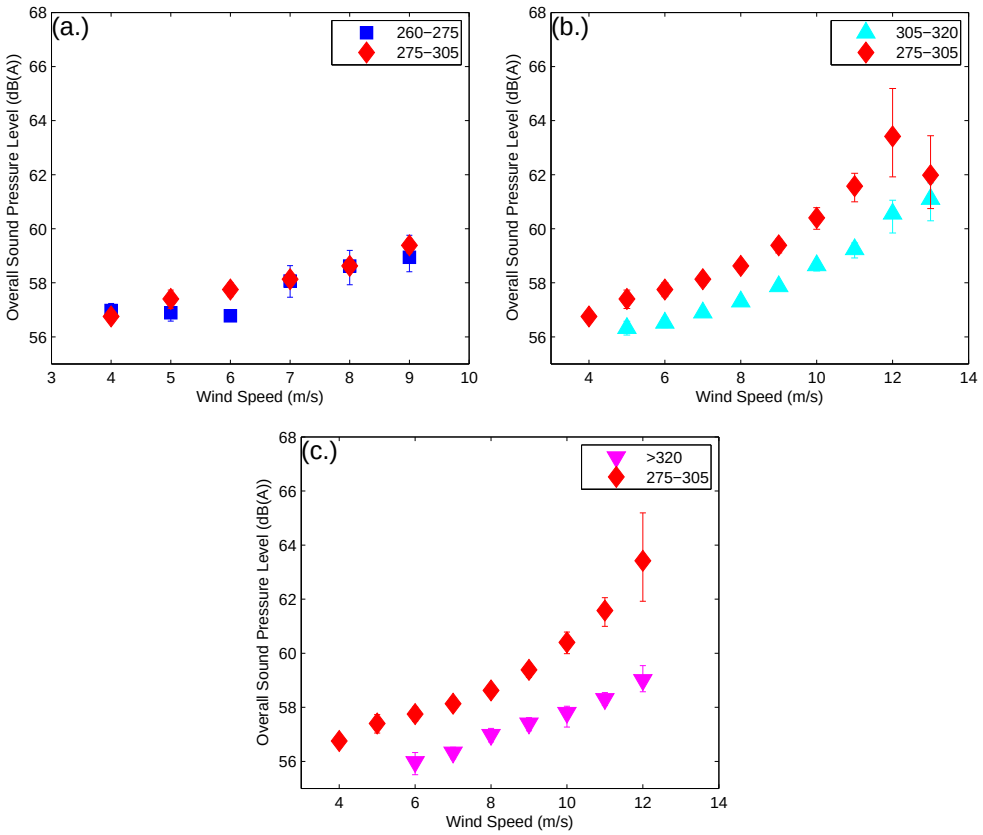

Figure 5.9: Average values of the combined noise OASPL values of different integer wind speed bins with respect to upstream wind direction as derived from the bootstrap sampling method. Bars indicating 95% confidence interval of the mean value a.) $260° - 275°$ b.) $305° - 320°$ c.) $> 320°$. All graphs are compared with the average value from the direction of $275° - 305°$.

Table 5.3: Sample size of combined noise datapoints in bins of yaw direction and wind speeds from 4 m/s to 13 m/s

20m RMY Wind Speed	**4 m/s**	**5 m/s**	**6 m/s**	**7 m/s**	**8 m/s**	**9 m/s**	**10 m/s**	**11 m/s**	**12 m/s**	**13 m/s**
$260° - 275°$ (Sample Size)	23	50	57	35	42	15	8	N/A	N/A	N/A
$275° - 305°$ (Sample Size)	12	65	143	350	436	406	254	140	43	18
$305° - 320°$ (Sample Size)	N/A	9	24	37	32	31	16	15	N/A	N/A
$> 320°$ (Sample Size)	N/A	N/A	9	12	N/A	2	3	2	N/A	N/A

behaves differently.

The wind turbine yaw direction was mostly found to be between the directions of $275° - 305°$; within $15°$ of the microphone position. At the same time, the wind direction is skewed with the many data points found from a direction greater than $305°$. Given the passive design of the yawing system, it was assumed that the upstream wind direction would, on average, be aligned with the wind turbine yaw direction. The results show a misalignment between the yaw direction and the upstream wind direction. The differences may be attributed to a mechanical resistance/stiffness in the yawing mechanism or the inertia associated with the wind turbine.

During the design of the experiment, the microphone location was selected based on the yaw direction (from data available up until that time). The location should be well aligned with the rotor plane of the wind turbine to allow for the best sound directivity. As the wind turbine contribution is expected to be the most prominent component in the combined noise measurement, this decision appears appropriate. Given the dynamic nature of the passive yawing system, it was not possible to keep the microphone directly perpendicular with the rotor at all times.

Given the yaw/upstream wind direction misalignment was observed for many of the datapoints, it is necessary to consider data points with upstream wind directions outside of $\pm 15°$ of the microphone. For the current study, all data from wind direction of $260° - 320°$ are included for consideration in the analysis. While this differs from the IEC standard [8], including the broader range of wind direction would be reflective of the turbine actual operating condition. The range of $260° - 320°$ was selected as the data does not differ greatly with the $275° - 305°$ range.

Examining the combined noise OASPL results with respect to the wind turbine yaw direction further, the average values of an integer wind speed bins for the various yaw direction intervals are shown in Figure 5.10. The directional intervals of $260° - 275°$, $305° - 320°$, $> 320°$ are shown in sub-figures a, b, and c respectively. Comparing with the upstream wind direction results from figure 5.9, the yaw direction results have smaller differences when comparing bin values between the directions of $275° - 305°$ with the other directional intervals. The differences between the direction-wise bin values are less than 2 dB. Although, from the confidence interval values, the differences are found to be statically significant.

It appears that the directivity of rotor noise is less sensitive in comparison with the directivity of noise from upstream wind. For future experimental designs, the directivity with the rotor may be less of an issue for consideration. For the current study, the wind turbine yaw direction results from $275° - 305°$ is considered.

As for other factors affecting the combined noise measurements related to the aerodynamics of the rotor, the pitch angle of the blade and rotor rpm can also be examined. From the review of airfoil self-noise mechanisms in section 2.1, the angle of attack has drastically affects the airfoil boundary layer conditions and therefore the mechanics of noise generation. The rpm affects the value of U_∞. Indeed, U_∞ is known to related to the sound pressure to the fifth power [36]. As such, there should be notable impact as well.

Figure 5.11 shows the relationship between the OASPL of the combined noise with the Wenvor turbine blade pitch angle. As a reference, the wind speed associated with each data point is indicated by color contours. At each blade pitch angle, there is a notable spread of the OASPL values. This is related to the varying wind speeds observed.

With decreasing blade pitch angle, the angle of attack throughout the blade increases, leading to blade stall and a increase in OASPL. Comparing the average OASPL values at various blade pitch angles, accounting for wind speed, only a minor influence was found. For the same integer wind speed, the average OASPL of when the blade is at operating pitch ($2.8°$) is found to be 1 to 2 dB lower on average than the noise emitted when the blade pitch is at the other end of the spectrum (i.e. $< -8°$).

For this study, the wind turbine noise at the operating pitch angle of $2.8°$ is further examined. While the wind turbine blades at various pitch angles are part of the normal operation of the wind turbine, examining the turbine noise output at the operating pitch controls one of the many variables affecting the wind turbine noise emission. Further discussion can be found in section 5.2.2.

As for rpm, the data points presented so far are collected when the wind turbine rotor was rotating at a fixed rpm due to the generator being synchronized with electrical

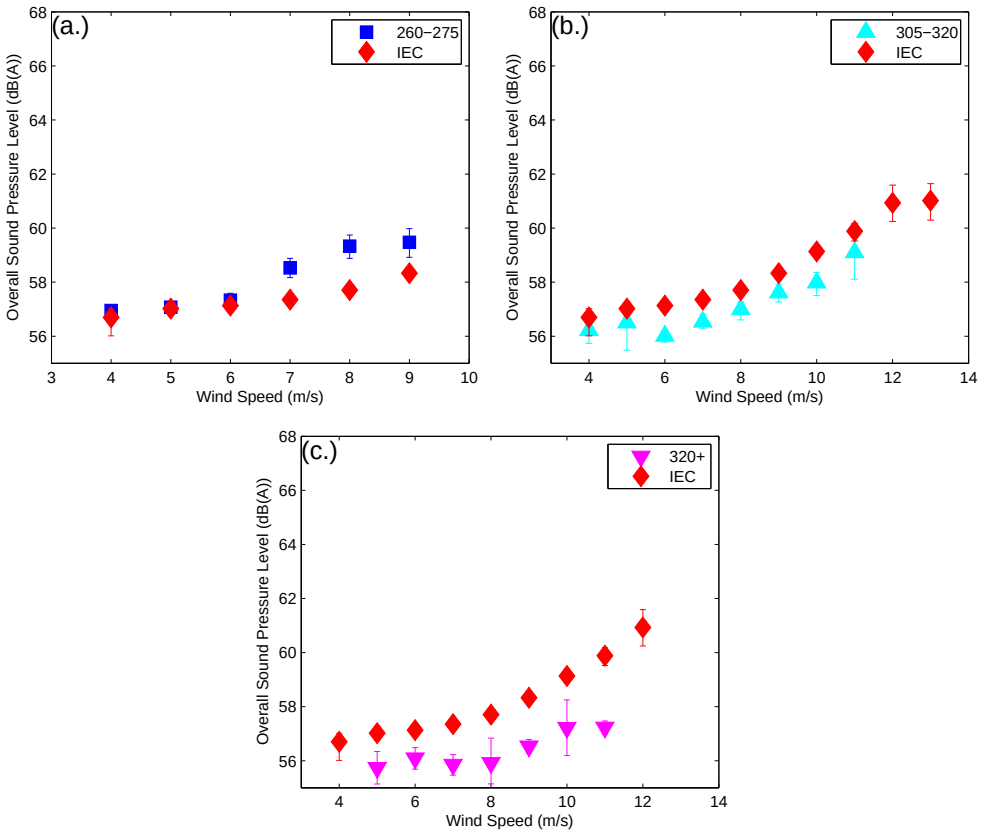

Figure 5.10: Average values of the combined noise OASPL values of different integer wind speed bins with respect to wind turbine yaw direction as derived from the bootstrap sampling method. The values compared with results from the yaw direction of $275° - 305°$. Bars indicating 95% confidence interval of the mean value a.) $260° - 275°$ b.) $305° - 320°$ c.) $> 320°$.

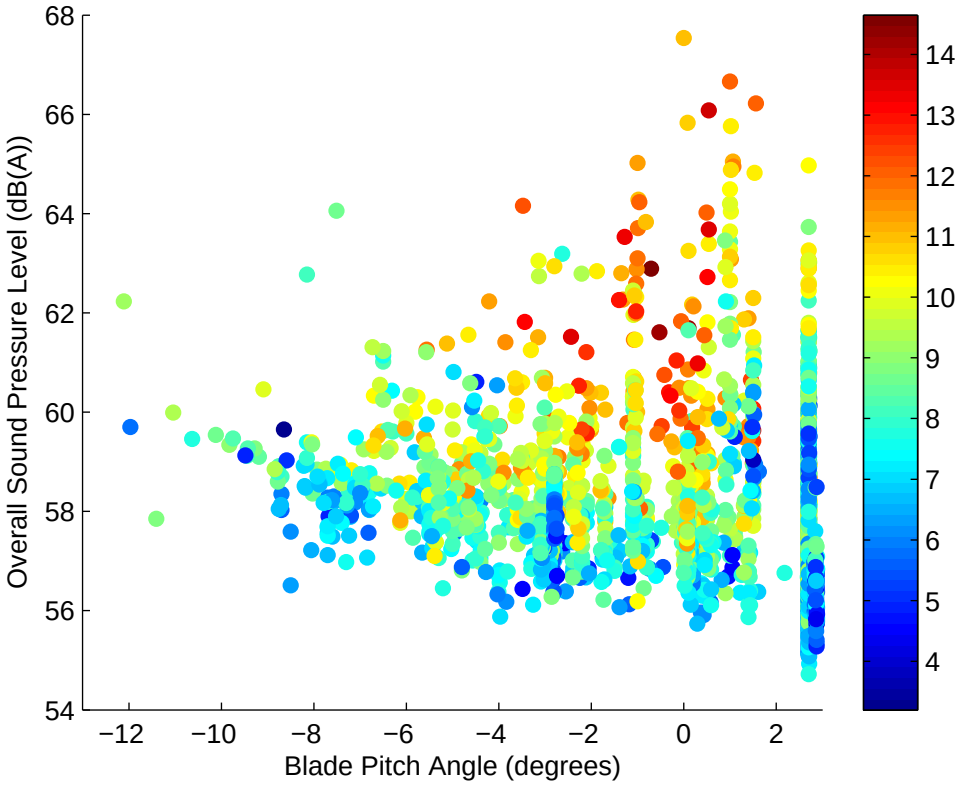

Figure 5.11: Combined noise OASPL values vs. wind turbine blade pitch angle for all days of experiment except February 22. Contour colors indicating wind speed (m/s)

power grid frequency. With gearing, the rotor is rotating at 122 rpm. The current study only discusses noise results when the wind turbine is grid-connected at this fixed rpm. However, as the wind turbine also operates when the rotor rpm is not fixed at 122 rpm: i.e. freewheeling when disconnected/awaiting grid connection. The effects of rpm on noise can be explore further in future studies and will only be discussed briefly.

Figure 5.12 shows the relationship between the combined noise OASPL with the Wenvor turbine rotor rpm. As a reference, the wind speed associated with each data point is indicated by the color contours. This dataset contains all data points presented so far (The 2827 data points previously shown in figure 5.7; located in the vertical grouping at 122 rpm). As well, all noise measurements taken during the days of experiments when the wind turbine was in freewheel are included in the figure (additional 1037 data points). The wind turbine rotor was found to vary between 100 rpm to greater than 140 rpm.

From figure 5.12, the OASPL of the combined noise is seen to increase with increasing wind turbine rotor rpm. The increase in U_∞ is known to related to increased airfoil self-noise [36]. However, the wind turbine rotor rpm during freewheel is related to the wind speed on site. During freewheeling, the higher rpm observed is a result of wind gusts and higher wind speeds. The results from figure 5.12 do not demostrate the relationship between OASPL and wind turbine rotor independently. Both factors are contributing to the increase in OASPL values.

5.2.2 Wind Turbine Noise at Operating Pitch Angle

The case of the wind turbine noise when the blade is pitched at its operating point is further examined in this section. During the combined noise measurements at grid connected conditions (2827 data points), the wind turbine blade pitch angle is most frequently observed to be at the operating point of 2.8°; accounting for 53% of the collected data points.

Figure 5.13 shows a scatterplot of OASPL vs. winds speed for all the background and combined noise data points used in the analysis of the current section. The data for February 22 and for the data for the other days are shown in sub figures a and b respectively. In total, there are 885 data points (180 of which was recorded on February 22) of combined noise measurements and 1522 data points (470 of which were recorded on February 22) of background noise measurements. The data set is limited to data points:

- when the wind turbine is grid connected (at a constant rotation of 122 rpm)
- when the upstream wind directions is between $260° - 320°$ (with effects as discussed in Section 5.1.1 and 5.2.1)

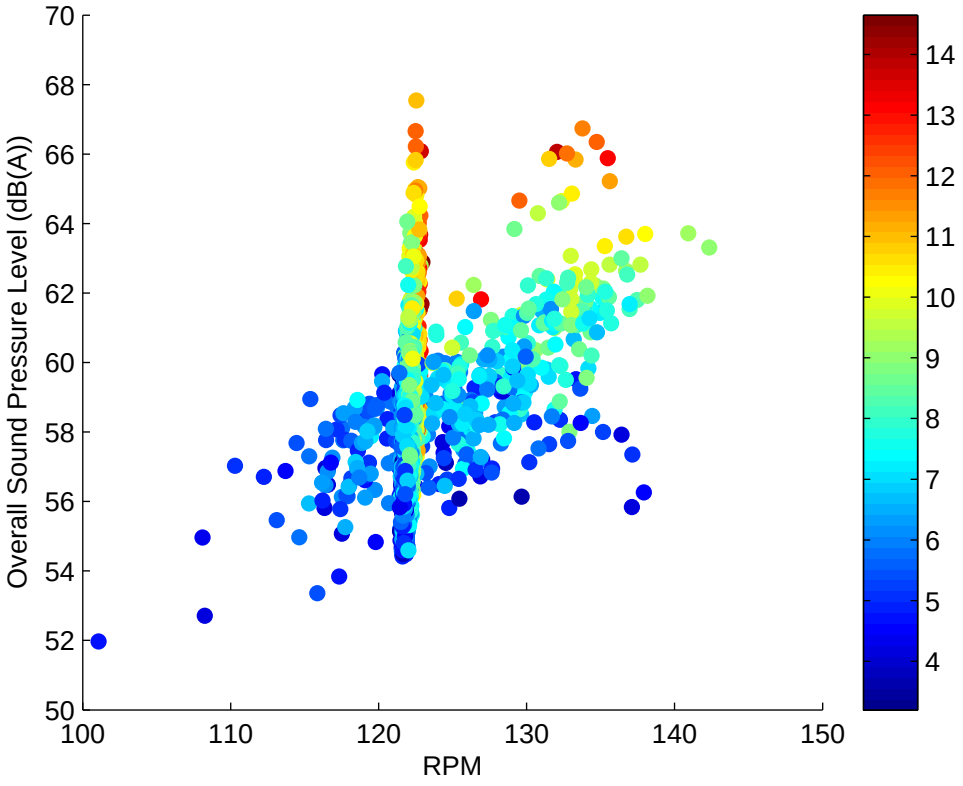

Figure 5.12: Combined noise OASPL vs. rpm for all days of experiment except February 22. Contour colour indicates wind speed (m/s)

Table 5.4: Second order regression of background and combined noise measurements for February 22 and other days of experiment

20m RMY Wind Speed (m/s)		4 m/s	5 m/s	6 m/s	7 m/s	8 m/s	9 m/s	10 m/s	11 m/s
Feb 22 (Background)	OASPL (dB)	44.3	45.1	46.1	47.3	48.6	50.2	N/A	N/A
	Type A Error (dB)	2.7	3.6	1.5	1.8	2.0	2.6	N/A	N/A
	Sample Size	101	97	97	85	34	5	N/A	N/A
Feb 22 (Combined)	OASPL (dB)	54.9	55.2	55.5	55.9	56.4	57.0	N/A	N/A
	Type A Error (dB)	0.3	0.3	0.6	0.7	0.5	0.5	N/A	N/A
	Sample Size	17	46	31	33	33	18	N/A	N/A
Other Days (Background)	OASPL (dB)	53.0	52.7	52.8	53.2	53.9	55.0	56.4	58.1
	Type A Error (dB)	0.9	1.3	1.2	1.4	2.0	1.9	2.5	2.8
	Sample Size	15	61	138	213	213	191	107	62
Other Days (Combined)	OASPL (dB)	56.5	56.6	56.9	57.2	57.6	58.1	58.7	59.4
	Type A Error (dB)	0.5	1.1	1.0	1.3	1.4	1.4	2.0	1.6
	Sample Size	6	32	69	166	189	147	70	21

- when the wind turbine yaw direction is between $275° - 305°$ (with effects as discussed in Section 5.2.1)
- when the wind turbine blade pitch angle is at 2.8° (for combined noise only)

The collected data is sorted into integer bins of site wind speeds and fitted to a second order regression. These results are shown in table 5.4 for the site wind speeds from 4m/s to 11 m/s. The Type A error (error associated with the regression fit, please see Appendix A) and the bin sample size are also presented in this table.

By subtracting the background noise OASPL from the combined noise OASPL, the wind turbine sound pressure levels ($L_{Aeq,SPL}$) can be derived. However, the sound pressure level should be at least 6 dB above the background noise signal [8]. Examining the values in table 5.4, the SNR is found to be low for the results excluding February 22. For all of the wind speed bins, the sound pressure level difference is less than 6 dB. The wind turbine sound pressure level ($L_{Aeq,SPL}$) and consequently the wind turbine sound power level ($L_{Aeq,SWL}$) could not be assessed.

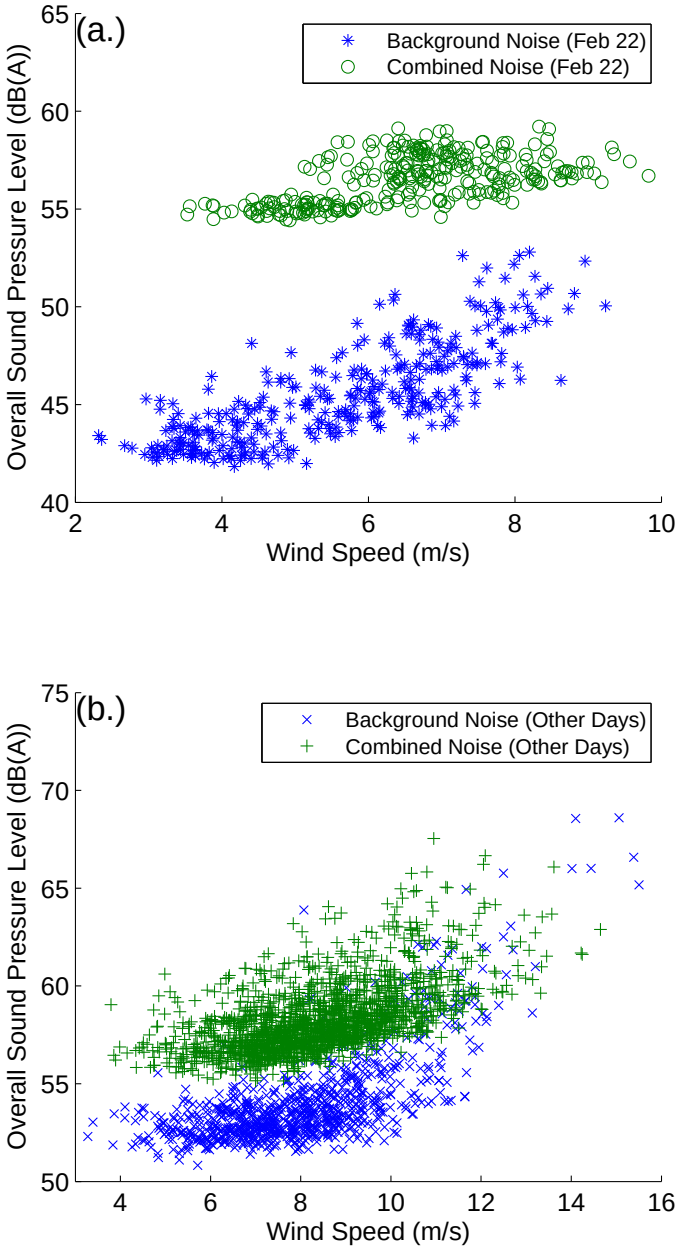

Figure 5.13: Comparison of combined noise measurements with background noise measurements a.) on Feb. 22 b.) on other days

Table 5.5: Sound pressure level of the wind turbine as calculated from experimental measurements on February 22

20m RMY Wind Speed (m/s)	**4 m/s**	**5 m/s**	**6 m/s**	**7 m/s**	**8 m/s**	**9 m/s**
$L_{Aeq,SPL}$, Feb 22 (dB)	54.5	54.7	55.0	55.3	55.6	56.0

Table 5.6: Sound power level of the wind turbine as calculated from experimental measurements on February 22

20m RMY Wind Speed (m/s)	**4 m/s**	**5 m/s**	**6 m/s**	**7 m/s**	**8 m/s**	**9 m/s**
$L_{Aeq,SWL}$, Feb 22 (dB)	92.8	93.1	93.3	93.7	94.0	94.3

For the measurements from the day of February 22, the SNR is strong due to the low OASPL of the background noise. On average, the combined noise is nearly 9 dB higher than the background noise of the same wind speed bins. The $L_{Aeq,SPL}$ and $L_{Aeq,SWL}$ (see eq. 2.6) can be calculated. The results are presented in table 5.5 and 5.6 respectively. The measurements are found to be similar to those seen in the NREL studies [54] [55] [56] [57] [58] [59].

As discussed in section 5.1.3, the wind turbine contributions from the combined noise measurements are found to be more resolved from the background noise in some parts of the frequency spectrum. From figure 5.6, it appears examining the 1/3 octave bands between 400 to 5000 Hz (or the 1/1 octave bands from 500-4000 Hz) would encompass the full range of frequencies where there is a strong SNR.

The band sound pressure level from the 1/3 octave bands of 400 Hz to 5000 Hz is calculated and binned according to their corresponding wind speed. The results are shown in table 5.7. The SNR is much improved, with many of the bins showing a greater tgab 6 dB difference. Table 5.8 and 5.9 $L_{Aeq,BPL}$ and $L_{Aeq,BWL}$ of the wind turbine noise from the days excluding February 22.

5.2.3 Narrowband Spectra

While examining the acoustic spectrum for tonal noise was not in the scope of the study, several unplanned FFT measurements were collected during the experiments. Figure 5.14 and 5.15 shows selected acoustic spectra measured at $-8°$ blade pitch angle and operating

Table 5.7: Second order regression of background and combined noise measurements when results are summed from 400 Hz to 5 kHz 1/3 octave bands, for all days except February 22

20m RMY Wind Speed (m/s)		**4 m/s**	**5 m/s**	**6 m/s**	**7 m/s**	**8 m/s**	**9 m/s**	**10 m/s**	**11 m/s**
Other Days (Background)	**BPL (dB)**	47.4	47.3	47.7	48.5	49.6	51.2	53.1	55.5
	Type A Error (dB)	1.8	2.3	2.0	2.4	3.1	2.9	3.5	3.7
	Sample Size	15	61	138	213	213	191	107	62
Other Days (Combined)	**BPL (dB)**	54.3	54.6	55.0	55.5	56.0	56.6	57.3	58.0
	Type A Error (dB)	0.2	1.3	1.2	1.5	1.6	1.5	2.2	1.8
	Sample Size	6	32	69	166	189	147	70	21

Table 5.8: Band sound pressure level of the wind turbine as calculated from experimental measurements on all days except February 22

20m RMY Wind Speed (m/s)	**4 m/s**	**5 m/s**	**6 m/s**	**7 m/s**	**8 m/s**	**9 m/s**	**10 m/s**	**11 m/s**
$L_{Aeq,BPL}$, Other Days (dB)	53.3	53.8	54.2	54.6	54.9	55.3*	56.0*	N/A

Table 5.9: Band sound power level of the wind turbine as calculated from experimental measurements on all days except February 22

20m RMY Wind Speed (m/s)	**4 m/s**	**5 m/s**	**6 m/s**	**7 m/s**	**8 m/s**	**9 m/s**	**10 m/s**	**11 m/s**
$L_{Aeq,BWL}$, Other Days (dB)	91.7	92.1	92.5	92.9	93.3	93.7*	94.3*	N/A

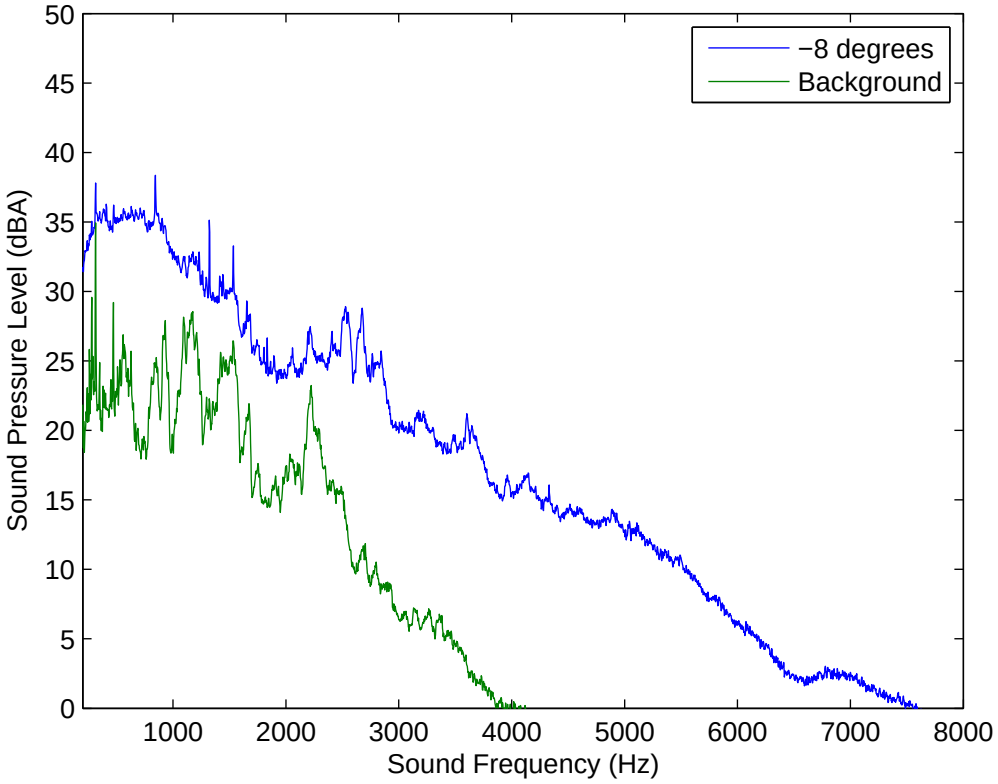

Figure 5.14: Narrowband acoustic spectra for combined noise and backgound noise at $-8°$ pitch

pitch angle of 2.8° respectively. For comparison, the background acoustic spectra are plotted in the figures.

The observations made during the experiment were not comprehensive as it was not possible to conduct the FFT measurements for the full range of observed wind speeds. Indeed, the right condition occur intermittently and it is difficult to collect sufficient data for analysis. For the measurements presented, the wind turbine had maintained the pitch angle for the duration of the recording however the wind turbine yaw direction and wind direction were misaligned in some cases. Despite the effects as discussed previously in section 5.1 and 5.2.1, some observations can still be made:

- Several tones can be observed in the narrowband acoustic spectra of the combined

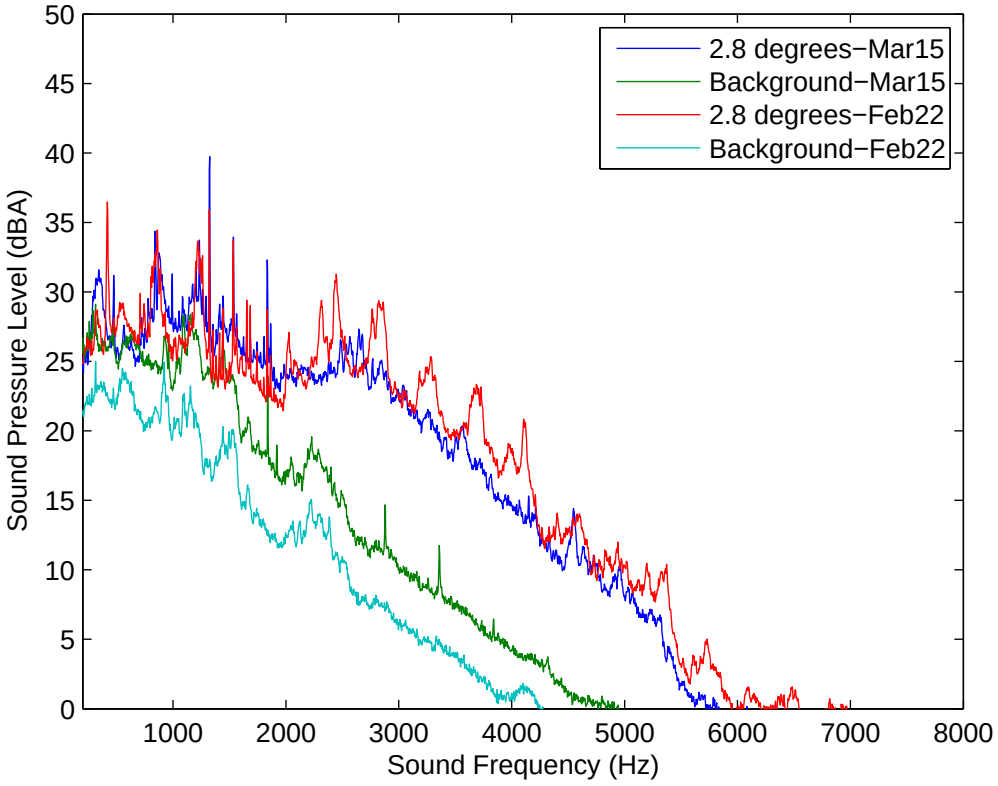

Figure 5.15: Narrowband acoustic spectra for combined noise and background noise at 2.8° pitch during February 22 and March 15

noise measurements. The tones appear to be more discernible from the ambient with the increase of blade pitch angle (decreasing angle of attack). This is evident from comparing figures 5.14 and 5.15.

- From the frequency between 400 Hz to 1800 Hz, the wind turbine noise narrowband acoustic spectra showed several prominent tones. The tones could be attributed to LBL-VS noise. Another possible explanation of the tones can be to attribute to mechanical noise from wind turbine components such as the gearbox. However, from observations on site during the experiment, mechanical noise is not apparent and does not seem to be a likely explanation.

- A broadband hump is seen at frequencies above 1800 Hz. The hump is roughly centered at 2500 Hz. Comparing figures 5.14 and 5.15, the broadband hump sound pressure levels appear to remain similar with decreasing blade pitch angles. However, at lower frequencies ($<$ 1800 Hz), with decreasing blade pitch angle, the sound pressure level is seen to have a broadband increase in noise. This is likely due to the increase in angle of attack and the promotion of turbulent boundary layer conditions and stalling conditions along the blades.

One possibility to improve the experimental setup is to make audio recordings of sufficient quality so they can be analyzed post-experiment for OASPL, 1/3 octave analysis and FFT analysis. At present, the equipment is not configured for this function. The two functions (octave analysis and FFT analysis) are separate and cannot be analyzed simultaneously.

5.3 Test Site Feasibility and Recommendations for Future Studies

In the current study, the noise emitted by the Wenvor wind turbine blades has been assessed at Wind Energy Group outdoor wind turbine test site. Even though on site noise from the nearby bio-gas power plant has contaminated the low end of the frequency spectrum, the wind turbine broadband noise was found to be centered at frequencies removed from the contamination; being very well resolved above the background noise at 1/3 octave bands greater than 500 Hz. It should be feasible to conduct further acoustic measurement on site, examining the noise emitted from the Wenvor wind turbine as well as examining the effects of noise reduction devices such as trailing edge serrations.

The effects with respect to upstream wind direction, wind turbine yaw direction, wind turbine rotor rpm and blade pitch angle have also been assessed. Upstream wind direction and yaw angle is recommended to be within $\pm 15^{\circ}$ alignment with the microphone measurement position to reduce variability of sound pressure level measurements. The wind turbine rotor rpm and blade pitch angle has also notable effects.

To further improve the understanding of current results, the results of the current experiment can be compared with known noise prediction model. Reviewed in section 2.2.2, the Acoustic Blade Element (ABE) method would be one such method. The contributions for each type of airfoil self-noise as well as from the noise generated from different radial positions can be better understood with this analysis. The relevant geometric information regarding the Wenvor wind turbine blade is readily available in section 3.2.2. The key to an accurate prediction would depend on accurately modelling the inflow condition. Examining variations due to azimuthal positions, effects from varying upstream conditions, rotational effects of the rotor and unsteady aerodynamic/dynamic stall effects would also enhance the accuracy of the prediction.

Relevant background on serration design at this Reynolds number regime have been reviewed in this study and found in section 2.4.1. Given the likely turbulent boundary layer flow experienced by the wind turbine, narrow serration aspect ratio λ/h are generally found to be more effective.

Chapter 6

Conclusion and Recommendations

In the current study, the objective to examined airfoil self-noise as it relates wind turbines. For small scale wind turbines, tonal noise can be generated by the LBL-VS noise mechanism. A portion of the current study was devoted to studying its characteristics and behaviour.

The experimental results show evidence to suggest noise orginated from generation mechanisms located on the suction side of the airfoil. The BPM noise prediction model, modified by using suction side boundary layer parameters as input, yields a reasonable prediction of the sound pressure levels. This can suggest that for small scale wind turbines experiencing similar chord Reynolds number flow regime ($Re_c < 10^5$) along the blade, noise reduction devices targeting LBL-VS noise should focus on targeting the suction side of the airfoil.

As wind turbines experience dynamic conditions which differ from the static conditions typically examined in wind tunnel conditions, the SD-7037 airfoil was examined under dynamically oscillating conditions previously studied aerodynamically by Gharali [6]. The experimental results show evidence to suggest the tonal noise may only exist at certain phases of the oscillation cycle. Overall, the tonal noise is found to be reduced compared with their static case counterparts at low angles of attack.

The side peak phenomonon, typically seen under static cases indicating an amplitude modulation of the main tone, is not found in the static case of the current study but in the dynamic case. The peak spacing corresponds to the oscillation frequency; suggesting the pressure fluctuation of the oscillation to contribute to the amplitude modulation in the main tone signal in this case. While this result doesn't contribute to the understanding of the cause in the static case (as it is still of some debate [21]), this may serve to be an indicator

in evaluating dynamic stall conditions experienced by the wind turbine. Although, more studies into the behaviour in other oscillating conditions are needed.

As part of the study, trailing edge sawtooth serrations were also examined for their noise reduction effects at low Reynolds number regime. The effects were found to be mixed.

Future studies should investigate the structures related to noise generation mechanism and pressure fluctuations near the surface of the airfoil to have validate the discussions in the current study.

Past studies [20] [25] [77] have analytically examined laminar flow instability/Tollmien Schlichting (TS) waves in relation with tonal noise using the Orr-Sommerfeld equation. Analytical identifying amplified frequencies of TS wave instabilities can predict expected tones and their behaviour to compare with experimental results. This can also serve to understand the role resonance had in the current study.

Numerical studies or experimental studies using spatial (ex. Particle Image Velocimetry) or time (ex. Laser Doppler Anemometry) resolved techniques can help understand the flow structures surrounding the airfoil. This can further validate their involvement as speculated in the discussion of this study.

If a resonance effect was found to be an issue, future experiments should consider investigating further the nature of the resonance effect, modify the closed circuit wind tunnel to reduce its impact or consider another platform for the experiment. While the background noise was observed to be high for the open jet blow down wind tunnel, noise reduction components (duct silencers, acoustic foam lined test section, outlet anechoic chamber) may serve as a suitable platform for future acoustic studies.

Another portion of the current study is devoted to examining airfoil self-noise as it relates to large scale wind turbines. Acoustic measurements were collected at the Wind Energy Group outdoor wind turbine test site. The quality of noise emitted from the Wenvor wind turbine was found. As well, it was the objective of the current study to assess the feasibility of conducting future acoustic experiments at the test site. Although the low frequency noise on site had obscured any qualities of interest below 500 Hz, the broadband noise emitted from the wind turbine rotor is well resolved above the background noise at 1/3 octave bands of mid to high frequency range.

Future studies can further examine the behaviour of noise with respect to different on site parameters in detail. It will also be possible to examine noise reduction devices such as trailing edge saw-tooth serrations. The good signal to noise ratio may make the test site suitable for future studies examining the effects of noise reduction devices.

Future studies should take into account the effects from changing upstream wind direction, wind turbine yaw direction, wind turbine rotor RPM and blade pitch angle as they were found to have an impact on the measured sound pressure levels. Further insight regarding the wind turbine can be gained by modelling the wind turbine rotor and comparing it with the experimental results.

References

[1] Canadian Wind Energy Association (CANWEA): Installed Capacity, 2015. http://canwea.ca/wind-energy/installed-capacity

[2] Statistics Canada: CANSIM, Table 127-0002: Electric Power Generation, by Class of Electricity Producer Monthly (Megawatt hour), 2015. http://www5.statcan.gc.ca/cansim/

[3] Global Wind Energy Council: Wnd Power Capacity in the World, 2015. http://www.gwec.net/global-figures/interactive-map/

[4] Noise Guidelines for Wind Farms. Government Report PIBS 4709e, Ministry of the Environment, Ontario, 2008.

[5] M. F. Barone. Survey of Techniques for Reduction of Wind Turbine Blade Trailing Edge Noise. Technical Report SAND2011-5252, Sandia National Laboratories, 2011.

[6] K. Gharali. Pitching Airfoil Study and Freestream Effects for Wind Turbine Applications, 2013. Ph.D Thesis, University of Waterloo

[7] K. Gharali, N. Tam, and D. A. Johnson. A PIV Load and Flow Structure Study of a Serrated Dynamic Airfoil. In *17th International Symposium on Applications of Laser and Imaging Techniques on Fluid Mechanics*, 2014.

[8] Wind Turbine Generator Systems- Part 11: Aoustic Noise Measurement Techniques. Standards Documentation IEC 61400-11: 2002+A1:2006(E), International Electrotechnical Commission, 2002.

[9] T. F. Brooks, D. S. Pope, and M. A. Marcolini. Airfoil Self Noise and Prediction. Technical Report 1218, National Aeronautics and Space Administration, 1989.

[10] A. McPhee. The Development of a Research Technique for Low Speed Aeroacoustics, 2008. M.A.Sc. Thesis, University of Waterloo

[11] R. Paterson, P. Vogt, M. Fink, and C. Munch. Vortex Noise of Isolated Airfoils. *Journal of Aircraft*, 10(5):296–302, 1973.

[12] C. K. W. Tam. Discrete Tones of Isolated Airfoils. *Journal of Acoustical Society of America*, 55(6):1173–1177, 1974.

[13] M. Fink. Prediction of Airfoil Tone Frequencies. *Journal of Aircraft*, 12(2):118–120, 1975.

[14] M. Lowson, S. Fiddes, and E. Nash. Laminar Boundary Layer Aeroacoustic Instabilities. In *32nd Aerospace Sciences Meeting and Exhibit*, volume 1994-358, pages 1–1–9, 1994.

[15] S. Akishita. Tone-like Noise from an Isolated Two Dimensional Airfoil. In *AIAA 10th Aeroacoustics Conference*, volume 1986, pages 1947–1–6, 1986.

[16] G. Desquesnes, M. Terracol, and P. Sagaut. Numerical Investigation of the Tone Noise Mechanism Over Laminar Airfoils. *Journal of Fluid Mechanics*, 591:155–182, 2007.

[17] H. Arbey and J. Bataille. Noise Generated by Airfoil Profiles Placed in a Uniform Laminar Flow. *Journal of Fluid Mechanics*, 134:33–47, 1983.

[18] E. Nash and M. Lowson. Noise due to Boundary Layer Instabilities. In *First Joint CEAS/AIAA Conference Aeroacoustic Conference*, volume 124, pages 875–875–884, 1995.

[19] E. Nash, M. Lowson, and A. McAlpine. Boundary-Layer Instability Noise on Aerofoils. *Journal of Fluid Mechanics*, 382:27–27–61, 1999.

[20] A. McAlpine, E. Nash, and M. Lowson. On the Generation of Discrete Frequency Tones by the Flow Around an Airfoil. *Journal of Sound and Vibration*, 222(5):753–753–779, 1999.

[21] S. Probsting, J. Serpieri, and F. Scarano. Experimental Investigation of Aerofoil Tonal Noise Generation. *Journal of Fluid Mechanics*, 747:656–687, 2014.

[22] T. Nakano and N. Fujisawa. Measurement of Tonal-Noise Characteristics and Periodic Flow Structure Around NACA0018 Airfoil. *Experiments in Fluids*, 40:482–482–490, 2006.

[23] Y. Takagi, N. Fujisawa, T. Nakano, and A. Nashimoto. Cylinder Wake Influence on the Tonal Noise and Aerodynamic Characteristics of a NACA0018 Airfoil. *Journal of Sound and Vibration*, 297:563–563–577, 2006.

[24] T. Nakano, N. Fujisawa, Y. Oguma, Y. Takagi, and S. Lee. Experimental Study on Flow and Noise Characteristics of NACA0018 airfoil. *Journal of Wind Engineering and Industrial Aerodynamics*, 95:511–511–531, 2006.

[25] T. P. Chong and P. Joseph. An Experimental Study of Tonal Noise Mechanism of Laminar Airfoils. In *15th AIAA/CAES Aeroacoustics Conference (30th AIAA Aeroacoustic Conference)*, volume 2009, page 3345, 2009.

[26] E. Arcondoulis, C. J. Doolan, and A. Zander. Airfoil Noise Measurements at Various Angles of Attack and Low Reynolds Number. In *ACOUSTICS 2009*, pages 1–1–8, 2009.

[27] T. Ikeda and T. Atobe. Self-Noise Effects on Aerodynamics of Cambered Airfoil at Low Reynolds Number. *AIAA Journal*, 53(8):1–1–14, 2015.

[28] B. Plogmann, A. Herrig, and W. Wurz. Experimental Investigation of a Trailing Edge Noise Feedback Mechanism on a NACA 0012 Airfoil. *Experiments in Fluids*, 54(1480):1–1–14, 2013.

[29] S. Probsting and F. Scarano. Experimental Investigation of Isolated Aerofoil Noise. In *The 21st International Congress on Sound and Vibration*, pages 1–1–8, 2014.

[30] S. Tomimatsu and N. Fujisawa. Measurement of Aerodynamic Noise and Unsteady Flow Field Around a Symmetic Airfoil. *Journal of Visualization*, 5(4):381–381–388, 2002.

[31] M. S. Howe. A Review of the Theory of Trailing Edge Noise. *Journal of Sound and Vibration*, 61((3)):437–465, 1978.

[32] C. A. Albarracin, C. J. Doolan, C. H. Hansen, and L. A. Brooks. Turbulent Trailing Edge Noise Estimation using a RANS-based Statistical Noise Model. In *ACOUSTICS 2011*, pages 1–1–5, 2011.

[33] *Wind Turbine Noise*. Multi-Science Publishing Co. Ltd, Brentwood, Essex, UK, 1st edition, 2011.

[34] A. Powell. On the Aerodynamic Noise of a Rigid Flat Plate Moving at Zero Incidence. *The Journal of the Acoustical Society of America*, 31(12):1649–1653, 1959.

[35] J. E. Ffowcs Williams and L. H. Hall. Aerodynamic Sound Generation by Turbulent Flow in the Vicinity of a Scattering Half Plane. *Journal of Fluid Mechanics*, 40(04):657–670, 3 1970.

[36] R. K. Amiet. Noise due to Turbulent Flow Past a Trailing Edge. *Journal of Sound and Vibration*, 47(3):387–393, 1976.

[37] S. Wagner, BareißR., and G. Guidati. *Wind Turbine Noise*. Springer Berlin Heidelberg, 2012.

[38] W. K. Blake. *Mechanics of Induced Flow Sound and Vibrations*. Academic Press, Waltham, Massachusetts, 1st edition, 1986.

[39] P. Moriarty and P. Migliore. Semi-Empirical Aeroacoustic Noise Prediction Code for Wind Turbines. Technical Report NREL/TP-500-34478, National Renewable Energy Laboratory, 2003.

[40] R. K. Amiet. Acoustic Radiation from an Airfoil in a Turbulent Stream. *Journal of Sound and Vibration*, 41(4):407, 1975.

[41] W. J. Zhu, N. Heilskov, W. Z. Shen, and J. N. Sorenson. Modeling of Aerodynamically Generated Noise from Wind Turbines. *Journal of Solar Energy Engineering*, 127(4):517–528, 06/09 2005. 10.1115/1.2035700.

[42] P. Fuglsang and H. A. Madsen. *Implementation and Verification of an Aeroacoustic Noise Prediction Model for Wind Turbines*. Risø National Laboratory, 1996.

[43] P. Moriarty, G. Guidati, and P. Migliore. *Recent Improvement of a Semi-Empirical Aeroacoustic Prediction Code for Wind Turbines*. American Institute of Aeronautics and Astronautics, 05/10; 2015/09 2004. 24; M1: 0; doi:10.2514/6.2004-3041.

[44] P. Moriarty, G. Guidati, and P. Migliore. *Prediction of Turbulent Inflow and Trailing-Edge Noise for Wind Turbines*. American Institute of Aeronautics and Astronautics, 05/23; 2015/09 2005. 25; M1: 0; doi:10.2514/6.2005-2881.

[45] W. J. Zhu, J. N. Sorenson, and W. Z. Shen. An Aerodynamic Noise Propagation Model for Wind Turbines. *Wind Engineering*, 29(2):129–142, 2005. http://dx.doi.org/10.1260/0309524054797168.

[46] K. Boorsma and J. G. Schepers. Enhanced Wind Turbine Noise Prediction Tool SILANT. In *Fouth International Meeting on Wind Turbine Noise*, volume ECN-M–12, pages 1–16, 2011.

[47] G. Leloudas, W. J. Zhu, J. N. Srensen, W. Z. Shen, and S. Hjort. Prediction and Reduction of Noise from a 2.3 MW Wind Turbine. *Journal of Physics: Conference Series*, 75(1):012083, 2007.

[48] M. Kamruzzaman, Th Lutz, W. Wrz, W. Z. Shen, W. J. Zhu, M. O. L. Hansen, F. Bertagnolio, and H. Aa Madsen. Validations and Improvements of Airfoil Trailing-Edge Noise Prediction Models using Detailed Experimental Data. *Wind Energy*, 15(1):45–61, 2012.

[49] J. G. Schepers, A. P. W. M. Curvers, S. Oerlemans, K. A. Braun, T. Lutz, A. Herrig, W. Wuerz, A. Matesanz, L. Garcillan, M. Fisher, K. Koegler, and T. Maeder. Sirocco: Silent Rotors by Acoustic Optimisation. In *Second International Meeting on Wind Turbine Noise*, 2007.

[50] J. F. Manwell, J. G. McGowan, and A. L. Rogers. *Wind Energy Explained: Theory, Design and Application*. Wiley Publishing, Chichester, UK, 2nd edition edition, 2010.

[51] M. Lowson. *Assessment and Prediction of Wind Turbine Noise*. Department of Trade and Industry W/13/00284/REP,. Department of Trade and Industry, 1993.

[52] M. Drela and H. Youngren. Xfoil 6.9 User Primer. User guide, Massachusetts Institute of Technology, 2001.

[53] S. Oerlemans and J. G. Schepers. Prediction of Wind Turbine Noise and Validation against Experiment. Technical Report NLR TP-2009-402, National Aerospace Laboratory NLR, 2009.

[54] P. Migliore, J. van Dam, and A. Huskey. Acoustic Tests of Small Wind Turbines. Technical Report CP-500-34662, NREL, 2003.

[55] J. Roadman and A. Huskey. Acoustic Noise Test Report for the Viryd CS8 Wind Turbine. Technical Report NREL/TP-5000-58565, NREL, 2013.

[56] A. Huskey. Wind Turbine Generator System Acoustic Noise Test Report for the Gaia Wund 11-kW Wind Turbine. Technical Report NREL/TP-5000-51828, NREL, 2011.

[57] A. Huskey and J. van Dam. Wind Turbine Generator System Acoustic Noise Test Report for the AOC 15/50 Wind Turbine. Technical Report NREL/EL-500-34021, NREL, 2003.

[58] A. Huskey and J. van Dam. Wind Turbine Generator System Acoustic Noise Test Report for the ARE 442 Wind Turbine. Technical Report NREL/TP-5000-49179, NREL, 2010.

[59] A. Huskey and M. Meadors. Wind Turbine Generator System Acoustic Noise Test Report for the Whisper H40 Wind Turbine. Technical Report NREL/EL-500-34383, NREL, 2003.

[60] Audio Weighting Filters, 2017. Mathworks. https://www.mathworks.com/help/audio/examples/audio-weighting-filters.html

[61] W. J. McCroskey. Unsteady Airfoils. *Annual Review of Fluid Mechanics*, 14:285–311, 1982.

[62] A. Laratro, M. Arjomandi, R. Kelso, and B. Cazzolato. A Disccusion of Wind Turbine Interaction and Stall Contributions to Wind Farm Noise. *Journal of Wind Engineering and Industrial Aerodynamics*, 127:1–10, 2014.

[63] S. Moreau, M. Roger, and J. Christophe. Flow Features and Self-Noise of Airfoils Near Stall or in Stall. In *15th AIAA/CEAS Aeroacoustic Conference (30th AIAA Aeroacoustic Conference)*, page 3198, 2009.

[64] S. Nagarajan, S. Hahn, and S. Lele. *Prediction of Sound Generated by a Pitching Airfoil: A Comparison of RANS and LES*. American Institute of Aeronautics and Astronautics, 05/08; 2015/09 2006. 25; M1: 0; doi:10.2514/6.2006-2516.

[65] S. Nagarajan and S. Lele. *Sound Generation by Unsteady Airfoil Motions: A Study Using Direct Computation and Acoustic Analogy*. American Institute of Aeronautics and Astronautics, 05/23; 2015/09 2005. 25; M1: 0; doi:10.2514/6.2005-2915.

[66] P. Totaro. Noise Reduction Technologies, Current and Future. In *EWEA 2014*, 2014.

[67] M. S. Howe. Aerodynamic Noise of a Serrated Trailing Edge. *Journal of Fluids and Structures*, 5:33–45, 1991.

[68] M. S. Howe. Noise Produced by a Sawtooth Trailing Edge. *Journal of Acoustical Society of America*, 90(1):482–487, 1991.

[69] K. A. Braun, A. Gordner, N. J. C. M. v. d. Borg, A. G. M. Dassen, F. Boorenspleet, and R. Parchen. Serrated Trailing Edge Noise (STENO) Publishable Final Report. Technical report, 1998.

[70] T. Dassen, R. Parchen, J. Bruggeman, and F. Hagg. Results of a Wind Tunnel Study on the Reduction of Airfoil Self-Noise by the Application of Serrated Blade Trailing Edges. Technical Report TP 96350 U, NLR, 1996.

[71] S. Oerlemans, M. Fisher, T. Maeder, and K. Kogler. Reduction of Wind Turbine Noise using Optimized Airfoils and Trailing Edge Serrations. Technical Report TP-2009-401, NLR, 2009.

[72] M. Gruber. Airfoil Noise Reduction by Edge Treatments, 2012. Ph.D Thesis, University of Southhampton

[73] A. Finez, E. Jondeau, and M. Roger. Broadband Noise Reduction of a Linear Casade with Trailing Edge Serrations. In *17th AIAA/CEAS Aeroacoustics Conference*, volume 2011, page 2874, 2011.

[74] S. Probsting. Coherent Structures at the Serrated Trailing-Edge of a NACA 0012, 2011.

[75] T. P. Chong, P. Joseph, and M. Gruber. An Experimental Study of Airfoil Instability Noise with Trailing Edge Serrations. In *16th AIAA?CEAS Aeroacoustic Conference (31st AIAA Aeroacoustic Conference)*, 2010.

[76] T. P. Chong, P. Joseph, A. Vathylakis, and M. Gruber. On the Noise and Wake Flow of an Airfoil with Broken and Serrated Trailing Edges. In *17th AIAA/CEAS Aeroacoustic Conference*, page 2860, 2011.

[77] T. P. Chong and P. Joseph. An Experimental Study of Airfoil Instability Tonal Noise with Trailing Edge Serrations. *Journal of Sound and Vibration*, 332:6335–6358, 2013.

[78] D. J. Moreau, L. A. Brooks, and C. J. Doolan. Flat Plate Self-Noise Reduction at Low-to-Moderate Reynolds Number with Trailing Edge Serrations. In *ACOUSTICS 2011*, volume Paper Number 46, pages 1–7, 2011.

[79] D. J. Moreau, L. A. Brooks, and C. J. Doolan. On the Noise Reduction Mechanism of a Flat Plate Serrated Trailing Edge at Low-to-Moderate Reynolds Number. *American Institute of Aeronautics and Astronautics*, 51(10):2513–2522, 2011.

[80] D. J. Moreau, L. A. Brooks, and C. J. Doolan. Experimental Investigation of Flat Plate Self-Noise Reduction using Trailing Edge Serrations. In *28th Interational Congess of the Aeronautical Sciences*, pages 1–9, 2012.

[81] D. J. Moreau and C. J. Doolan. Tonal Noise from Trailing Edge Serrations at Low Reynolds Numbers. In *19th AIAA/CEAS Aeroacoustics Conference*, volume 2013, page 2010, 2013.

[82] L. E. Jones and R. Sandberg. Numerical Investigation of Tonal Airfoil Self-Noise Generated by an Acoustic Feedback-Loop. In *16th AIAA/CEAS Aeroacoustic Conference*, page 3701, 2010.

[83] R. Sandberg and L. E. Jones. Direct Numerical Simulation of Low Reynolds Number Flow over Airfoils with Trailing-Edge Serrations. *Journal of SOund and Vibration*, 330:3818–3831, 2011.

[84] L. E. Jones and R. Sandberg. Acoustic and Hydrodynamic Analysis of the Flow Around an Aerofoil with Trailing-Edge Serrations. *Journal of Fluid Mechanics*, 706:295–322, 2012.

[85] S. M. Orlando. Laser Doppler Anemometry and Acoustic Measurements of an S822 Airfoil at Low Reynolds Numbers, 2011. M.A.Sc. Thesis, University of Waterloo

[86] B. Sperandei. The Application of Particle Image Velocimetry in a Small Scale Wind Tunnel, 2002.

[87] R. Parker. Resonance Effects in Wake Shedding from Parallel Plates: Calculation of Resonant Frequencies. *Journal of Sound and Vibration*, 5(2):330, 1967.

[88] T. Ikeda, T. Atobe, Y. Konishi, H. Nagai, and K. Sasi. Numerical Study of Wind-Tunnel Acoustic Resonance Induced by Two-Dimensional Airfoil Flow at Low Reynolds Number. In *29th Congress of the International Council of the Aeronautical Sciences*, 2014.

[89] J. B. Barlow, W. H. Rae, and A. Pope. *Low-Speed Wind Tunnel Testing*. Wiley-Interscience, 3rd edition, 1999.

[90] A. Abdelrahman. Noise Location and Reduction using Trailing Edge Serrations on a Small Scale Wind Turbine. Univeristy of waterloo course me770, fall 2011, Individual, 2011.

[91] C. Torrence and G. Compo. A Practical Guide to Wavelet Analysis. *Bulletin of American Meteorological Society*, 79(1):61–61–78, 1998.

[92] S. Probsting, F. Scarano, and C. Morris. Regimes of Tonal Noise on an Airfoil at Moderate Reynolds Number. *J.Fluid Mech.*, 780:407–438, 2015.

[93] Wavelet Toolbox, 2017. Mathworks. https://www.mathworks.com/products/wavelet.html

[94] P. Moriarty. NAFNoise User's Guide. User's guide, National Renewable Energy Laboratory, 2005.

[95] V. Lam. Development of Wind Resource Assessment Methods and Application to the Waterloo Region, 2013. M.A.Sc. Thesis, University of Waterloo

[96] N. Swytink-Binnema. Digital Tuft Flow Visualisation of Wind Turine Blade Stall, 2014. M.A.Sc. Thesis, University of Waterloo

[97] Wind, Waves, & Weather Forecast Kitchener/Waterloo Airport, 2015. http://www.windfinder.com/

[98] A. Paulissen. Wenvor Technologies inc., 2009. http://www.wenvortechnologies.com/

[99] N. Tam and D. A. Johnson. Implementing a Monitoring System on a 30kW Wind Turbine. In D. A. Johnson, editor, *Canadian Wind Energy Association Annual Conference (CANWEA 2013)*, Waterloo, Ontario, 2013.

[100] N. Swytink-Binnema, C. Knischewsky, N. Tam, T. Gallant, and D. Dwaorakowski. The Wenvor Turbine Field Site. Internal report/ documentation, Wind Energy Group, University of Waterloo, 2014.

[101] Google. Google Earth: Satellite Images, 2016.

[102] Bruel and Kjaer. *Technical Documentation: Hand-held Analyzers Types 2250 and 2270 with Microphone Type 4189*. 2011.

[103] R. Gu. Blade Element Momentum Modeling in Support of Experimental Measurements on a 30kW Wind Turbine. In *1000 Islands Energy Research Forum*, 2013.

APPENDICES

Appendix A

Uncertainties for Outdoor Noise Measurements

In the analysis of the experimental results, there are two types of uncertainty that has to be considered. Type A uncertainty concerns the statistical uncertainty associated with the regression analysis of the sound pressure level readings measured at 10 second intervals. Type B uncertainty is associated with the instrument/ chain of measurement equipment. The IEC standard [8] outlines the method to estimates the different types of uncertainties.

Type A uncertainty, U_A, is defined in the IEC standard [8] as:

$$U_A = \sqrt{\frac{\Sigma(y - y_{est})^2}{N - 2}} \tag{A.1}$$

where y is the individual datapoints of sound pressure level measured on site, y_{est} is the value of sound pressure level estimated from the 2nd order regression fit with respect to wind speed and N is the number of measurements used in the regression. The values are presented in the discussion for the current study.

Type B uncertainty are estimated from values found in table A.1.

The total uncertainty is defined from [8] as:

$$U_{total} = \sqrt{U_A^2 + \Sigma U_{Bn}^2} \tag{A.2}$$

where ΣU_{Bn}^2 is the sum of the square of the various Type B uncertainty values. The value for ΣU_{Bn}^2 is found to be 1.26 dB. In the current study, the minimal total error is 1.26

Table A.1: Estimated values of the Type B uncertainties for the current study. These are typical values that can be found for the experiment according to the IEC standard [8]

Uncertainty Type	**Estimated Value**
Calibration, U_{B1}	0.2 dB
Instrument, U_{B2}	0.2 dB
Board, U_{B3}	0.3 dB
Distance, U_{B4}	0.1 dB
Impedance, U_{B5}	0.1 dB
Turbulence, U_{B6}	0.4 dB
Wind Speed, U_{B7}	0.9 dB
Direction, U_{B8}	0.3 dB
Background, U_{B9}	0.1 dB

dB (for when Type A error was 0.2 dB) and 3.9 dB (for when the Type A uncertainty was 3.7 dB).